FUNCTIONALIZING THE MITOCHONDRIAL PROTEOME-

MITOCHONDRIAL METABOLISM, PROTEIN

QUALITY CONTROL AND BEYOND

by

Yu-Chan Chen

A dissertation submitted to the faculty of
The University of Utah
in partial fulfillment of the requirements for the degree of

Doctor of Philosophy

Department of Biochemistry

The University of Utah

August 2015

The University of Utah Graduate School

STATEMENT OF DISSERTATION APPROVAL

The dissertation of Yu-Chan Chen

has been approved by the following supervisory committee members:

Jared P. Rutter	, Chair	**April 29, 2015** Date Approved
Wesley I. Sundquist	, Member	**April 29, 2015** Date Approved
Janet M. Shaw	, Member	**April 29, 2015** Date Approved
Dennis R. Winge	, Member	**April 29, 2015** Date Approved
Donald E. Ayer	, Member	**April 29, 2015** Date Approved

and by Wesley I. Sundquist , Chair of

the Department of Biochemistry

and by David B. Kieda, Dean of The Graduate School.

ABSTRACT

This dissertation is to characterize two evolutionarily conserved but uncharacterized mitochondrial proteins using yeast and mammalian cells. The first protein, which we named respiratory supercomplex factor 1 (Rcf1), is required for the assembly of respiratory supercomplexes. Deletion of the *RCF1* gene causes destabilization of respiratory supercomplexes, impaires respiration and elevates mitochondrial oxidative stress. We also show that *HIG2A*, a mammalian homolog of *RCF1*, performs the same function in mammalian cells. Therefore, we suggest that Rcf1 and HIG2A are members of a conserved protein family that acts to maintain the homeostasis of mitochondrial metabolism by promoting respiratory supercomplex assembly. The second protein on which my dissertation research was based, originally annotated as mitochondrial sorting of protein 1 (Msp1), performs multiple tasks. The first function is its role in facilitating the removal of tail-anchored (TA) proteins that are mislocalized to mitochondria. Disruption of the guided entry of tail-anchored protein (GET) system was shown to cause a subset of TA proteins to mislocalize to mitochondria. The AAA+ ATPase Msp1 can limit the accumulation of mislocalized TA proteins on mitochondria. The human homolog of Msp1, ATAD1, also limits the mitochondrial mislocalization of TA proteins in mammalian cells. Therefore, Msp1 and ATAD1 are conserved members of a mitochondrial protein quality control system that

functions to promote the extraction and degradation of mislocalized TA proteins to maintain mitochondrial integrity. The second role of Msp1 and ATAD1 is in a novel vesicular trafficking system from mitochondria to peroxisomes in an ATPase activity-dependent manner. Impaired peroxisome biogenesis and mislocalization of peroxins (peroxisomal biogenesis factors) to the mitochondria has been observed in cells from Zellweger patients. Overexpression of *ATAD1* facilitates the removal of these peroxins from mitochondria and the accumulation in vesicle-like structures of unknown character and function. We speculate that these vesicles might sort the peroxins to peroxisomes for peroxisomal biogenesis. Therefore, we propose that Msp1 and ATAD1 participate in a novel vesicular trafficking pathway, which is likely associated with protein sorting from mitochondria to peroxisomes. In conclusion, our findings provide a better understanding of mitochondrial biology, which further sheds light on the etiology of human mitochondrial diseases.

This dissertation is dedicated to my beloved parents and families

TABLE OF CONTENTS

LIST OF FIGURES

LIST OF TABLES

ACKNOWLEDGEMENTS

Many faculty members, colleagues, families and friends played a critical role in helping me to finish my dissertation. Without their mentorship and support, it would not be possible for me to accomplish the most important goal in my career. I am grateful for being surrounded by them and I thank them from the bottom of my heart.

I would like to express my gratitude to my dissertation advisor, Dr. Jared Rutter, for his endless patience and scientific breadth in guiding me in the path of my graduate career. Jared accepted me into his lab without any hesitation and he has mentored me based on my own personality. He had so much faith in me even when I experienced some bumpiness in the beginning of my graduate career. His encouragement and criticism have always spurred me to constantly improve myself to become an independent scientist. He was always supportive when I undertook risk in different projects. I am grateful for his generosity, support, encouragement and patience.

I gratefully thank many faculty members who have helped and encouraged me during my graduate career. Dr. Janet Shaw, Dr. Dennis Winge, Dr. Wesley Sundquist and Dr. Don Ayer who served as my committee members have used their expertise in guiding me to always stay on the right track. Scientifically, they always offer brilliant ideas and comments to help with the project. Personally, they give me the best guidance to help me thrive in my career. I also thank Dr. Adam Frost for his scientific insight in

my project. Furthermore, it would not have been possible to complete my dissertation without all of the successful collaborations with fantastic scientists in our field. Dr. Noah Dephore in Dr. Steven Gygi's laboratory and Dr. George Umanah in Dr. Ted Dawson's laboratory have put tremendous effort into making my projects better. I thank them for their time and effort.

I also want to show my appreciation to all my past and current lab members: Jin-Mi Heo, Caleb Cardon, Thomas Orsake, Addie Walkup, Eric Taylor, Aline Tonhato, Eric Fredrickson, Sarah Fogarty, Amy Hawkins, Chintan Kikani, Jason Nielson, Kristofor Olson, John Schell, Wojciech Swiatek, Cameron Waller, Peng Wei, Sarah Nowinski, Jonathan Van Vranken, Xiaoying Wu. A collaborative and cheerful lab environment is established by all of them. I also thank many colleagues across the campus for their scientific communication and technical support, especially, Oleh Khalimonchuk, Un Na, Sajjan Koirala, Qian Guo, Tammy Nguyen, Huyen Bui, Warren Voth and others.

Without family, I would not have been able to accomplish this most important task in my career. I am extremely fortunate to be the daughter-of-my-father, Shih-Pao Chen, and my mother, A-Mei Kao. Neither of them received higher education but they have always encouraged and supported me to pursue my goals. Their never-give up attitude towards life has shaped me into what I am today. To me, they are the best parents and best mentors. I also thank my four sisters and the little brother who gave me a perfect childhood that established my outgoing personality and ability to work with different people. Most importantly, I want to thank my dearest husband for his love, support and understanding. It was both of our dreams to obtain doctorate degrees and we have now

both accomplished this goal. During this process, we understood and embraced each other.

Finally, as a foreign student who does not have many family members here, friends have served as family to me. I want to express my appreciation to many friends who have supported me outside my scientific life; particularly, Lisha Niu, Ya-Chi Yang, Kuan-Lin Kuo and others. I thank them for their company throughout my graduate life.

CHAPTER 1

INTRODUCTION

Mitochondria and human diseases

Mitochondria have two membranes, the outer mitochondrial membrane (OMM) and the inner mitochondrial membrane (IMM). The dual membranes divide this organelle into two distinct compartments, the matrix and the inter-membrane space (IMS) (Ernster and Schatz, 1981; Frey and Mannella, 2000). The OMM hosts aqueous channels that are made by porin, a highly abundant transporter and by the protein import machinery. The porin channels allow molecules that are smaller than 5 kilodaltons to diffuse freely across the OMM. Thus, the microenvironment of the IMS is thought to be quite similar to the cytosol. In contrast, the IMM is highly specialized, containing a unique lipid molecule, cardiolipin, that prevents ions from moving across its interface. Ions and metabolites must therefore be selectively transported across this membrane, in and out of matrix, by specific transporters. Among many reactions that occur in the matrix, is the well-known citric acid cycle (also know as tricarboxylic acid cycle, TCA cycle or Krebs cycle). The TCA cycle accounts for oxidation of a large proportion of the carbon compounds in the cell. The electrons produced from these oxidative reactions are passed to the electron transport chain (ETC) in the IMM and are eventually used to generate adenosine triphosphate (ATP), the energy currency of life. Hence, mitochondria are commonly referred to as "the power house" of the cell. In addition to catabolism and ATP production, mitochondria are also known to participate in diverse cellular processes including synthesis of metabolites, redox balance, cell signaling, inflammatory responses and cell death.

Probably due to the multifaceted function of the mitochondria, mitochondrial dysfunction has been linked to the pathogenesis of many human diseases, including

common metabolic diseases such as diabetes and obesity (Abdul-Ghani and DeFronzo, 2008). Because most cellular ATP is produced in mitochondria, high energy-demanding tissues or organs such as the heart and muscle are particularly susceptible to mitochondrial damage. Therefore, many forms of muscular or cardiovascular disease are associated with the impairment of this organelle; specifically myopathy, ischaemic heart disease, cardiomyopathy and atherosclerotic vascular disease (Dominic et al., 2014). The redox capacity of mitochondria also determines the cellular level of reactive oxygen species (ROS), which directly impacts the lifespan and aging process of organisms (Dai et al., 2014). It is becoming obvious that mitochondrial dysfunction is an important contributor to many forms of neurodegenerative disease, such as Parkinson's disease, Huntington's disease, Alzheimer's disease, Amyotrophic lateral sclerosis, Friedreich's ataxia and Charcot-Marie-Tooth disease (Chaturvedi and Flint Beal, 2013; Witte et al., 2014). Although there have been an increasing number of human diseases that are directly or indirectly linked to impaired mitochondria, their underlying molecular mechanisms await discovery. Future work is needed to uncover the molecular mechanisms that underly these human diseases, which will enable the development of novel therapeutics.

Rationale for studying uncharacterized mitochondrial proteins

The mitochondria proteome is contributed by two separate genomes, the mitochondrial and nuclear genoms. Mitochondrial DNA (mtDNA) exists in multiple and circular copies in the mitochondrial matrix. Human mtDNA encodes ribosomal RNAs, transfer RNAs and only 13 proteins. The nuclear genome encodes the majority of

mitochondrial proteins, which must be transported and imported into mitochondria via designated import machinery. While much is understood about the mitochondrion and its functions, much is still unknown and awaits discovery. Recent advances in organelle separation, mass spectrometry and bioinformatic analysis have enabled more precise definition of the mitochondrial proteome of different organisms (Elstner et al., 2009; Meisinger et al., 2008; Pagliarini et al., 2008; Prokisch et al., 2004; Reinders et al., 2006; Schmidt et al., 2010; Sickmann et al., 2003; Wiederhold et al., 2010). The most comprehensive proteomic analyses have identified approximately 850 mitochondrial proteins in *Saccharomyces cerevisiae* (baker's yeast) and nearly 1100 mitochodnrial proteins in mouse. Remarkably, more than 20% of mitochondrial proteins remain uncharacterized, including many that are highly conserved across the eukaryotic kingdom. Their evolutionary conservation implies that these proteins play fundamentally important roles in mitochondrial function, and perhaps may be associated with human diseases (Bricker et al., 2012; Chen et al., 2011; Chen et al., 2012; Chen et al., 2014; Hao et al., 2009; Heo et al., 2010).

After carefully examining the yeast and human mitochondrial proteomes, we identified 29 conserved protein families that are uncharacterized in both yeast and humans. We undertook a systematic and multitiered approach to study these proteins. Initially, we use yeast as a model system to categorize these proteins based on their loss-of-function phenotypes and sub-mitochondrial localization. Based upon the initial results, we select proteins of interest for in-depth biochemical and genetic studies using *S. cerevisiae*, which is a powerful model organism for molecular biochemistry and genetics. Finally, we pursue the function of the homolog in higher eukaryotes such as cultured

mammalian cells or mouse models. We have employed this scheme successfully to characterize proteins that perform conserved functions in different aspects of mitochondrial biology (Bricker et al., 2012; Chen et al., 2011; Chen et al., 2012; Chen et al., 2014; Hao et al., 2009; Heo et al., 2010). In this dissertation, I will describe how we have discovered the functions of two conserved mitochondrial proteins, Yml030 and Ygr028, in both yeast and mammalian cells.

YML030W

Yml030 (Aim31), which we renamed respiratory supercomplex factor 1 or Rcf1 is encoded by *YML030W* on yeast chromosome XIII. Rcf1 is a 159-amino acid polypeptide that has two predicted transmembrane domains (TMD), spanning amino acids 32-54 and 64-85. HIG1 domain family members 2A and 1A (HIG2A and HIG1A) share sequence homology with Rcf1 and also have unknown mitochondrial functions. Our initial characterization showed that deletion of *YML030W* impairs growth of yeast cultivated on nonfermentable carbon sources.

YGR028W

Ygr028 (Yta4 or mitochondrial sorting of proteins, Msp1) is encoded by *YGR028W* on yeast chromosome VII. It is a 362-amino acid polypeptide that contains a predicted TMD at the N-terminus and a conserved AAA+ domain (ATPase associated with various cellular activities) at the C-terminus. Msp1 was initially characterized as a protein that might participate in protein sorting into mitochondria based on a questionable assay (Nakai et al., 1993). The mammalian homologue of Msp1, ATAD1 (AAA domain

containing 1) was previously reported to play a role in recycling the AMPAR receptor from the plasma membrane (Zhang et al., 2011). No other mitochondrial functions have been reported prior to my study.

Mitochondrial electron transport chain (ETC)

The majority of cellular ATP is produced in the mitochondria through oxidative phosphorylation (Saraste, 1999). Mitochondria use amino acids, carbohydrates and fatty acids as fuels that are then converted into acetyl CoA. Through oxidation of the acetyl group in acetyl CoA via the TCA cycle in the matrix, the electrons are transferred to and carried by NADH and $FADH_2$. These high-energy electrons are then transferred to the ETC in the mitochondrial inner membrane. As the electrons move between the ETC complexes, energy is captured as an electrochemical proton gradient across the IMM, which then drives ATP synthesis by ATP synthase, as illustrated in Figure 1.1.

The ETC is composed of four membrane bound protein complexes (Complex I-IV). Complex I (also known as the NADH dehydrogenase complex or NADH-Q oxidoreductase) is the largest complex in the ETC (~1 megadaltons). It is present in the majority of eukaryotic organisms, but is absent in *S. cerevisiae*. It contains more than forty protein subunits, a flavin and eight to nine iron-sulfur (Fe-S) clusters. Two electrons are released from NADH and passed through the flavin and Fe-S clusters to reduce ubiquinone (Q). In parallel, Complex I translocates four protons from the matrix to the IMS to establish a proton gradient across the IMM (Brandt, 2006).

Complex II (also known as succinate dehydrogenase or succinate-coenzyme Q reductase) is the only complex that directly couples the TCA cycle with the ETC. It

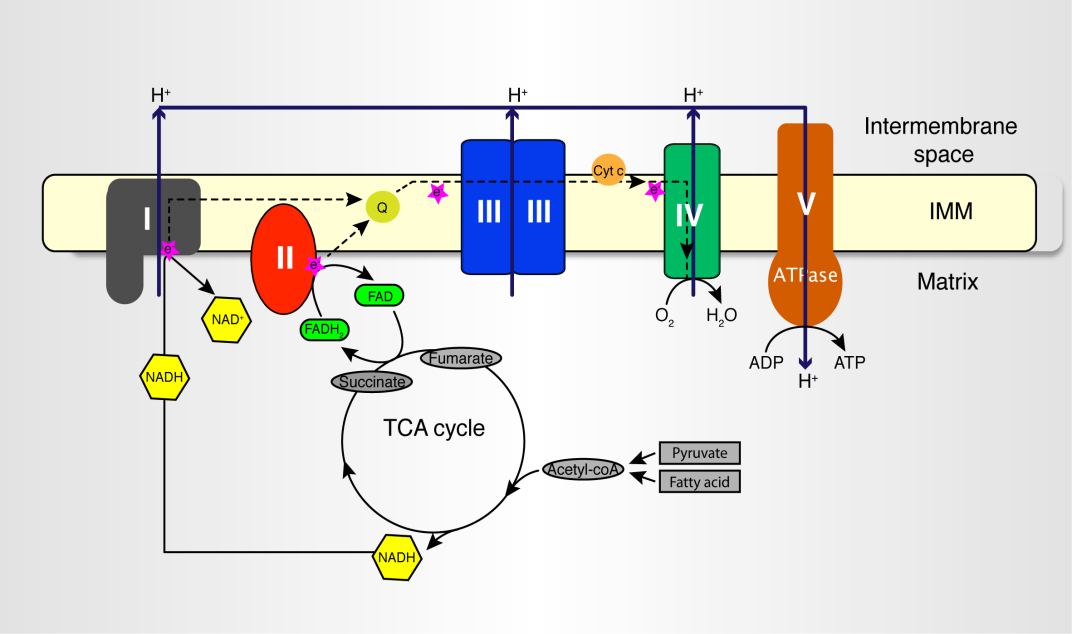

Figure 1-1. The electron transport chain

Electrons derived from NADH and $FADH_2$ are transferred through Complex I and Complex II, respectively, to reduce quinone (Q). Electrons transported *via* Complex III, cytochrome *c* (Cyt *c*) and Complex VI are accepted by O_2 molecules to form water. The proton gradient established in the intermembrane space is then utilized by Complex V to convert ADP into ATP.

contains four proteins subunits (SDHA, SDHB, SDHC, SDHD), a covalently bound flavin adenine dinucleotide (FAD) cofactor, and three iron-sulfur (Fe-S) clusters. In the TCA cycle, it catalyzes the oxidation of succinate to fumarate and the electrons released are transferred through FAD and iron-sulfur clusters to reduce Q. Mutations affecting all the subunits of Complex II are associated with an array of human diseases including cancer and neurologic disease (Hoekstra and Bayley, 2013).

Complex III (also known as cytochrome *b*-c_1 complex or coenzyme Q: cytochrome *c* oxidoreductase) is composed of eleven protein subunits and it exists as a stable dimer in the IMM. Three subunits that have prosthetic groups and participate in electron transfer are CYTB, CYTC and Rieske iron-sulfur protein (RIP1). There are two core proteins, CORE1 (or Qcr1 in yeast) and CORE2 (or Qcr2 in yeast) and six accessory proteins that maintain the stability and fine-tune the activity of this complex. The complex catalyzes the oxidation of Q and transfers electrons though hemes and the iron-sulfur cluster, eventually reducing cytochrome *c,* a small heme protein that is peripherally attached to the IMM. Concomitantly, Complex III translocates four protons across the IMM to the IMS (Berry et al., 2000).

Complex IV (also known as the cytochrome *c* oxidase complex) is the terminal protein complex of the ETC. It is composed of fourteen protein subunits, two hemes and two copper centers. COX1 and COX2 are the active subunits and contain all of the metal prosthetic sites. Four electrons are transferred from cytochrome *c* sequentially and passed through heme and copper centers, ultimately reducing one oxygen molecule to two water molecules. Complex IV concomitantly exports four protons across the IMM to the IMS (Tsukihara et al., 1996).

The electrochemical proton gradient across the IMM that is established by Complexes I, II III and IV of the ETC, drives ATP synthesis by ATP synthase (also known as Complex V). It is a multi-subunit protein complex residing in the IMM that acts by rotary catalysis. The enzymatic portion (F1 sector) of the complex protrudes into the matrix side and is anchored to the membrane by a "rotor," which comprises a ring of transmembrane proteins (F0 sector). Protons turn the rotor as they flow down their electrochemical gradient through the hydrophilic channel of ATP synthase, while the F1 sector phosphorylates ADP to generate ATP (Boyer, 1997).

Supra-molecular organization of the ETC

The random collision model, which suggests that ETC complexes are randomly dispersed on the mitochondrial inner membrane, was long the prevailing model. In this model, electrons are transported via random collision of two mobile electron carriers, ubiquinone and cytochrome *c*, that diffuse laterally on the inner membrane (Hackenbrock et al., 1986). However, this idea has been challenged in the past decade by another model by which the ETC complexes associate into massive supercomplexes through which electrons can be transported via direct channeling (Cruciat et al., 2000; Schagger and Pfeiffer, 2000, 2001).

Biochemical and structural evidence now supports the model that ETC complexes are physically associated into a huge energy-converting machine, called the respiratory supercomplex or respirasome. The concept of this superstructure was proposed more than fifty years ago, but only in recent decades, multiple laboratories started to revisit this old idea by utilizing Blue-Native gel electrophoresis (Blue-Native PAGE). The

association of the ETC subunits into supercomplexes has been observed using Blue-Native PAGE to analyze multiple in species, including mitochondria from yeast, mouse or human cultured cells, rodent tissue, bovine heart and plant mitochondria. These studies typically employed the mild nonionic detergent, digitonin to avoid disassociating the complexes (Dudkina et al., 2006; Juszczuk and Rychter, 2009; Krause et al., 2004a; Krause et al., 2004b; Reifschneider et al., 2006; Schagger, 2002; Schagger et al., 2004; Schagger and Pfeiffer, 2000). There has been a concern, however, that respiratory supercomplexes revealed on Blue-Native PAGE might reflect artifacts caused by the use of digitonin. However, the same higher-order complexes have been using other detergents such as TritonX-100, NP-40 and Tween-20 (Acin-Perez et al., 2008). Cytochrome *c* and ubiquinone are also present in these respiratory supercomplexes, which further supports the idea that they can exist as functional electron transporting units (Acin-Perez et al., 2008). It appears that respiratory supercomplexes are ancient, as respirasome-like structures have also been reported in bacteria (Stroh et al., 2004).

The structure of the yeast and mammalian mitochondria respiratory superomplex has been visualized by electron microscopy (Althoff et al., 2011; Dudkina et al., 2005; Dudkina et al., 2011; Heinemeyer et al., 2007; Mileykovskaya et al., 2012; Schafer et al., 2007). Kinetic data from flux control analyses suggest that either Complex I-III or Complex I-III-IV function together as a single enzyme to control nicotinamide adenine dinucleotide (NADH) oxidation in bovine heart and potato tuber mitochondria (Fato et al., 1993; Genova et al., 2008). Furthermore, *in vitro* isolated respiratory supercomplexes are fully active in transferring electrons from NADH to molecular oxygen, suggesting that respiratory supercomplexes exist as functional entities (Acin-Perez et al., 2008).

S. cerevisiae does not possess Complex I, and the yeast respiratory supercomplex is therefore composed of a dimeric Complex III and one or two copies of Complex IV (III_2VI_2 or III_2IV) (Heinemeyer et al., 2007). Fractions of Complex III exist as free dimers and Complex IV as monomers. The partitioning of these two species between free and respiratory supercomplexes changes under different growth conditions. Complex II usually exists in the free form in yeast, and it is controversial whether it is ever a component of the respiratory supercomplex in mammals. Complex V can homo-oligomerize to form dimers, but can also present as monomers in both yeast and mammalian cells (Arnold et al., 1998; Schagger and Pfeiffer, 2000). In mammals, the composition of the respiratory supercomplex is more complicated due to the presence of Complex I. Most Complex I and III subunits are associated with other complexes to form distinct forms of supercomplexes. Once again, different mammalian supercomplex assembly appears to be quite dynamic, and respond to the mitochondrial microenvironment (*e.g.*, lipid composition and mitochondrial membrane potential) (Genova and Lenaz, 2014; Porras and Bai, 2015). It is unclear, however, how cells adjust the compositions of different forms of respiratory supercomplexes. Prior to my work, the only molecules that had been shown to be important for the assembly or stability of respiratory supercomplexes were the lipid cardiolipin and the ADP/ATP translocase Aac2. Loss of either of these molecules was found to destabilize supercomplexes in yeast (Dienhart and Stuart, 2008; Zhang et al., 2002).

Functional arguments can help to explain why cells form respiratory supercomplexes. First, they provide additional stability to each of the individual complexes. Second, the close association of ETC complexes shortens the distance that electrons must travel

between complexes. Reactive intermediates are therefore more effectively sequestered and the generation of reactive oxygen species is minimized. In both mice and humans, mutation in one complex impairs of the stability and activity of other complexes, indicating the interdependency of the ETC complexes, most likely by disrupting direct physical associations (Acin-Perez et al., 2004; Diaz et al., 2006; Gil Borlado et al., 2010; Vempati et al., 2009). Moreover, there is also evidence suggesting that dissociation of the respiratory supercomplex elevates mitochondrial oxidative stress (Ghelli et al., 2013; Lenaz et al., 2010; Maranzana et al., 2013). This finding places the respiratory supercomplex at the heart of the aging process and the pathogenesis of chronic diseases.

Mitochondrial protein quality control

Mitochondria play critical roles in the determination of cell survival and cell death, and damage to this organelle is associated with many human diseases. This critical importance requires cells to employ a multitiered and interconnected quality control (QC) system to maintain mitochondrial integrity (Rugarli and Langer, 2012).

The first line of defense consists of intramitochondrial chaperones and proteases that promote the folding of newly imported proteins and enable the degradation of misfolded or damaged proteins. Heat-shock protein 60 and 70 (Hsp60 and Hsp70) are matrix-localized chaperons that help the import, fold and assembly of mitochondrial proteins (Cheng et al., 1989; Kang et al., 1990; Pellegrino et al., 2013). Two inner membrane-associated AAA+ proteases, *m*-AAA and *i*-AAA, catalyze the degradation of misfolded and damaged proteins in the matrix and intermembrane space compartments, respectively (Gerdes et al., 2012; Janska et al., 2013). Lon and ClpXP are two additional soluble

AAA+ proteases that patrol the matrix to maintain protein quality (Truscott et al., 2011; Venkatesh et al., 2012). All of these proteins have AAA+ domains which, in most cases, oligomerize to form central channels that unfold protein substrates using the energy derived from ATP hydrolysis (Gerdes et al., 2012; Hanson and Whiteheart, 2005). The unfolded polypeptides are subsequently degraded by an associated proteolytic domain (Sauer and Baker, 2011). Cells employ an analogous QC system on the mitochondrial outer membrane, which enables the extraction and proteasomal degradation of proteins exposed to the cytosol (Taylor and Rutter, 2011). This system also appears to utilize a AAA+ ATPase, Cdc48 in yeast or p97 in mammals, to extract proteins prior to proteasome engagement (Heo et al., 2010; Tanaka et al., 2010; Xu et al., 2011). Furthermore, the capacity of mitochondrial QC systems can be modulated by a specialized transcriptional program, known as the mitochondrial unfolded protein response (mtUPR). Upon mitochondrial stress, the mtUPR can induce transcription of mitochondrial proteases and chaperones to fulfill the cellular demands for these activities (Haynes and Ron, 2010; Nargund et al., 2012; Zhao et al., 2002).

When mitochondria depolarize, cells initiate the autophagic degradation of mitochondria (mitophagy) as a second line of defense (Ashrafi and Schwarz, 2013; Youle and Narendra, 2011). Mitophagy is a selective process that removes and degrades damaged mitochondria. PTEN-induced kinase (PINK1) and Parkin are key regulators of mitophagy in mammalian cells. PINK1 is a mitochondrial serine/threonine kinase and it acts upstream of Parkin, which is a cytoplasmic E3 ubiquitin ligase. Under normal conditions, PINK1 is imported into mitochondria in a membrane potential ($\Delta\Psi$)-dependent manner and instantly degraded by the PARL protease (Jin et al., 2010).

However, when mitochondrial ΔΨ is dissipated, PINK1 import is stalled and PINK1 is retained on the outer membrane. PINK1 then recruits Parkin and phosphorylates it to activate Parkin ubiquitin ligase activity (Lazarou et al., 2012; Lazarou et al., 2013). Ubiquitination of mitochondrial OMM proteins initiates the autophagic removal of defective mitochondria (Sarraf et al., 2013). Parkin and PINK were recently shown to participate in a noncanonical form of mitophagy *via* a vesicular trafficking pathway that degrades mitochondria subjected to oxidative stress (McLelland et al., 2014). Mitochondria are very dynamic organelles, which undergo constant fission and fusion. It is clear that both fusion and fission are critical for sequestering damaged mitochondria prior to engagement with lysosomes (Twig et al., 2008). In animals, neurons seem to be particularly sensitive to the presence of damaged mitochondria and to defects in the mitochondrial QC system. Mutations in PINK1 and Parkin cause familial Parkinson's disease (Kitada et al., 1998; Valente et al., 2004). Beyond that, an increasing number of neurodegenerative diseases, including spastic paraplegia, spinocerebellar ataxia, Alzheimer's disease and peripheral neurophathies, are linked to defective mitochondrial quality control systems (Rugarli and Langer, 2012).

References

Abdul-Ghani, M.A., and DeFronzo, R.A. (2008). Mitochondrial dysfunction, insulin resistance, and type 2 diabetes mellitus. Current Diabetes Reports *8*, 173-178.

Acin-Perez, R., Bayona-Bafaluy, M.P., Fernandez-Silva, P., Moreno-Loshuertos, R., Perez-Martos, A., Bruno, C., Moraes, C.T., and Enriquez, J.A. (2004). Respiratory Complex III is required to maintain Complex I in mammalian mitochondria. Mol Cell *13*, 805-815.

Acin-Perez, R., Fernandez-Silva, P., Peleato, M.L., Perez-Martos, A., and Enriquez, J.A. (2008). Respiratory active mitochondrial supercomplexes. Mol Cell *32*, 529-539.

Althoff, T., Mills, D.J., Popot, J.L., and Kuhlbrandt, W. (2011). Arrangement of electron transport chain components in bovine mitochondrial I(1)III(2)IV(1). Embo J. *30*, 4652-4664

Arnold, I., Pfeiffer, K., Neupert, W., Stuart, R.A., and Schagger, H. (1998). Yeast mitochondrial F1F0-ATP synthase exists as a dimer: identification of three dimer-specific subunits. Embo J *17*, 7170-7178.

Ashrafi, G., and Schwarz, T.L. (2013). The pathways of mitophagy for quality control and clearance of mitochondria. Cell Death and Differentiation *20*, 31-42.

Berry, E.A., Guergova-Kuras, M., Huang, L.S., and Crofts, A.R. (2000). Structure and function of cytochrome bc complexes. Annual Review of Biochemistry *69*, 1005-1075.

Boyer, P.D. (1997). The ATP synthase--a splendid molecular machine. Annual Review of Biochemistry *66*, 717-749.

Brandt, U. (2006). Energy converting NADH:quinone oxidoreductase (Complex I). Annual Review of Biochemistry *75*, 69-92.

Bricker, D.K., Taylor, E.B., Schell, J.C., Orsak, T., Boutron, A., Chen, Y.C., Cox, J.E., Cardon, C.M., Van Vranken, J.G., Dephoure, N.*, et al.* (2012). A mitochondrial pyruvate carrier required for pyruvate uptake in yeast, Drosophila, and humans. Science *337*, 96-100.

Chaturvedi, R.K., and Flint Beal, M. (2013). Mitochondrial diseases of the brain. Free Radical Biology & Medicine *63*, 1-29.

Chen, Y.C., Taylor, E.B., Dephoure, N., Heo, J.M., Tonhato, A., Papandreou, I., Nath, N., Denko, N.C., Gygi, S.P., and Rutter, J. (2012). Identification of a protein mediating respiratory supercomplex stability. Cell Metab *15*, 348-360.

Chen, Y.C., Umanah, G.K., Dephoure, N., Andrabi, S.A., Gygi, S.P., Dawson, T.M., Dawson, V.L., and Rutter, J. (2014). Msp1/ATAD1 maintains mitochondrial function by facilitating the degradation of mislocalized tail-anchored proteins. Embo J *33*, 1548-1564.

Cheng, M.Y., Hartl, F.U., Martin, J., Pollock, R.A., Kalousek, F., Neupert, W., Hallberg, E.M., Hallberg, R.L., and Horwich, A.L. (1989). Mitochondrial heat-shock protein hsp60 is essential for assembly of proteins imported into yeast mitochondria. Nature *337*, 620-625.

Cruciat, C.M., Brunner, S., Baumann, F., Neupert, W., and Stuart, R.A. (2000). The cytochrome bc1 and cytochrome c oxidase complexes associate to form a single supracomplex in yeast mitochondria. J Biol Chem *275*, 18093-18098.

Dai, D.F., Chiao, Y.A., Marcinek, D.J., Szeto, H.H., and Rabinovitch, P.S. (2014). Mitochondrial oxidative stress in aging and healthspan. Longevity & Healthspan *3*, 6.

Diaz, F., Fukui, H., Garcia, S., and Moraes, C.T. (2006). Cytochrome c oxidase is required for the assembly/stability of respiratory Complex I in mouse fibroblasts. Mol Cell Biol *26*, 4872-4881.

Dienhart, M.K., and Stuart, R.A. (2008). The yeast Aac2 protein exists in physical association with the cytochrome bc1-COX supercomplex and the TIM23 machinery. Mol Biol Cell *19*, 3934-3943.

Dominic, E.A., Ramezani, A., Anker, S.D., Verma, M., Mehta, N., and Rao, M. (2014). Mitochondrial cytopathies and cardiovascular disease. Heart (British Cardiac Society) *100*, 611-618.

Dudkina, N.V., Eubel, H., Keegstra, W., Boekema, E.J., and Braun, H.P. (2005). Structure of a mitochondrial supercomplex formed by respiratory-chain Complexes I and III. Proc Natl Acad Sci USA *102*, 3225-3229.

Dudkina, N.V., Heinemeyer, J., Sunderhaus, S., Boekema, E.J., and Braun, H.P. (2006). Respiratory chain supercomplexes in the plant mitochondrial membrane. Trends in Plant Science *11*, 232-240.

Dudkina, N.V., Kudryashev, M., Stahlberg, H., and Boekema, E.J. (2011). Interaction of Complexes I, III, and IV within the bovine respirasome by single particle cryoelectron tomography. Proc Natl Acad Sci USA *108*, 15196-15200.

Elstner, M., Andreoli, C., Klopstock, T., Meitinger, T., and Prokisch, H. (2009). The mitochondrial proteome database: MitoP2. Methods Enzymol *457*, 3-20.

Ernster, L., and Schatz, G. (1981). Mitochondria: a historical review. The Journal of Cell Biology *91*, 227s-255s.

Fato, R., Cavazzoni, M., Castelluccio, C., Parenti Castelli, G., Palmer, G., Degli Esposti, M., and Lenaz, G. (1993). Steady-state kinetics of ubiquinol-cytochrome c reductase in bovine heart submitochondrial particles: diffusional effects. Biochem J *290 (Pt 1)*, 225-236.

Frey, T.G., and Mannella, C.A. (2000). The internal structure of mitochondria. Trends in Biochemical Sciences *25*, 319-324.

Genova, M.L., Baracca, A., Biondi, A., Casalena, G., Faccioli, M., Falasca, A.I., Formiggini, G., Sgarbi, G., Solaini, G., and Lenaz, G. (2008). Is supercomplex organization of the respiratory chain required for optimal electron transfer activity? Biochim Biophys Acta *1777*, 740-746.

Genova, M.L., and Lenaz, G. (2014). Functional role of mitochondrial respiratory supercomplexes. Biochim Biophys Acta *1837*, 427-443.

Gerdes, F., Tatsuta, T., and Langer, T. (2012). Mitochondrial AAA proteases--towards a molecular understanding of membrane-bound proteolytic machines. Biochim Biophys Acta *1823*, 49-55.

Ghelli, A., Tropeano, C.V., Calvaruso, M.A., Marchesini, A., Iommarini, L., Porcelli, A.M., Zanna, C., De Nardo, V., Martinuzzi, A., Wibrand, F.*, et al.* (2013). The cytochrome b p.278Y>C mutation causative of a multisystem disorder enhances superoxide production and alters supramolecular interactions of respiratory chain complexes. Human Molecular Genetics *22*, 2141-2151.

Gil Borlado, M.C., Moreno Lastres, D., Gonzalez Hoyuela, M., Moran, M., Blazquez, A., Pello, R., Marin Buera, L., Gabaldon, T., Garcia Penas, J.J., Martin, M.A.*, et al.* (2010). Impact of the mitochondrial genetic background in Complex III deficiency. PLoS One *5*.

Hackenbrock, C.R., Chazotte, B., and Gupte, S.S. (1986). The random collision model and a critical assessment of diffusion and collision in mitochondrial electron transport. Journal of Bioenergetics and Biomembranes *18*, 331-368.

Hanson, P.I., and Whiteheart, S.W. (2005). AAA+ proteins: have engine, will work. Nat Rev Mol Cell Biol *6*, 519-529.

Hao, H.X., Khalimonchuk, O., Schraders, M., Dephoure, N., Bayley, J.P., Kunst, H., Devilee, P., Cremers, C.W., Schiffman, J.D., Bentz, B.G.*, et al.* (2009). SDH5, a gene required for flavination of succinate dehydrogenase, is mutated in paraganglioma. Science *325*, 1139-1142.

Haynes, C.M., and Ron, D. (2010). The mitochondrial UPR - protecting organelle protein homeostasis. J Cell Sci *123*, 3849-3855.

Heinemeyer, J., Braun, H.P., Boekema, E.J., and Kouril, R. (2007). A structural model of the cytochrome C reductase/oxidase supercomplex from yeast mitochondria. J Biol Chem *282*, 12240-12248.

Heo, J.M., Livnat-Levanon, N., Taylor, E.B., Jones, K.T., Dephoure, N., Ring, J., Xie, J., Brodsky, J.L., Madeo, F., Gygi, S.P.*, et al.* (2010). A stress-responsive system for mitochondrial protein degradation. Mol Cell *40*, 465-480.

Hoekstra, A.S., and Bayley, J.P. (2013). The role of Complex II in disease. Biochim Biophys Acta *1827*, 543-551.

Janska, H., Kwasniak, M., and Szczepanowska, J. (2013). Protein quality control in organelles - AAA/FtsH story. Biochim Biophys Acta *1833*, 381-387.

Jin, S.M., Lazarou, M., Wang, C., Kane, L.A., Narendra, D.P., and Youle, R.J. (2010). Mitochondrial membrane potential regulates PINK1 import and proteolytic destabilization by PARL. The Journal of Cell Biology *191*, 933-942.

Juszczuk, I.M., and Rychter, A.M. (2009). BN-PAGE analysis of the respiratory chain complexes in mitochondria of cucumber MSC16 mutant. Plant Physiology and Biochemistry: PPB / Societe francaise de physiologie vegetale *47*, 397-406.

Kang, P.J., Ostermann, J., Shilling, J., Neupert, W., Craig, E.A., and Pfanner, N. (1990). Requirement for hsp70 in the mitochondrial matrix for translocation and folding of precursor proteins. Nature *348*, 137-143.

Kitada, T., Asakawa, S., Hattori, N., Matsumine, H., Yamamura, Y., Minoshima, S., Yokochi, M., Mizuno, Y., and Shimizu, N. (1998). Mutations in the parkin gene cause autosomal recessive juvenile parkinsonism. Nature *392*, 605-608.

Krause, F., Reifschneider, N.H., Vocke, D., Seelert, H., Rexroth, S., and Dencher, N.A. (2004a). "Respirasome"-like supercomplexes in green leaf mitochondria of spinach. J Biol Chem *279*, 48369-48375.

Krause, F., Scheckhuber, C.Q., Werner, A., Rexroth, S., Reifschneider, N.H., Dencher, N.A., and Osiewacz, H.D. (2004b). Supramolecular organization of cytochrome c oxidase- and alternative oxidase-dependent respiratory chains in the filamentous fungus Podospora anserina. J Biol Chem *279*, 26453-26461.

Lazarou, M., Jin, S.M., Kane, L.A., and Youle, R.J. (2012). Role of PINK1 binding to the TOM complex and alternate intracellular membranes in recruitment and activation of the E3 ligase Parkin. Developmental Cell *22*, 320-333.

Lazarou, M., Narendra, D.P., Jin, S.M., Tekle, E., Banerjee, S., and Youle, R.J. (2013). PINK1 drives Parkin self-association and HECT-like E3 activity upstream of mitochondrial binding. The Journal of Cell Biology *200*, 163-172.

Lenaz, G., Baracca, A., Barbero, G., Bergamini, C., Dalmonte, M.E., Del Sole, M., Faccioli, M., Falasca, A., Fato, R., Genova, M.L*., et al.* (2010). Mitochondrial respiratory chain Super-complex I-III in physiology and pathology. Biochim Biophys Acta *1797*, 633-640.

Maranzana, E., Barbero, G., Falasca, A.I., Lenaz, G., and Genova, M.L. (2013). Mitochondrial respiratory supercomplex association limits production of reactive oxygen species from Complex I. Antioxidants & Redox Signaling *19*, 1469-1480.

McLelland, G.L., Soubannier, V., Chen, C.X., McBride, H.M., and Fon, E.A. (2014). Parkin and PINK1 function in a vesicular trafficking pathway regulating mitochondrial quality control. Embo J *33*, 282-295.

Meisinger, C., Sickmann, A., and Pfanner, N. (2008). The mitochondrial proteome: from inventory to function. Cell *134*, 22-24.

Mileykovskaya, E., Penczek, P.A., Fang, J., Mallampalli, V.K., Sparagna, G.C., and Dowhan, W. (2012). Arrangement of the respiratory chain complexes in Saccharomyces

cerevisiae Supercomplex III2IV2 revealed by single particle cryo-electron microscopy. J Biol Chem *287*, 23095-23103.

Nakai, M., Endo, T., Hase, T., and Matsubara, H. (1993). Intramitochondrial protein sorting. Isolation and characterization of the yeast MSP1 gene which belongs to a novel family of putative ATPases. J Biol Chem *268*, 24262-24269.

Nargund, A.M., Pellegrino, M.W., Fiorese, C.J., Baker, B.M., and Haynes, C.M. (2012). Mitochondrial import efficiency of ATFS-1 regulates mitochondrial UPR activation. Science *337*, 587-590.

Pagliarini, D.J., Calvo, S.E., Chang, B., Sheth, S.A., Vafai, S.B., Ong, S.E., Walford, G.A., Sugiana, C., Boneh, A., Chen, W.K.*, et al.* (2008). A mitochondrial protein compendium elucidates Complex I disease biology. Cell *134*, 112-123.

Pellegrino, M.W., Nargund, A.M., and Haynes, C.M. (2013). Signaling the mitochondrial unfolded protein response. Biochim Biophys Acta *1833*, 410-416.

Porras, C.A., and Bai, Y. (2015). Respiratory supercomplexes: plasticity and implications. Frontiers in Bioscience (Landmark edition) *20*, 621-634.

Prokisch, H., Scharfe, C., Camp, D.G., 2nd, Xiao, W., David, L., Andreoli, C., Monroe, M.E., Moore, R.J., Gritsenko, M.A., Kozany, C.*, et al.* (2004). Integrative analysis of the mitochondrial proteome in yeast. PLoS Biology *2*, e160.

Reifschneider, N.H., Goto, S., Nakamoto, H., Takahashi, R., Sugawa, M., Dencher, N.A., and Krause, F. (2006). Defining the mitochondrial proteomes from five rat organs in a physiologically significant context using 2D blue-native/SDS-PAGE. Journal of Proteome Research *5*, 1117-1132.

Reinders, J., Zahedi, R.P., Pfanner, N., Meisinger, C., and Sickmann, A. (2006). Toward the complete yeast mitochondrial proteome: multidimensional separation techniques for mitochondrial proteomics. Journal of Proteome Research *5*, 1543-1554.

Rugarli, E.I., and Langer, T. (2012). Mitochondrial quality control: a matter of life and death for neurons. Embo J *31*, 1336-1349.

Saraste, M. (1999). Oxidative phosphorylation at the fin de siecle. Science *283*, 1488-1493.

Sarraf, S.A., Raman, M., Guarani-Pereira, V., Sowa, M.E., Huttlin, E.L., Gygi, S.P., and Harper, J.W. (2013). Landscape of the PARKIN-dependent ubiquitylome in response to mitochondrial depolarization. Nature *496*, 372-376.

Sauer, R.T., and Baker, T.A. (2011). AAA+ proteases: ATP-fueled machines of protein destruction. Annual Review of Biochemistry *80*, 587-612.

Schafer, E., Dencher, N.A., Vonck, J., and Parcej, D.N. (2007). Three-dimensional structure of the respiratory chain Supercomplex $I1III_2IV_1$ from bovine heart mitochondria. Biochemistry *46*, 12579-12585.

Schagger, H. (2002). Respiratory chain upercomplexes of mitochondria and bacteria. Biochim Biophys Acta *1555*, 154-159.

Schagger, H., de Coo, R., Bauer, M.F., Hofmann, S., Godinot, C., and Brandt, U. (2004). Significance of respirasomes for the assembly/stability of human respiratory chain Complex I. J Biol Chem *279*, 36349-36353.

Schagger, H., and Pfeiffer, K. (2000). Supercomplexes in the respiratory chains of yeast and mammalian mitochondria. EMBO J *19*, 1777-1783.

Schagger, H., and Pfeiffer, K. (2001). The ratio of oxidative phosphorylation Complexes I-V in bovine heart mitochondria and the composition of respiratory chain supercomplexes. J Biol Chem *276*, 37861-37867.

Schmidt, O., Pfanner, N., and Meisinger, C. (2010). Mitochondrial protein import: from proteomics to functional mechanisms. Nat Rev Mol Cell Biol *11*, 655-667.

Sickmann, A., Reinders, J., Wagner, Y., Joppich, C., Zahedi, R., Meyer, H.E., Schonfisch, B., Perschil, I., Chacinska, A., Guiard, B.*, et al.* (2003). The proteome of Saccharomyces cerevisiae mitochondria. Proc Natl Acad Sci USA *100*, 13207-13212.

Stroh, A., Anderka, O., Pfeiffer, K., Yagi, T., Finel, M., Ludwig, B., and Schagger, H. (2004). Assembly of respiratory Complexes I, III, and IV into NADH oxidase supercomplex stabilizes Complex I in Paracoccus denitrificans. J Biol Chem *279*, 5000-5007.

Tanaka, A., Cleland, M.M., Xu, S., Narendra, D.P., Suen, D.F., Karbowski, M., and Youle, R.J. (2010). Proteasome and p97 mediate mitophagy and degradation of mitofusins induced by Parkin. The Journal of Cell Biology *191*, 1367-1380.

Taylor, E.B., and Rutter, J. (2011). Mitochondrial quality control by the ubiquitin-proteasome system. Biochemical Society Transactions *39*, 1509-1513.

Truscott, K.N., Bezawork-Geleta, A., and Dougan, D.A. (2011). Unfolded protein responses in bacteria and mitochondria: a central role for the ClpXP machine. IUBMB life *63*, 955-963.

Tsukihara, T., Aoyama, H., Yamashita, E., Tomizaki, T., Yamaguchi, H., Shinzawa-Itoh, K., Nakashima, R., Yaono, R., and Yoshikawa, S. (1996). The whole structure of the 13-subunit oxidized cytochrome c oxidase at 2.8 A. Science *272*, 1136-1144.

Twig, G., Elorza, A., Molina, A.J., Mohamed, H., Wikstrom, J.D., Walzer, G., Stiles, L., Haigh, S.E., Katz, S., Las, G.*, et al.* (2008). Fission and selective fusion govern mitochondrial segregation and elimination by autophagy. Embo J *27*, 433-446.

Valente, E.M., Abou-Sleiman, P.M., Caputo, V., Muqit, M.M., Harvey, K., Gispert, S., Ali, Z., Del Turco, D., Bentivoglio, A.R., Healy, D.G.*, et al.* (2004). Hereditary early-onset Parkinson's disease caused by mutations in PINK1. Science *304*, 1158-1160.

Vempati, U.D., Han, X., and Moraes, C.T. (2009). Lack of cytochrome c in mouse fibroblasts disrupts assembly/stability of respiratory Complexes I and IV. J Biol Chem *284*, 4383-4391.

Venkatesh, S., Lee, J., Singh, K., Lee, I., and Suzuki, C.K. (2012). Multitasking in the mitochondrion by the ATP-dependent Lon protease. Biochim Biophys Acta *1823*, 56-66.

Wiederhold, E., Veenhoff, L.M., Poolman, B., and Slotboom, D.J. (2010). Proteomics of Saccharomyces cerevisiae Organelles. Mol Cell Proteomics *9*, 431-445.

Witte, M.E., Mahad, D.J., Lassmann, H., and van Horssen, J. (2014). Mitochondrial dysfunction contributes to neurodegeneration in multiple sclerosis. Trends in Molecular Medicine *20*, 179-187.

Xu, S., Peng, G., Wang, Y., Fang, S., and Karbowski, M. (2011). The AAA-ATPase p97 is essential for outer mitochondrial membrane protein turnover. Mol Biol Cell *22*, 291-300.

Youle, R.J., and Narendra, D.P. (2011). Mechanisms of mitophagy. Nat Rev Mol Cell Biol *12*, 9-14.

Zhang, J., Wang, Y., Chi, Z., Keuss, M.J., Pai, Y.M., Kang, H.C., Shin, J.H., Bugayenko, A., Wang, H., Xiong, Y.*, et al.* (2011). The AAA+ ATPase Thorase regulates AMPA receptor-dependent synaptic plasticity and behavior. Cell *145*, 284-299.

Zhang, M., Mileykovskaya, E., and Dowhan, W. (2002). Gluing the respiratory chain together. Cardiolipin is required for supercomplex formation in the inner mitochondrial membrane. J Biol Chem *277*, 43553-43556.

Zhao, Q., Wang, J., Levichkin, I.V., Stasinopoulos, S., Ryan, M.T., and Hoogenraad, N.J. (2002). A mitochondrial specific stress response in mammalian cells. Embo J *21*, 4411-4419.

Bonekamp, N.A., Sampaio, P., de Abreu, F.V., Luers, G.H., and Schrader, M. (2012). Transient complex interactions of mammalian peroxisomes without exchange of matrix or membrane marker proteins. Traffic (Copenhagen, Denmark) *13*, 960-978.

CHAPTER 2

IDENTIFICATION OF A PROTEIN MEDIATING RESPIRATORY SUPERCOMPLEX STABILITY

Yu-Chan Chen, Eric B. Taylor, Noah Dephoure, Jin-Mi Heo, Aline Tonhato, Ioanna Papandreou, Nandita Nath, Nicolas C. Denko, Steven P. Gygi, Jared Rutter

Reprinted from Elsevier, Vol. 15(3), pp. 348-360. Yu-Chan Chen, Eric B. Taylor, Noah Dephoure, Jin-Mi Heo, Aline Tonhato, Ioanna Papandreou, Nandita Nath, Nicolas C. Denko, Steven P. Gygi, Jared Rutter. Identification of a protein mediating respiratory Supercomplex stability.

Cell Metabolism
Article

Identification of a Protein Mediating Respiratory Supercomplex Stability

Yu-Chan Chen,[1] Eric B. Taylor,[1] Noah Dephoure,[2] Jin-Mi Heo,[1] Aline Tonhato,[1] Ioanna Papandreou,[3] Nandita Nath,[3] Nicolas C. Denko,[3] Steven P. Gygi,[2] and Jared Rutter[1,*]
[1]Department of Biochemistry, University of Utah School of Medicine, Salt Lake City, UT 84112, USA
[2]Department of Cell Biology, Harvard Medical School, Boston, MA 02115, USA
[3]Division of Radiation and Cancer Biology, Department of Radiation Oncology at Stanford University School of Medicine, Stanford, CA 94305, USA
*Correspondence: rutter@biochem.utah.edu
DOI 10.1016/j.cmet.2012.02.006

SUMMARY

The complexes of the electron transport chain associate into large macromolecular assemblies, which are believed to facilitate efficient electron flow. We have identified a conserved mitochondrial protein, named respiratory supercomplex factor 1 (Rcf1—Yml030w), that is required for the normal assembly of respiratory supercomplexes. We demonstrate that Rcf1 stably and independently associates with both Complex III and Complex IV of the electron transport chain. Deletion of the *RCF1* gene caused impaired respiration, probably as a result of destabilization of respiratory supercomplexes. Consistent with the hypothetical function of these respiratory assemblies, loss of *RCF1* caused elevated mitochondrial oxidative stress and damage. Finally, we show that knockdown of *HIG2A*, a mammalian homolog of *RCF1*, causes impaired supercomplex formation. We suggest that Rcf1 is a member of an evolutionarily conserved protein family that acts to promote respiratory supercomplex assembly and activity.

INTRODUCTION

Mitochondria are unique and complex organelles that perform essential functions in many aspects of cell biology. It is not surprising, therefore, that mitochondrial dysfunction is associated with many forms of human disease. This includes relatively common disorders, such as cancer (Kroemer and Pouyssegur, 2008), diabetes (Patti and Corvera, 2010), and neurodegenerative disease (Lessing and Bonini, 2009). Beyond these common disorders, which are all age-related, mitochondrial dysfunction has been associated with the aging process itself. Manipulation of mitochondrial function, including by modulation of mitochondrial oxidative stress and mitochondrial DNA (mtDNA) mutability, has striking effects on longevity (Schriner et al., 2005; Trifunovic et al., 2004).

The intimate connection between oxidative stress, mitochondrial dysfunction, and age-related disorders is thought to derive from the physical proximity of the electron transport chain (ETC) and the mtDNA. The ETC is the major source of reactive oxygen species (ROS) in most cells. This ROS load is then in immediate proximity to the mtDNA, which is highly sensitive to mutagenic insult. Mutated mtDNA is then postulated to be a causal factor in further ETC dysfunction, leading to a vicious cycle of ROS production (Wallace, 2005). The challenge for the ETC is to conduct reactive electrons via soluble carriers, through three distinct multiprotein complexes, to oxygen. When this conduction process is disturbed, the risk of ROS production increases. Because this oxidative stress/ETC/aging axis is of such relevance to human disease, it is of great importance to understand the mechanisms that have evolved to prevent inappropriate ROS production. One biochemical phenomenon that has been postulated to control ETC malfunction and prevent mitochondrial ROS production is the assembly of the individual ETC complexes into massive conduction machines called respiratory supercomplexes (Cruciat et al., 2000; Lenaz and Genova, 2009).

The clear importance of mitochondria has led to extensive efforts to define the mitochondrial proteome in many species. The best current inventory of mammalian mitochondrial-resident proteins consists of 1,098 proteins (Pagliarini et al., 2008). Surprisingly, nearly 300 of these proteins are largely or completely unstudied (Pagliarini et al., 2008). Included among this number are many that are conserved throughout the eukaryotic kingdom. Such conservation implies that they perform a function that is of fundamental importance for cell viability. As a result, we initiated a project to identify the functions of a subset of these highly and evolutionarily conserved but uncharacterized mitochondrial proteins. We previously described the function of *SDH5*/*SDHAF2*, which is required for assembly of ETC Complex II and is mutated in multiple families afflicted with the paraganglioma tumor syndrome (Bayley et al., 2010; Hao et al., 2009). We also described Vms1, which plays an important role in stress-responsive recruitment of the ubiquitin-proteasome machinery to mitochondria for protein degradation (Heo et al., 2010).

Herein, we describe the function of Rcf1, which we show is a stable component of ETC supercomplexes and is required for their normal stability. In *Saccharomyces cerevisiae*, ETC supercomplexes are assemblies in the mitochondrial inner membrane that contain, among other proteins, both cytochrome bc1 complex (Complex III) and cytochrome c oxidase complex (Complex IV) and perhaps Complex II as well (Stuart, 2008). In mammals, supercomplexes often also contain Complex I

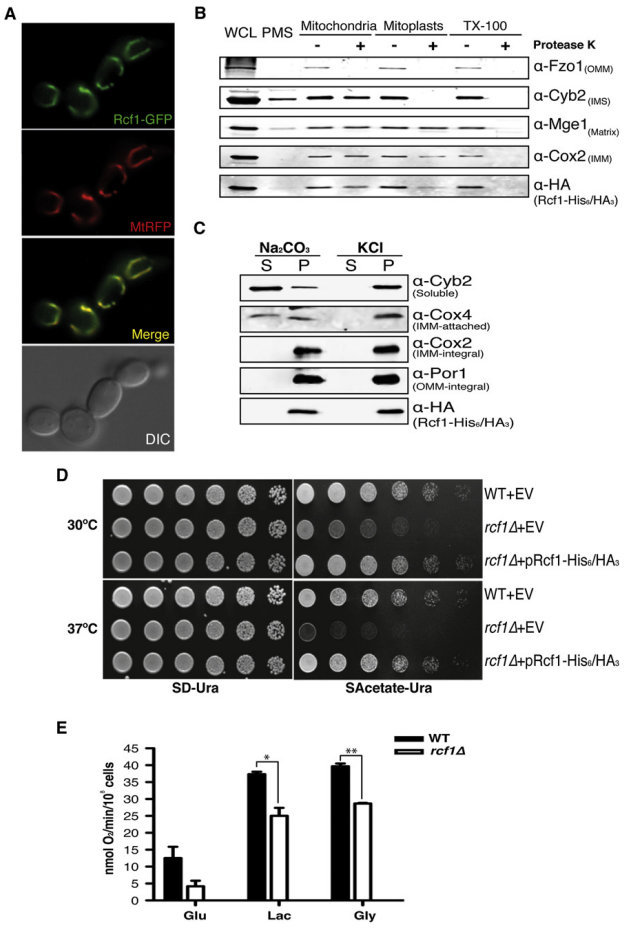

Figure 1. Rcf1 Is a Mitochondrial Inner Membrane Protein Important for Respiration

(A) The *rcf1*Δ mutant expressing Rcf1-GFP and MtRFP grown to log phase in SD medium was imaged by fluorescence microscopy.

(B) Intact mitochondria, hypotonic-swollen mitoplasts, and Triton X-100–solubilized mitochondria of a strain expressing Rcf1-His_6/HA_3 were treated either with (+) or without (–) Proteinase K and analyzed by immunoblot with the whole-cell lysate (WCL) and postmitochondrial supernatant (PMS). Cox2, Mge1, Cyb2, and Fzo1 are inner membrane, matrix, intermembrane space, and outer membrane proteins, respectively.

(C) Soluble (S) and pellet (P) fractions from alkali and high-salt extracted mitochondria expressing Rcf1-His_6/HA_3 were analyzed by immunoblot. Cyb2 is a soluble intermembrane space protein; Cox4 is an inner membrane-associated protein; Cox2 is an integral inner membrane protein; and Por1 is an integral outer membrane protein.

(D) Five-fold serial dilutions of the indicated strains harboring an empty vector (EV) or a plasmid expressing Rcf1-His_6/HA_3 were spotted on plates and incubated at 30°C and 37°C.

(E) WT and *rcf1*Δ mutant strains of the BY4741 background were grown in glucose, lactate, or glycerol to log phase and the rate of oxygen consumption was measured. Data shown is representative of three independent experiments and mean + SD is shown. *$p < 0.05$; **$p < 0.01$.

See also Figure S1.

(Acín-Pérez et al., 2008; Wittig and Schägger, 2009). These huge macromolecular assemblies are believed to enable more efficient electron flow between complexes and to promote complex stability (Suthammarak et al., 2010). This efficiency is believed to reduce electron loss from ETC and ROS generation (Genova et al., 2008). Not surprisingly, we show that the *rcf1*Δ mutant, which exhibits decreased supercomplex assembly, has increased mitochondrial oxidative damage. We also show that knockdown of *HIG2A*, one of the mammalian orthologs of *RCF1*, impairs supercomplex assembly in mouse cells. We, therefore, speculate that the *RCF1* gene family plays an evolutionarily conserved role in maintaining mitochondrial function through the optimal assembly of electron transport chain complexes. Thereby, it might be a component of the cellular system to delay ROS-induced and age-associated degeneration.

RESULTS

Rcf1 Is an Integral Mitochondrial Inner Membrane Protein Required for Normal Respiration

Using the yeast *S. cerevisiae* as the primary model system, we first verified mitochondrial localization of the Rcf1 (Yml030w/Aim31) protein using two complementary methods. First, we generated a strain expressing an Rcf1-GFP fusion protein from the native promoter, which is fully functional as assessed by suppression of the *rcf1*Δ phenotype (data not shown). This strain was cotransformed with a plasmid expressing a mitochondria-targeted red fluorescent protein (MtRFP). As seen in Figure 1A, we observed complete overlap between the mitochondrial RFP signal and the Rcf1-GFP signal. Under no conditions did we find extramitochondrial GFP fluorescence.

In parallel, we also biochemically examined the localization of an Rcf1 fusion protein with a dual His_6/HA_3-tag at its C terminus. This fusion protein, which is expressed from the native promoter, was also demonstrated to be fully functional (see Figure 1D).

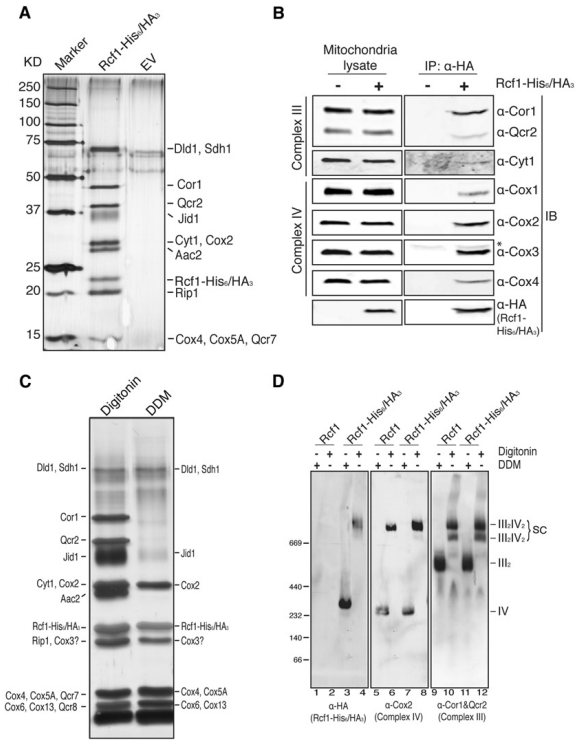

Figure 2. Rcf1 Physically Interacts with Respiratory Complex III and IV

(A) Mitochondria from an EV-containing WT strain or an *rcf1*Δ mutant strain expressing Rcf1-His_6/HA_3 were subjected to two-step purification. The final eluate was analyzed by silver staining. Discrete bands were excised and the protein identity was determined by mass spectrometry as indicated in the text.

(B) Digitonin-solubilized mitochondria extracted from yeast strains either expressing Rcf1-His_6/HA_3 (+) or not (−) were immunoprecipitated using anti-HA antibody. One percent of the mitochondrial lysate and the final eluate were immunoblotted using anti-Cor1&Qcr2, Cyt1, Cox1, Cox2, Cox3, Cox4, and HA antibodies. * indicates IgG light chain.

(C) Rcf1-His_6/HA_3 was purified from digitonin and DDM-solubilized mitochondria, respectively. The final eluate was visualized by silver stain, and protein identities were determined by mass spectrometry. Cox3 is indicated based on SDS-PAGE/western blot because it was not detected by mass spectrometry.

(D) Mitochondria extracted from a strain harboring a plasmid expressing Rcf1 or Rcf1-His_6/HA_3 were solubilized by digitonin or DDM and subjected to BN-PAGE/western blot. Rcf1, Complex III, and Complex IV were immunoblotted by anti-HA, Cor1&Qcr 2, and Cox2 antibodies, respectively.

Upon biochemical fractionation, Rcf1- His_6/HA_3 was detected in the whole-cell lysate, but was essentially absent from the post-mitochondrial supernatant (Figure 1B). The purified mitochondria fraction was subjected to either proteinase K digestion with or without swelling to rupture the outer membrane (mitoplasts) or with Triton X-100 to rupture all membranes. Rcf1 was partially degraded in mitoplasts and was completely degraded upon Triton X-100 treatment. This pattern is similar to that observed for Cox2, which is an integral protein of the mitochondrial inner membrane (Figure 1B). Independently, we found that this same Rcf1 fusion protein was stably associated with mitochondrial membranes even following high salt and bicarbonate extraction (Figure 1C). This is consistent with the bioinformatic prediction that Rcf1 and its relatives have two transmembrane domains and are therefore likely to be integral membrane proteins (Figure S1A available online). Taken together, these results suggest that Rcf1 is an integral protein of the mitochondrial inner membrane, as was found for one of the mammalian orthologs of *RCF1* (Wang et al., 2006).

To begin to understand the role of Rcf1 in mitochondrial function, we generated an *rcf1*Δ mutant and subjected it to growth assays in comparison to a wild-type (WT) strain. The *rcf1*Δ mutant exhibited impaired growth on all nonfermentable carbon sources tested, including acetate (Figure 1D). This phenotype was exacerbated when the experiment was conducted at 37°C (Figure 1D, bottom), consistent with a destabilization of proteins or protein complexes in the *rcf1*Δ mutant. This slow-growth phenotype on nonfermentable carbon sources is consistent with a partial failure in respiration in the *rcf1*Δ mutant. To directly assess respiration, we measured oxygen consumption in the WT and *rcf1*Δ mutant strains. The *rcf1*Δ mutant had roughly 30% of WT oxygen consumption on glucose medium and substantial respiratory defects on lactate and glycerol medium (Figures 1E and S1B). Together, these results demonstrate that Rcf1 is an integral protein of the mitochondrial inner membrane that is required for normal respiratory activity.

Rcf1 Stably Associates with Complex III and Complex IV of the Electron Transport Chain

To determine the biochemical mechanism that underlies the role of Rcf1 in mitochondrial respiration, we identified proteins associated with Rcf1-His_6/HA_3 expressed at endogenous levels. After two-step purification, we observed at least nine discrete bands, which were absent in the empty vector negative control, in the sample from the Rcf1-His_6/HA_3 strain (Figure 2A). These bands primarily contained subunits of either Complex III or Complex IV from the electron transport chain (Figure 2A and Table S1). We also observed the ATP/ADP carrier, Aac2, which was previously shown to associate with electron transport chain complexes (Dienhart and Stuart, 2008). Bands containing Dld1, Sdh1, and Jid1 were also observed. Copurification of multiple

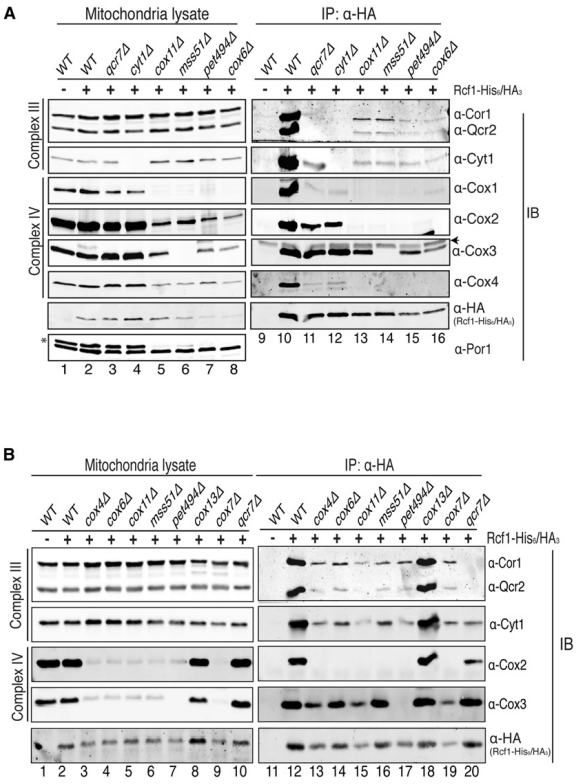

Figure 3. Rcf1 Interacts with Complex III and Complex IV Independently

(A) Rcf1 was immunoprecipitated using anti-HA antibodies from the digitonin-solubilized mitochondria of the indicated strains harboring either with (+) or without (–) a plasmid expressing Rcf1-His_6/HA_3. Both 1% crude lysate and final eluate were immunoblotted using anti-Cor1&Qcr2, Cyt1, Cox1, Cox2, Cox3, Cox4, HA, and Por1 antibodies, respectively. Asterisk on the anti-Por1 blot indicates the Cox2 signal from a previous exposure; arrowhead on the anti-Cox3 blot indicates IgG light chain. (B) Mitochondria from the indicated strains were analyzed as in (A).

See also Figure S2.

components of both Complex III and Complex IV with Rcf1 was confirmed using immunoprecipitation of the Rcf1-His_6/HA_3 fusion protein (Figure 2B). Note that we observed a clear interaction with Cox3. Perhaps due to its sequence and chemical properties, Cox3 was not detected by mass spectrometry of the Rcf1 eluate (Table S1).

It is well known that Complex III and Complex IV physically associate with one another, forming respiratory supercomplexes (Schägger and Pfeiffer, 2000; Wittig and Schägger, 2009). Therefore, it was not surprising that those two complexes simultaneously copurify with Rcf1. To further explore the interrelationships between Rcf1, Complex III, and Complex IV, we repeated the Rcf1-His_6/HA_3 purification experiment using both digitonin-solubilized and dodecylmaltoside (DDM)-solubilized mitochondria. Although we again observed the same set of Complex III and Complex IV subunits in the digitonin sample, the Complex III subunits did not copurify with Rcf1-His_6/HA_3 in the DDM-solubilized sample (Figure 2C). Digitonin has been shown to be mild enough to maintain Complex III/Complex IV associations in III_2/IV and III_2/IV_2 supercomplexes, whereas DDM disrupts these interactions. This pattern of associations in the two detergents was confirmed by mass spectrometry of the entire eluate from the purifications. All complex IV subunits were observed in both digitonin and DDM, but Complex III subunits were associated only with Rcf1 in digitonin (Table S1). This implies that the interaction of Rcf1 with Complex IV is likely to be more stable than the interaction with Complex III. Interestingly, Complex II subunits also were detected in the Rcf1 eluate, albeit at apparently lower stoichiometry (Table S1). These observations were also confirmed using blue native-PAGE (BN-PAGE) electrophoresis. In DDM-solubilized mitochondrial lysates, Rcf1-His_6/HA_3 migrated in a complex of similar mobility to monomeric Complex IV, as exemplified by Cox2 (Figure 2D, lane 3). In digitonin, however, Rcf1-His_6/HA_3 primarily migrated at the position of the III_2/ IV_2 heterotetrameric supercomplex (Figure 2D, lane 4). These data indicate that Rcf1 maintains strong association with Complex IV in either detergent condition but loses the association with Complex III in DDM.

This pattern of associations between Rcf1 and the ETC complexes suggested two possibilities. One possible interpretation is that Rcf1 associates directly with Complex IV and the copurification with Complex III is indirect, occurring via the Complex III/Complex IV interaction. The other possibility is that Rcf1 interacts with both complexes independently, perhaps even serving as a contact point between the two complexes. To systematically address this question, we monitored the association between Rcf1 and Complex III subunits (Cor1, Qcr2, and Cyt1) and between Rcf1 and Complex IV subunits (Cox1, Cox2, Cox3, and Cox4) in mutants that lead to the loss of either Complex III or Complex IV (Figure 3A). The copurification of Complex IV with Rcf1 in DDM conditions was recapitulated in this assay. A *qcr7*Δ mutant causes severe failure of Complex III assembly and Rcf1 shows no association with Cor1 or Qcr2 in this mutant (Figures 3A, lane 11, and 3B, lane 20), even though both Cor1 and Qcr2 are present in the mitochondrial lysate (Figures 3A, lane 3, and 3B, lane 10).

Interestingly, deletion of *QCR7* does not destroy the interaction between Rcf1 and Cyt1, raising the possibility that Rcf1 might be associated more closely with Cyt1 than Cor1 or Qcr2. As expected, deletion of *CYT1* also leads to the loss of Rcf1 interaction with Cor1 and Qcr2 (Figure 3A, lane 12). In both of these mutants, however, the Rcf1 interactions with Cox1, Cox2, Cox3, and Cox4 were maintained. For Cox1, Cox2, and Cox4, Rcf1 interactions were compromised but remained significantly above background. Interestingly, the Rcf1/Cox3 interaction was not negatively affected by either the *qcr7*Δ or *cyt1*Δ mutations, suggesting that it might be more proximal to the Rcf1 interaction site than Cox1, Cox2, or Cox4. These data demonstrate that Rcf1 interacts stably with Complex IV even in the absence of association with Complex III.

The more interesting question, however, is whether Rcf1 maintains an association with Complex III in the absence of Complex IV. To address this question, we monitored association between Rcf1 and Complex III subunits in four different mutants lacking properly assembled Complex IV. They each lead to distinct defects in the expression, translation, or assembly of different Complex IV subunits. Deletion of *COX11*, which encodes a Cox1 assembly factor, causes impaired synthesis of Cox1 (Barrientos et al., 2004; Horng et al., 2004). Pet494 and Mss51 are translational activators of *COX3* and *COX1*, respectively, and their deletion causes loss of their respective target (Costanzo and Fox, 1986; Perez-Martinez et al., 2003). Cox6 is a Complex IV subunit that might play a role in oxygen sensing and is indispensible for the stability and activity of Complex IV (Wright et al., 1995). None of these mutants has intact, properly assembled Complex IV. In all cases, however, Cor1, Qcr2, and Cyt1 copurified with Rcf1, albeit at a reduced level compared to the WT strain (Figure 3A, lanes 13–16). As observed earlier, we again saw that Cox3 maintained an association with Rcf1 when other Complex IV subunits did not. In spite of this, depletion of Cox3 by mutation of *PET494* did not prevent the association of Rcf1 with Complex III subunits (Figure 3A, lane 15). Even after a stringent two-step purification, the same results were obtained for the WT, *qcr7*Δ, and *cox11*Δ strains (Figures S2A and S2B).

The recent publication of higher resolution structures of respiratory supercomplexes (Althoff et al., 2011; Dudkina et al., 2011) has provided some insight into the more intimate relationship between Rcf1 and Cox3. These structures show that Cox3, Cox7, and Cox13 comprise the majority of the interface with Complex III. As shown above, loss of Cox3 failed to abolish the ability of Rcf1 to coprecipitate Complex III subunits (Figure 3B, lane 17). Additionally, neither loss of Cox7 or Cox13 abrogated the Rcf1/Complex III interaction (Figure 3B, lanes 18 and 19). Unlike the other Complex IV mutants, the *cox13*Δ mutant had no deleterious effect on the Rcf1 interaction with either Complex III subunits (Cor1, Qcr2, and Cyt1) or Complex IV subunits (Cox2 and Cox3). Therefore, even the loss of those proteins that are likely to be most intimately associated with Rcf1 within Complex IV doesn't abolish the Rcf1 interaction with Cor1, Qcr2, and Cyt1. Although it is possible that subcomplexes of Complex IV remain in any one of these mutants and could mediate the interaction between Rcf1 and Complex III, it is unlikely that the same subcomplex bearing that bridging activity is found in each of these many mutants. We therefore conclude that Rcf1 has the rather unusual property of interacting directly with components of Complex III and Complex IV, independent of association with the other.

Rcf1 Promotes the Stability of Complex III/Complex IV Supercomplexes

If Rcf1 interacts directly with both Complex III and Complex IV and, therefore, serves as a point of contact between the two complexes, it is possible that an *rcf1*Δ mutant might exhibit defects in their association. BN-PAGE analysis was conducted on the WT and *rcf1*Δ mutant grown in raffinose medium to induce mitochondrial biogenesis. As assessed by α-Cor1/Qcr2 immunoblot, Complex III migration in the WT strain was almost completely as the Complex III_2/Complex IV_2 tetramer (Figure 4A, left). A small amount of the III_2/IV complex was observed, but we detected no free Complex III. Complex III in the *rcf1*Δ mutant, however, showed a loss of association with Complex IV. There was a shift from the fully assembled III_2/IV_2 complex toward the III_2/IV complex and some free III_2 dimer was detected. Examination of Complex IV (Cox3 immunoblot) showed a similar loss of the III_2/IV_2 complex and an increase in the III_2/IV complex and free Complex IV in the *rcf1*Δ mutant (Figure 4A, middle). A similar phenotype was observed for the *rcf1*Δ mutant in stationary phase cultures grown in glucose (Figure S3A). Again, we observed a shift from the fully assembled III_2/IV_2 complex toward the III_2/IV and III_2 complexes. We detected free Complex IV in the WT strain that was decreased in the *rcf1*Δ mutant, raising the possibility that Complex IV might be less stable to BN-PAGE analysis under some conditions in the absence of Rcf1. This appears to not be general, however, because we observed increased free Complex IV in the *rcf1*Δ mutant grown in raffinose medium (Figure 4A). The migration of Complex V was unaffected by loss of Rcf1 (Figure S3A). In both raffinose and glucose cultures, these effects on supercomplex organization occurred in the absence of any substantial effect on the steady-state levels of Complex III or Complex IV subunits (Figures 4B and S3B). Although the *rcf1*Δ mutant may exhibit a defect in Complex IV assembly or stability, these data strongly suggest that there is a specific defect in the Complex III/Complex IV association.

Measurement of complex activity following BN-PAGE was consistent with these results. As expected, Complex V/ATP synthase exhibited normal activity in the *rcf1*Δ mutant (Figures S3C and S4C). Total Complex IV activity was decreased in the *rcf1*Δ mutant, and this impairment was due primarily to a loss of activity in the III_2/IV_2 complex (Figures S3C and S4C). The loss of Complex IV activity could be due to an intrinsic defect in Complex IV or to loss of association with Complex III, which has been shown to result in Complex IV defects in mammalian systems (Acín-Pérez et al., 2008; Gil Borlado et al., 2010). Quantitative assays confirmed these results and also showed that Complex III activity is unaffected by deletion of *RCF1* (Figure 4C). We also noticed a slight but reproducible defect in the activity of Complex II in the *rcf1*Δ mutant (Figure S3C), possibly indicating that the interactions between Rcf1 and Complex II subunits (Table S1) have functional importance.

Rcf1 doesn't appear to be a stoichiometric constituent of the Complex III/Complex IV supercomplex. When we immunoprecipitate Rcf1, we coprecipitate a smaller amount of both

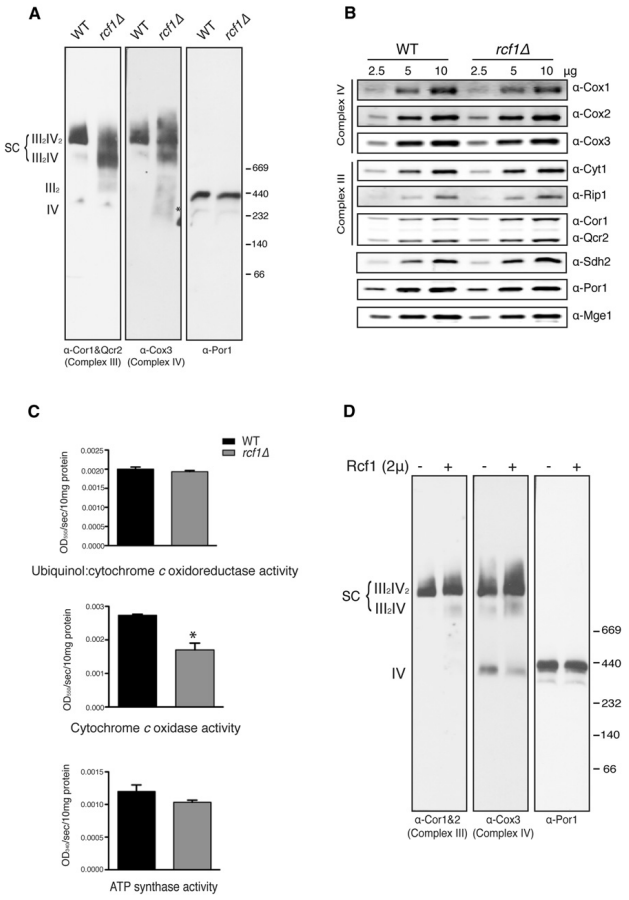

Figure 4. Respiratory Supercomplexes Are Impaired in the Absence of *RCF1*

(A) Mitochondria from WT and the *rcf1*Δ mutant grown to log phase in synthetic raffinose medium were analyzed by BN-PAGE/western blot. Complex III and Complex IV were immunoblotted by anti-Cor1&Qcr2 and Cox3 antibodies, respectively. Asterisk indicates the position of free Complex IV monomer. Porin serves as a control.

(B) The mitochondria from (A) were subjected to SDS-PAGE and immunoblotted using Cox1, Cox2, Cox3, Cor1&Qcr2, Cyt1, Rip1, and Sdh2 antibodies. Por1 and Mge1 are loading controls.

(C) Enzymatic activities of Complex III, Complex IV, and Complex V were measured in lysates of the WT and *rcf1*Δ mutant grown in synthetic raffinose media to log phase. Each was measured in three independent cultures and data shown is mean + SD. $^*p < 0.05$.

(D) Mitochondria from the WT strain with or without a 2μ-based plasmid overexpressing Rcf1 grown in raffinose medium to log phase were analyzed by BN-PAGE/Western blot. Complex III, Complex IV and porin complex were immunoblotted by anti-Cor1&Qcr2, Cox3 and Por1 antibodies, respectively.

See also Figure S3.

Complex III subunits (Cor1, Qcr2, and Cyt1) and Complex IV subunits (Cox1, Cox2, Cox3, and Cox4) than when we immunoprecipitate a typical Complex IV subunit, Cox4 (Figure S3D). Based on that and its apparent function, we reasoned that overexpression of Rcf1 might increase the amount of respiratory supercomplexes. As seen in Figure 4D, expression of Rcf1 from a multicopy 2μ plasmid caused a subtle shift in the Complex IV migration pattern in cells grown in raffinose. Free Complex IV was lost and both the III_2IV and III_2IV_2 complexes were increased in abundance, indicating that increased Rcf1 dosage can promote supercomplex formation. Although subtle, this effect is reproducible under distinct growth conditions—stationary phase in glucose medium (Figure S3E).

RCF1 Genetically Interacts with *AAC2* and *COX13* to Stabilize Respiratory Supercomplexes

Two other molecules have been shown previously to be important for the assembly of respiratory supercomplexes: the lipid cardiolipin and the ADP/ATP translocase Aac2. Loss of either of these molecules was found to destabilize supercomplexes (Dienhart and Stuart, 2008; Zhang et al., 2002). We wanted to examine the genetic relationship between *RCF1*, *AAC2*, and the gene encoding cardiolipin synthase *CRD1*, which is required for cardiolipin synthesis. Therefore, we constructed strains lacking these three genes in all possible combinations and examined their growth under different conditions. The *aac2*Δ strain exhibited a complete inability to grow on nonfermentable carbon sources, making it impossible to use such medium to examine respiratory growth (Figure S4A). As an alternative, we examined the survival of these strains in stationary phase, which is also an indicator of respiratory capability (Gray et al., 2004). When grown at 30°C to log phase, all mutants exhibited normal survival (Figure 5A, left panel). Even at day 4 of stationary phase, the three single mutants and the *crd1*Δ *rcf1*Δ double mutant showed no loss of viability. However, both of the other double mutants showed a substantial defect in survival and the triple-mutant was even more severely affected (Figure 5A, right). When grown at 37°C, the same general pattern was evident, but the synergistic growth defects were more pronounced. These data demonstrated that loss of the *RCF1* and *CRD1* genes does not

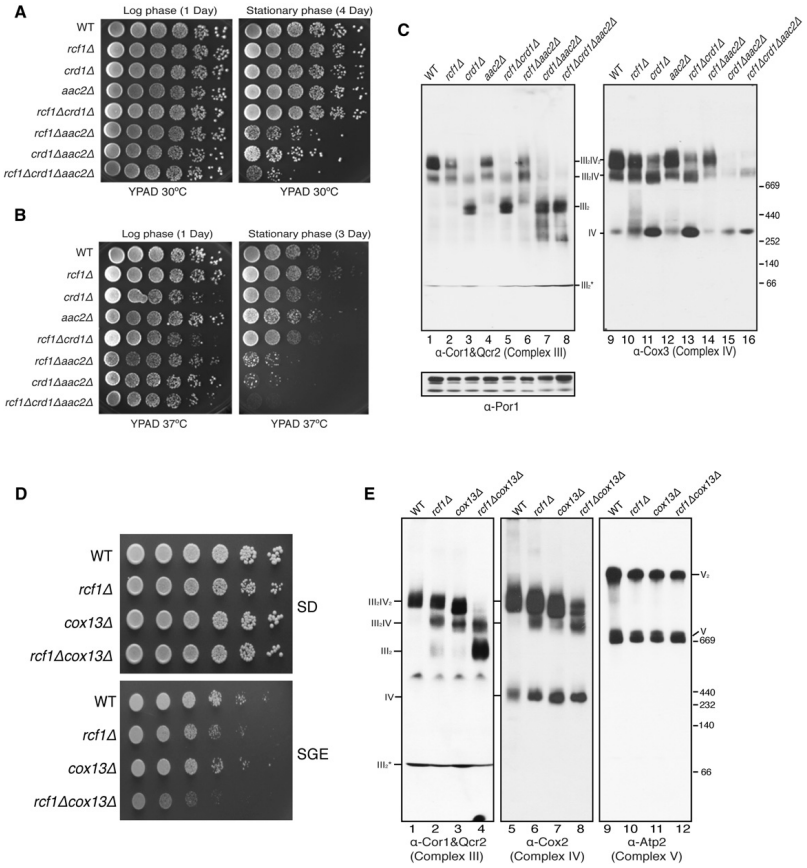

Figure 5. *RCF1* Genetically Interacts with *AAC2* and *COX13* to Stabilize Respiratory Supercomplexes

(A and B) The indicated strains were grown in YPAD media to log or stationary phase as indicated were spotted on YPAD plates and incubated at 30°C (A) or 37°C (B).

(C) Mitochondria from the indicated strains grown in raffinose medium to log phase were analyzed by BN-PAGE/western blot. Complex III, Complex IV, and porin complex were immunoblotted by anti-Cor1&Qcr2, Cox3, and Por1 antibodies, respectively. III_2* indicates a Complex III intermediate.

(D) The indicated strains were spotted on SD and SGlycerol/ethanol plates and incubated at 30°C. (E) Mitochondria from the indicated strains grown in 1% glucose medium for 1 day were analyzed by BN-PAGE/western blot. Complex III, Complex IV, and Complex V were immunoblotted by anti-Cor1&Qcr2, Cox2, and Atp2 antibodies, respectively. III_2* indicates a Complex III intermediate.

See also Figure S4.

result in a synergistic or even an additive phenotype. One possible explanation is that these two genes act in the same pathway to promote respiration, a conclusion that is supported by biochemical data described below. On the other hand, loss of *AAC2* causes a synergistic survival defect with both the *rcf1*Δ and *crd1*Δ mutants, a result that is consistent with Aac2 acting in parallel with both Rcf1 and Crd1 to promote supercomplex assembly or stability. Both Aac2 and cardiolipin have significant roles outside of supercomplex stabilization, which makes it difficult to draw mechanistic conclusions from genetic interactions.

To directly assess the assembly and stability of respiratory supercomplexes in these mutants, we subjected the same strains to BN-PAGE analysis after growth in raffinose. As

observed before, the *rcf1*Δ mutant showed depletion of the III_2/IV_2 complex, as determined both by Complex III and Complex IV immunoblot (Figure 5C, lanes 2 and 10). The *aac2*Δ mutant exhibited a very similar phenotype (Figure 5C, lanes 4 and 12). The *crd1*Δ single mutant showed a stronger defect, with an almost complete absence of the III_2/IV_2 complex and a significant amount of the III_2 and IV species (Figure 5C, lanes 3 and 11). As seen in the growth assays, the *crd1*Δ *rcf1*Δ double mutant showed no additive phenotype and was nearly identical to the *crd1*Δ single mutant (Figure 5C, lanes 5 and 13). The *aac2*Δ *rcf1*Δ double mutant on the other hand showed a more substantial loss of the III_2/IV_2 complex than either single mutant (Figure 5C, lanes 6 and 14). There was a clear synthetic phenotype in the *aac2*Δ *crd1*Δ double mutant, which had a nearly complete loss of all supercomplexes (Figure 5C, lanes 7 and 15). Although deletion of *AAC2* and *CRD1* caused a decrease in the steady-state levels of some Complex IV subunits, deletion of *RCF1* caused no effect on any Complex III or Complex IV subunits, even in the context of double mutants that had a synthetic effect on supercomplex organization (Figure S4B). Similar phenotypes were also observed in BN-PAGE analysis of these strains, which were grown to stationary phase in glucose (Figure S4C). Another factor that occupies the predicted interface between Complex III and Complex IV is Cox13. In isolation, the *cox13*Δ mutant exhibits WT growth on both glucose and glycerol/ethanol plates (Figure 5D). The *cox13*Δ *rcf1*Δ double mutant, however, has a more dramatic growth phenotype than the *rcf1*Δ single mutant when grown under respiratory conditions (Figure 5D). This growth phenotype is accompanied by a severe loss of higher-order respiratory supercomplexes, as determined by BN-PAGE analysis on the strain grown in different conditions. The *cox13*Δ single mutant shows depletion of the III_2/IV_2 complex similar to that observed in the *rcf1*Δ mutant (Figure 5E). The *cox13*Δ *rcf1*Δ double mutant, however, shows almost a complete loss of the intact III_2/IV_2 supercomplex and a marked shift to lower order complexes.

Increased Mitochondrial Oxidative Stress in the *rcf1*Δ Mutant

The physiological importance of mitochondrial ETC supercomplexes has not been precisely defined. It has been speculated, however, that the assembly of individual complexes into supercomplexes enables more efficient electron flow and decreases the risk of electron stalling. One predicted physiological manifestation of reduced electron stalling would be decreased generation of reactive oxygen species (ROS) by the ETC. As a means of assessing the level of oxidative damage in the mitochondrial matrix of the *rcf1*Δ mutant, we measured the activity of aconitase. This mitochondrial enzyme is highly susceptible to inactivation by ROS, due to oxidation of an exposed Fe/S cluster. Therefore, aconitase activity is a measure of the in vivo burden of oxidative stress and damage in the mitochondrial matrix (Criscuolo et al., 2005; Gardner et al., 1995). In log phase cultures, we observed an ~20% decrease in aconitase activity in the *rcf1*Δ mutant, compared to an ~60% decrease in activity in a mutant lacking the mitochondrial Mn^{2+}-dependent superoxide dismutase, Sod2 (Figure 6A). In stationary phase cultures, which are subject to enhanced respiratory activity and elevated oxidative stress, the aconitase activity was more severely affected in both mutants. We previously showed that overexpression of *RCF1* caused a modest stabilization of higher-order supercomplex structures. *RCF1* overexpression also caused a nearly 2-fold increase in aconitase activity (Figure 6B). As described previously, additional loss of *COX13* confers a synergistic growth and supercomplex assembly phenotype upon the *rcf1*Δ mutant strain. The *cox13*Δ *rcf1*Δ double mutant also exhibited a more profound loss of aconitase activity relative to either of the two single mutants (Figure 6C).

We also monitored the susceptibility of WT and mutant strains to exogenous hydrogen peroxide. Mutants with higher in vivo production of ROS are typically more sensitive to this exogenous stress. Compared to WT, the dose-dependent lethality in response to hydrogen peroxide is exacerbated in the *rcf1*Δ mutant (Figure 6D). In addition, we also measured the expression of the endogenous ROS defense system, as exemplified by the mitochondria-specific superoxide dismutase Sod2. The *rcf1*Δ mutant has elevated Sod2 protein levels relative to the WT control (Figure 6E), which is consistent with this mutant having elevated endogenous oxidative stress, particularly in mitochondria. We hypothesize that this increased oxidative damage and sensitivity result from accelerated ROS production by the electron transport chain. This ETC dysfunction is a predictable result of impaired assembly of individual complexes into supercomplexes, which promotes reliable, solid-state electron transmission. As another manifestation of ETC dysfunction, the *rcf1*Δ mutant exhibited impaired maximal respiration in the presence of CCCP, which causes dissipation of the mitochondrial membrane potential and a compensatory acceleration of respiration in WT cells (Figure S5; compare to Figure 1E). The impaired stimulated respiration in the *rcf1*Δ mutant was accompanied by markedly increased sensitivity to CCCP-induced cell death (Figure 6F).

The *HIG2A* Mammalian Homolog of *RCF1* Plays a Role in Supercomplex Stability

As previously described, our selection of *RCF1* for detailed study was based partially upon evolutionary conservation among eukaryotes. We were interested to determine whether the role we discovered for Rcf1 in supercomplex organization might also extend to *RCF1* orthologs in other species. The mouse and human genomes contain five homologs of *RCF1*, which are subdivided into two classes that are defined by the two genes with the broadest expression pattern, *HIG1A* and *HIG2A* (Figure S1A). *HIG1A* was originally described as being strongly inducible by hypoxia in a HIF-1-dependent manner (Denko et al., 2000; Kasper and Brindle, 2006). To determine whether either *HIG1A* or *HIG2A* were required for normal supercomplex assembly or stability in mammalian cells, we transfected cells with siRNAs targeted to these two genes. Knockdown of *HIG1A* (Figure S6B) had no effect on the pattern of supercomplex assembly (Figure S6A), which is more complicated in mammalian cells due to the presence of Complex I and the stable incorporation of both Complex II and Complex V (Acín-Pérez et al., 2008). On the other hand, knockdown of *HIG2A* (Figure 7B) caused a depletion of all higher order supercomplexes that contain Complex IV, particularly the I+II+III+IV (#3), I+III+IV (#4), and III+IV (#6) species (Figure 7A) (Acín-Pérez et al., 2008). Supercomplex species that do not contain Complex IV,

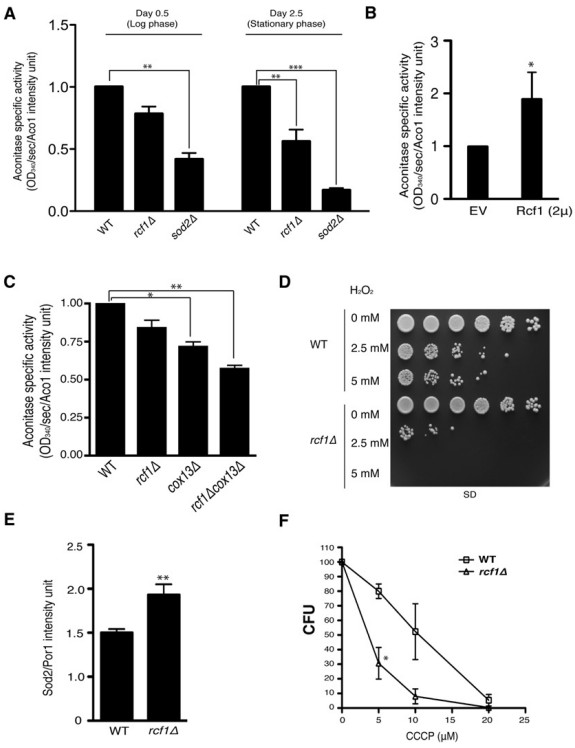

Figure 6. Increased Mitochondrial Oxidative Stress in the Absence of *RCF1*

(A) Cell lysates of the indicated strains grown in SD media for 0.5 and 2.5 days were subjected to aconitase activity assay and immunoblotted with anti-Aco1 antibody. Aconitase activity was determined specifically by normalizing the NADP reduction rate to Aco1 protein-band intensity. *sod2*Δ was used as a control. Mean ± SD of three independent cultures is shown. **p < 0.01; ***p < 0.0005.

(B) The WT strain harboring either EV or a 2μ-based plasmid overexpressing Rcf1 were grown for 1 day in 1% glucose and analyzed as in (A). Mean ± SD of three independent cultures is shown. *p < 0.05.

(C) The indicated strains were harvested after being grown in SD media for 0.5 day and analyzed as in (A). Mean ± SD of three independent cultures is shown. *, p < 0.05; **p < 0.01.

(D) Log phase cultures (0.5 day) of the WT and *rcf1*Δ mutant were pretreated with H_2O_2 for 2 hr, spotted on synthetic glucose medium, and incubated at 30°C.

(E) Log phase cultures (0.5 day) of the indicated strains were harvested and immunoblotted for Sod2, which was normalized to Por1 intensity. Mean ± SD of six independent cultures is shown. **p < 0.01.

(F) WT and the *rcf1*Δ mutant strains of the BY4741 background were grown to log phase in glucose media and an equal number of cells were plated on media containing the indicated concentration of CCCP. Number of colonies was counted after 48 hr. Mean ± SD of three independent cultures is shown. *p < 0.05.

See also Figure S5.

DISCUSSION

Based on the data presented herein, we conclude that Rcf1 is a component of respiratory supercomplexes and is required for their normal stability. We also conclude that although Rcf1 is not essential for basal mitochondrial function, but is essential for optimally efficient ETC function and respiration. Evidence that supports these conclusions is detailed below.

First, Rcf1 directly interacts with respiratory supercomplexes. When we purified Rcf1, we copurified stoichiometric amounts of both Complex III and Complex IV, the major components of *S. cerevisiae* ETC supercomplexes. We considered the alternative explanation that Rcf1 is a previously unidentified component of Complex IV. The association with Complex III could be indirect, occurring only as a consequence of the interaction between Complex III and Complex IV. The fact that extraction of mitochondria with the relatively harsh detergent DDM causes the loss of Rcf1/Complex III association could be seen as supporting this view. However, none of the seven distinct COX mutants that we have analyzed, six of which exhibit failed assembly of Complex IV and the destruction of many of its subunits, have lost the association of Rcf1 with Complex III subunits. Interactions of Rcf1 with Cor1, Qcr2, and Cyc1 are maintained in spite of the fact that Rcf1 has lost all detectable interaction with Cox1, Cox2, Cox3, Cox4, and, presumably, other Complex IV subunits for which we do not have usable antibodies. Similarly, loss of the Complex III subunit Cyt1 leads to a complete failure

such as the two I+III+V complexes (#1 and #5), were either unaffected or slightly increased upon *HIG2A* depletion (Figure 7A). To more rigorously evaluate a role for *HIG2A* and its encoded protein in supercomplex stability, we generated three additional siRNAs targeted to *HIG2A*, two of which caused significant depletion of the *HIG2A* mRNA; the other did not (Figure 7D). The two additional efficacious siRNAs (Si2 and Si3) caused an identical phenotype to that observed for Si1 (Figure 7C). Specifically, we again observed a loss of supercomplex species containing Complex IV and either unaffected or increased levels of Complex IV-independent species. At longer exposure of the anti-Cox1 immunoblot, we also saw a profound depletion of the #2 I+II+III+IV species in Si2- and Si3-treated cells (Figure 7C, panel 5). We observed a slight reduction in the amount of free, fully assembled Complex IV and a slight increase in an incomplete Complex IV (IV*). Although these results demonstrate a role for *HIG2A* in C2C12 myoblast cells, it is possible that the four additional mammalian *HIG* family members serve a related function in different cell types or different conditions. Determining their precise roles and contributions in Complex IV and supercomplex assembly and stability requires additional study.

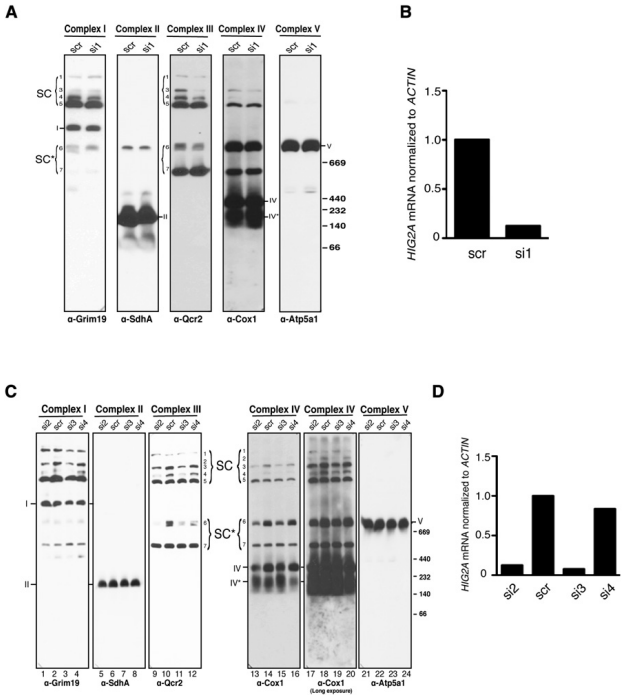

Figure 7. Mammalian *HIG2A* is Critical for Normal Respiratory Supercomplex Organization

(A) Mitochondria extracted from C2C12 cells transfected with either scrambled (scr) or *HIG2A*-targeted siRNA (si1) were solubilized in 2% digitonin and resolved by BN-PAGE, followed by immunoblotting with the indicated antibodies. Respiratory complex species are indicated following the convention of (Acín-Pérez et al., 2008), specifically: 1 (I+III+V); 2 (I+II+III+IV); 3 (I+II+III+IV); 4 (I+III+IV); 5 (I+III+V); 6 (III+IV); 7 (III+IV)*.

(B) *HIG2A* mRNA level normalized to *ACTIN* was measured from cells in (A) using quantitative RT-PCR.

(C) Mitochondria extracted from C2C12 cells transfected with scrambled (scr) or one of three unique *HIG2A*-targeted siRNA (si2, 3, 4) were treated as in (A). A longer exposure of the anti-Cox1 immunoblot is shown to enable visualization of the supercomplexes #1, 2, and 4. Note that si4 is not efficacious in *HIG2A* knockdown.

(D) *HIG2A* mRNA level normalized to *ACTIN* was measured from cells in (C) using quantitative RT-PCR.

See also Figure S6.

of Rcf1 to interact with central Complex III subunits Cor1 and Qcr2, although interactions with Complex IV subunits are maintained.

In general, although mutations impairing either Complex III or IV assembly do not eliminate the interaction of Rcf1 with the other Complex, the interactions are significantly weakened. One exception to this is the Complex IV subunit, Cox3. The *qcr7*Δ and *cyt1*Δ (Complex III) mutations eliminate the interaction of Rcf1 with the core Cor1 and Qcr2 subunits of Complex III. They also greatly impair the Rcf1 interaction with Complex IV subunits Cox1, Cox4, and, to a lesser extent, Cox2. The Rcf1 interaction with Cox3, however, is essentially unaffected. The Rcf1/Cox3 interaction also seems to be unusually persistent in the face of Complex IV destruction. The *cox11*Δ, *mss51*Δ, and *cox6*Δ (all Complex IV) mutations each eliminate the interaction of Rcf1 with Cox1, Cox2, and Cox4, but the interaction with Cox3 is maintained, albeit at a reduced level. In spite of this seemingly special relationship between Cox3 and Rcf1, loss of Pet494, which completely blocks the expression of Cox3, does not destroy the interaction of Rcf1 with Complex III.

The data demonstrating an intimate association between Rcf1 and Cox3 has been confusing until recently. If Rcf1 interacts independently with both Complex III and Complex IV, it must occupy a position close to the interface between them in the respiratory supercomplex. The structure of the III_2/IV_2 supercomplex from *S. cerevisiae*, however, suggested that Cox3 was situated on the face of Complex IV that was opposite to the Complex III interaction site (Heinemeyer et al., 2007). This model was based on low-resolution data, and the rotational orientation of Complex IV was quite speculative. Recently, much higher-resolution electron microscopy reconstructions of the bovine $I/III_2/IV$ supercomplex were completed and published (Althoff et al., 2011; Dudkina et al., 2011). These data clearly show the Complex IV orientation to be rotated relative to Complex III, placing Cox3 at the site of the Complex III/Complex IV interface. Interestingly, the docking of the crystal structures of Complex III and Complex IV into the EM model demonstrated a clear gap between the two complexes, particularly in the juxtamembrane region (Dudkina et al., 2011). Based on its small size and two transmembrane domains, this is the region that should be occupied by Rcf1. It is possible that in addition to cardiolipin, which was postulated to occupy this position, Rcf1 fills this space and stabilizes the Complex III/Complex IV interaction.

Second, *RCF1* has a robust genetic interaction with *AAC2*, which has been implicated previously in stabilizing ETC supercomplexes (Dienhart and Stuart, 2008). In assays of stationary phase survival, *RCF1* and *AAC2* exhibited a profound synthetic phenotype, particularly at elevated temperature. Such a growth phenotype is potentially due to destabilization of supercomplexes, as we showed using blue native-PAGE. *AAC2* has a nearly identical relationship with *CRD1*, which encodes cardiolipin synthase and is necessary for the synthesis of this lipid.

Like Aac2, cardiolipin has also been implicated in the stability of respiratory supercomplexes. There was no additivity, on the other hand, between *RCF1* and *CRD1*. Although we don't yet know how these molecules interrelate in their stabilization of supercomplexes, these varied genetic interactions imply that they don't all function identically or independently.

We also observed a strong genetic interaction between *RCF1* and *COX13*. The Cox13 protein is predicted to occupy the interface between Complex III and Complex IV. Our data shows a modest loss of the III_2/IV_2 supercomplexes in the *cox13*Δ single mutant, which is dramatically exacerbated in the *cox13*Δ *rcf1*Δ double mutant. This synergistic loss of supercomplexes is accompanied by a synthetic growth defect and accelerated generation of oxidative stress, as determined by loss of aconitase activity. These phenotypes are consistent with the proposed role of Rcf1 in supercomplex stabilization and with the proposed role of supercomplexes in prevention of oxidant production.

Finally, loss of Rcf1 leads to a loss of the fully assembled III_2/IV_2 supercomplexes and an increase in lower order structures. The majority of Complex III and IV appears to assume the III_2/IV assemblage but a significant amount of both complexes dissociate completely from the other. It is important to note that this effect seems to be specific because assembly of the other OXPHOS complexes is not impaired. *HIG2A*, one of the mammalian homologs of *RCF1*, appears to play a similar role in mouse cells. Treatment with any of three siRNAs that deplete the *HIG2A* mRNA causes a reduction of all Complex IV-containing respiratory supercomplexes.

Although we have not explored this possibility to date, it is likely that the extent and nature of respiratory supercomplexes is tightly regulated and responsive to environmental conditions. For example, we predict that nutrient availability, oxygen concentration, and ATP demand are all likely stimuli for the adjustment of supercomplex status. This could be accomplished through transcriptional or posttranscriptional regulation of *RCF1* or its homologs in other species. *HIG1A*, the mouse ortholog of *RCF1* whose depletion had no effect on supercomplex organization in C2C12 cells, is robustly induced by hypoxia (Denko et al., 2000). Perhaps *HIG1A* plays a more prominent role under hypoxia or in different cells. Indeed, it has been shown to protect pancreatic β-cells from apoptosis in response to a variety of stimuli (Wang et al., 2006). Due to its relatively simple supercomplex content, *S. cerevisiae* has only one interaction that can be targeted for regulation, between Complex III and Complex IV. In mammals, however, a much more complicated pattern exists. Complexes I, II, III, IV, and V are all components of respiratory supercomplexes, and their inclusion and stoichiometry is variable (Acín-Pérez et al., 2008). The makeup of these complexes is a likely target of metabolic regulation.

We certainly do not fully understand the consequences of the loss of supercomplex formation. We do observe, however, that there is a substantial reduction in respiratory activity, as measured by total oxygen consumption in the *rcf1*Δ mutant. Perhaps of more interest, it appears that the *rcf1*Δ mutant also has elevated oxidative stress and damage in the mitochondrial matrix. This was determined by the loss of aconitase activity, hypersensitivity to exogenous hydrogen peroxide, and an upregulation of the endogenous oxidative stress defenses. These are common phenotypes among strains that combat an elevated level of endogenous oxidative stress. One of the factors that have kept us from an understanding of the effects of supercomplex assembly and disassembly is an inability to genetically manipulate supercomplex formation without disrupting other mitochondrial functions. As best we can determine, *RCF1* deletion causes a specific defect in supercomplex formation in yeast and *HIG2A* silencing does the same in mouse cells. These will be valuable tools in understanding the role and importance of the assembly of these intricate machines.

EXPERIMENTAL PROCEDURES

Assessment of Submitochondrial Localization

These experiments were performed following a protocol adapted from (Boldogh and Pon, 2007). Mitochondria were incubated in the isotonic SH buffer or hypertonic H buffer (20 mM HEPES-KOH) with and without 1% Triton X-100. Protease K was added and incubated on ice for 20–30 min, and digestion was stopped by adding PMSF. Samples were denatured in 6X *Laemmli* buffer and resolved by 12% SDS-PAGE, followed by immunoblot. To assess the solubility of Rcf1, intact mitochondria were extracted by 100 mM Na_2CO_3 and 1 M KCl for 20 min on ice. Supernatant was isolated by centrifuging samples at 100,000 × *g* for 20 min (MLA-130, Beckman Coulter) and precipitated in 15% TCA. The precipitated supernatant fraction and insoluble membrane fraction were solubilized in 1X *Laemmli* buffer, and resolved by 12% SDS-PAGE, followed by immunoblot.

Two-Step Rcf1-His_6/HA_3 Purification

Crude mitochondria isolated from strains grown in synthetic glycerol/ethanol medium were solubilized in 0.8% digitonin or dodecylmaltoside (DDM) for 1 hr at 4°C. For the first step of the purification, cleared mitochondria lysate was incubated with equilibrated Ni-NTA beads for 1 hr at 4°C. Beads were washed 5 times with buffer containing 20 mM imidazole. Protein was eluted by 250 mM imidazole. For the second step of the purification, final eluates of the first purification were mixed with anti-HA antibody conjugated agarose (Sigma) for 1 hr at 4°C. Agarose was washed 5 times and eluted by 1 mg/ml HA peptide. Eighty percent of the final precipitate was dissolved in *Laemmli* buffer and resolved by SDS-PAGE, followed by silver stain. Protein bands excised from the gel and the rest of 20% of the final precipitate were analyzed by mass spectrometry.

Blue-Native Polyacrylamide Gel Electrophoresis (BN-PAGE)

BN-PAGE was performed as described previously (Wittig et al., 2006). Yeast mitochondria were solubilized in 1% digitonin or DDM and mammalian mitochondria were solubilized in 2% digitonin. Lysate was resolved on a 3%–13% gradient native gel using a PROTEAN® II xi Cell gel running system (Bio-rad). Western blot was performed as the regular procedure using a Trans-Blot transfer cell (Bio-rad). Membrane was blocked in 5% nonfat milk/TBS and probed with antibodies as indicated.

Solution ETC Complex Activity Assay

These experiments were performed following a protocol adapted from (Magri et al., 2010). Ubiqinol:cytochrome *c* oxidoreductase (Complex III) activity was determined by measuring the rate of cytochrome *c* reduction by ubiquinol at 550 nm. Complex III specific activity was calculated by deducing the rate of cytochrome *c* reduction of a parallel reaction with antimycin A. Cytochrome *c* oxidase (Complex IV) activity was determined by measuring the rate of cytochrome c oxidation. Complex IV-specific activity was verified by adding KCN into the reaction mixture. ATP synthase (Complex V) activity was determined by measuring the rate of NADH oxidation. ATP synthase specific activity was verified by adding oligomycin to stop the reaction. The specific Complex V activity was calculated by deducing the rate of NADH oxidation in the presence of oligomycin.

Isolation of Mammalian Mitochondria

The procedure was adapted from (Bozidis et al., 2007). C2C12 cells were washed twice with PBS, scraped from dishes, and pelleted. Roughly 150 mg

cell pellet was resuspended in 2 ml of ice-cold MTE buffer. Cells were lysed by sonication (continuous pulse on power setting of 3.5) 3 times for 10 s each. Cell debris and nuclei were pelleted at 1,400 × g for 10 min. Crude mitochondria were recovered from the supernatant fraction by centrifuging at 10,000 × g for 10 min. Mitochondrial pellet was rinsed with MTE and resuspended in it. Protein concentration was determined by Bradford assay.

Statistics

Data are presented as the means ± standard deviation (SD). Statistical significance was evaluated by the Student's t test. *, $p < 0.05$; **, $p < 0.01$; ***, $p < 0.0005$.

SUPPLEMENTAL INFORMATION

Supplemental Information includes Supplemental Experimental Procedures, Figures S1–S6, and Tables S1 and S2 and can be found with this article online at doi:10.1016/j.cmet.2012.02.006.

ACKNOWLEDGMENTS

We thank members of the Rutter laboratory as well as the laboratories of Dennis Winge, Tim Formosa, David Stillman, Janet Shaw, Jindrich Kopecek, Jerry Kaplan, and Vincenzo Zara for technical support and helpful discussions. We especially thank the Winge laboratory and Oleh Khalimonchuk for many ETC antibodies, protocols, and instruction on BN-PAGE and oxygen consumption assays. We thank the Shaw laboratory for the anti-Fzo1, Mge1 antibodies and mito-RFP constructs, and fluorescence microscopy, and the Kopecek laboratory for the preparation of DBH_2. We also thank Kaplan laboratory for the anti-Sod2 antibody and Dr. Vincenzo Zara for the anti-Cor1&Qcr2, Rip1 antibodies. This work was supported by NIH grants RO1GM087346 (to J.R.) and R24DK092784 (to J.R.).

Received: September 26, 2011
Revised: December 27, 2011
Accepted: February 8, 2012
Published online: March 6, 2012

REFERENCES

Acín-Pérez, R., Fernández-Silva, P., Peleato, M.L., Pérez-Martos, A., and Enriquez, J.A. (2008). Respiratory active mitochondrial supercomplexes. Mol. Cell *32*, 529–539.

Althoff, T., Mills, D.J., Popot, J.L., and Kühlbrandt, W. (2011). Arrangement of electron transport chain components in bovine mitochondrial supercomplex I1III2IV1. EMBO J. *30*, 4652–4664.

Barrientos, A., Zambrano, A., and Tzagoloff, A. (2004). Mss51p and Cox14p jointly regulate mitochondrial Cox1p expression in Saccharomyces cerevisiae. EMBO J. *23*, 3472–3482.

Bayley, J.P., Kunst, H.P., Cascon, A., Sampietro, M.L., Gaal, J., Korpershoek, E., Hinojar-Gutierrez, A., Timmers, H.J., Hoefsloot, L.H., Hermsen, M.A., et al. (2010). SDHAF2 mutations in familial and sporadic paraganglioma and phaeochromocytoma. Lancet Oncol. *11*, 366–372.

Boldogh, I.R., and Pon, L.A. (2007). Purification and subfractionation of mitochondria from the yeast Saccharomyces cerevisiae. Methods Cell Biol. *80*, 45–64.

Bozidis, P., Williamson, C.D., and Colberg-Poley, A.M. (2007). Isolation of endoplasmic reticulum, mitochondria, and mitochondria-associated membrane fractions from transfected cells and from human cytomegalovirus-infected primary fibroblasts. Curr. Protoc. Cell Biol. *37*, 3.27.1–3.27.23.

Costanzo, M.C., and Fox, T.D. (1986). Product of Saccharomyces cerevisiae nuclear gene PET494 activates translation of a specific mitochondrial mRNA. Mol. Cell. Biol. *6*, 3694–3703.

Criscuolo, F., Gonzalez-Barroso, Mdel.M., Le Maho, Y., Ricquier, D., and Bouillaud, F. (2005). Avian uncoupling protein expressed in yeast mitochondria prevents endogenous free radical damage. Proc. Biol. Sci. *272*, 803–810.

Cruciat, C.M., Brunner, S., Baumann, F., Neupert, W., and Stuart, R.A. (2000). The cytochrome bc1 and cytochrome c oxidase complexes associate to form a single supracomplex in yeast mitochondria. J. Biol. Chem. *275*, 18093–18098.

Denko, N., Schindler, C., Koong, A., Laderoute, K., Green, C., and Giaccia, A. (2000). Epigenetic regulation of gene expression in cervical cancer cells by the tumor microenvironment. Clin. Cancer Res. *6*, 480–487.

Dienhart, M.K., and Stuart, R.A. (2008). The yeast Aac2 protein exists in physical association with the cytochrome bc1-COX supercomplex and the TIM23 machinery. Mol. Biol. Cell *19*, 3934–3943.

Dudkina, N.V., Kudryashev, M., Stahlberg, H., and Boekema, E.J. (2011). Interaction of complexes I, III, and IV within the bovine respirasome by single particle cryoelectron tomography. Proc. Natl. Acad. Sci. USA *108*, 15196–15200.

Gardner, P.R., Raineri, I., Epstein, L.B., and White, C.W. (1995). Superoxide radical and iron modulate aconitase activity in mammalian cells. J. Biol. Chem. *270*, 13399–13405.

Genova, M.L., Baracca, A., Biondi, A., Casalena, G., Faccioli, M., Falasca, A.I., Formiggini, G., Sgarbi, G., Solaini, G., and Lenaz, G. (2008). Is supercomplex organization of the respiratory chain required for optimal electron transfer activity? Biochim. Biophys. Acta *1777*, 740–746.

Gil Borlado, M.C., Moreno Lastres, D., Gonzalez Hoyuela, M., Moran, M., Blazquez, A., Pello, R., Marin Buera, L., Gabaldon, T., Garcia Peñas, J.J., Martín, M.A., et al. (2010). Impact of the mitochondrial genetic background in complex III deficiency. PLoS ONE *5*, e12801.

Gray, J.V., Petsko, G.A., Johnston, G.C., Ringe, D., Singer, R.A., and Werner-Washburne, M. (2004). "Sleeping beauty": quiescence in Saccharomyces cerevisiae. Microbiol. Mol. Biol. Rev. *68*, 187–206.

Hao, H.X., Khalimonchuk, O., Schraders, M., Dephoure, N., Bayley, J.P., Kunst, H., Devilee, P., Cremers, C.W., Schiffman, J.D., Bentz, B.G., et al. (2009). SDH5, a gene required for flavination of succinate dehydrogenase, is mutated in paraganglioma. Science *325*, 1139–1142.

Heinemeyer, J., Braun, H.P., Boekema, E.J., and Kouril, R. (2007). A structural model of the cytochrome C reductase/oxidase supercomplex from yeast mitochondria. J. Biol. Chem. *282*, 12240–12248.

Heo, J.M., Livnat-Levanon, N., Taylor, E.B., Jones, K.T., Dephoure, N., Ring, J., Xie, J., Brodsky, J.L., Madeo, F., Gygi, S.P., et al. (2010). A stress-responsive system for mitochondrial protein degradation. Mol. Cell *40*, 465–480.

Horng, Y.C., Cobine, P.A., Maxfield, A.B., Carr, H.S., and Winge, D.R. (2004). Specific copper transfer from the Cox17 metallochaperone to both Sco1 and Cox11 in the assembly of yeast cytochrome C oxidase. J. Biol. Chem. *279*, 35334–35340.

Kasper, L.H., and Brindle, P.K. (2006). Mammalian gene expression program resiliency: the roles of multiple coactivator mechanisms in hypoxia-responsive transcription. Cell Cycle *5*, 142–146.

Kroemer, G., and Pouyssegur, J. (2008). Tumor cell metabolism: cancer's Achilles' heel. Cancer Cell *13*, 472–482.

Lenaz, G., and Genova, M.L. (2009). Structural and functional organization of the mitochondrial respiratory chain: a dynamic super-assembly. Int. J. Biochem. Cell Biol. *41*, 1750–1772.

Lessing, D., and Bonini, N.M. (2009). Maintaining the brain: insight into human neurodegeneration from Drosophila melanogaster mutants. Nat. Rev. Genet. *10*, 359–370.

Magri, S., Fracasso, V., Rimoldi, M., and Taroni, F. (2010). Preparation of yeast mitochondria and in vitro assay of respiratory chain complex activities. Protoc. Exchange. Published online March 7, 2010. 10.1038/nprot.2010.25.

Pagliarini, D.J., Calvo, S.E., Chang, B., Sheth, S.A., Vafai, S.B., Ong, S.E., Walford, G.A., Sugiana, C., Boneh, A., Chen, W.K., et al. (2008). A mitochondrial protein compendium elucidates complex I disease biology. Cell *134*, 112–123.

Patti, M.E., and Corvera, S. (2010). The role of mitochondria in the pathogenesis of type 2 diabetes. Endocr. Rev. *31*, 364–395.

Perez-Martinez, X., Broadley, S.A., and Fox, T.D. (2003). Mss51p promotes mitochondrial Cox1p synthesis and interacts with newly synthesized Cox1p. EMBO J. *22*, 5951–5961.

Schägger, H., and Pfeiffer, K. (2000). Supercomplexes in the respiratory chains of yeast and mammalian mitochondria. EMBO J. *19*, 1777–1783.

Schriner, S.E., Linford, N.J., Martin, G.M., Treuting, P., Ogburn, C.E., Emond, M., Coskun, P.E., Ladiges, W., Wolf, N., Van Remmen, H., et al. (2005). Extension of murine life span by overexpression of catalase targeted to mitochondria. Science *308*, 1909–1911.

Stuart, R.A. (2008). Supercomplex organization of the oxidative phosphorylation enzymes in yeast mitochondria. J. Bioenerg. Biomembr. *40*, 411–417.

Suthammarak, W., Morgan, P.G., and Sedensky, M.M. (2010). Mutations in mitochondrial complex III uniquely affect complex I in Caenorhabditis elegans. J. Biol. Chem. *285*, 40724–40731.

Trifunovic, A., Wredenberg, A., Falkenberg, M., Spelbrink, J.N., Rovio, A.T., Bruder, C.E., Bohlooly-Y, M., Gidlöf, S., Oldfors, A., Wibom, R., et al. (2004). Premature ageing in mice expressing defective mitochondrial DNA polymerase. Nature *429*, 417–423.

Wallace, D.C. (2005). A mitochondrial paradigm of metabolic and degenerative diseases, aging, and cancer: a dawn for evolutionary medicine. Annu. Rev. Genet. *39*, 359–407.

Wang, J., Cao, Y., Chen, Y., Chen, Y., Gardner, P., and Steiner, D.F. (2006). Pancreatic beta cells lack a low glucose and O2-inducible mitochondrial protein that augments cell survival. Proc. Natl. Acad. Sci. USA *103*, 10636–10641.

Wittig, I., and Schägger, H. (2009). Supramolecular organization of ATP synthase and respiratory chain in mitochondrial membranes. Biochim. Biophys. Acta *1787*, 672–680.

Wittig, I., Braun, H.P., and Schägger, H. (2006). Blue native PAGE. Nat. Protoc. *1*, 418–428.

Wright, R.M., Simpson, S.L., and Lanoil, B.D. (1995). Oxygen regulation of the cytochrome c oxidase subunit VI gene, COX6, in Saccharomyces cerevisiae. Biochem. Biophys. Res. Commun. *216*, 676–685.

Zhang, M., Mileykovskaya, E., and Dowhan, W. (2002). Gluing the respiratory chain together. Cardiolipin is required for supercomplex formation in the inner mitochondrial membrane. J. Biol. Chem. *277*, 43553–43556.

Cell Metabolism, *Volume 15*

Supplemental Information

Identification of a Protein Mediating Respiratory Supercomplex Stability

Yu-Chan Chen, Eric B. Taylor, Noah Dephoure, Jin-Mi Heo, Aline Tonhato, Ioanna Papandreou, Nandita Nath, Nicolas C. Denko, Steven P. Gygi, and Jared Rutter

Supplemental Experimental Procedures

Yeast Strains and Growth Conditions

Saccharomyces cerevisiae (W303a *MATa, his3 leu2 met15 trp1 ura3*) was used as the wild-type strain in most experiments in this study, with BY4741 also being used in isolated experiments as indicated. Each mutant strain was derived from a W303 diploid strain using a standard PCR-based homologous recombination method. Each haploid strain was generated by sporulation and tetrad dissection. The genotypes of all yeast strains used in this study are listed in Table 1. Yeast transformation was performed by the standard TE/LiAc method and the transformed cells were recovered and grown in synthetic complete dextrose (SD) medium lacking the appropriate amino acid(s) for selection purposes. Medium used in this study includes standard YP and synthetic minimal medium supplemented with 1 or 2% dextrose, 2% raffinose, 3% glycerol and 2% ethanol or 2% acetate.

Plasmid Construction

The plasmids expressing C-terminal His_6/HA_3 or GFP tagged Rcf1 were generated by PCR amplification of the *RCF1* (NM_001182388) flanked with its upstream 500-bp promoter region. This fragment was ligated into a pRS416-based vector containing a C-terminal His_6/HA_3 or GFP tag. The plasmid expressing C-terminal HA tagged Cox4 was constructed as Rcf1. The plasmid for *RCF1* overexpression was generated by amplifying the *RCF1* gene flanked by the

endogenous promoter and terminator and ligating into a pRS426 vector. The sequence of each fragment was confirmed by DNA sequencing.

Fluorescence Microscopy

The rcf1Δ mutant strain transformed with plasmids expressing GFP-Rcf1 and MtRFP was grown in SD medium overnight. Cells were diluted in fresh medium to 0.1 OD and grown at 30°C for 6 hours. Images were captured using a Zeiss Axioplan 2 Imaging microscope (Carl Zeiss).

Isolation of Yeast Mitochondria

Yeast cells were harvested at early log phase, unless indicated otherwise. Preparation of crude mitochondria was as described previously (Boldogh and Pon, 2007). Cell pellet was washed once with ddH_2O and resuspended in TD buffer (100 mM Tris-SO_4, pH 9.4 and 100 mM DTT) for 15 min at 30°C. Spheroplasts were obtained by incubating cells in SP buffer (1.2 M Sorbitol and 20 mM potassium phosphate, pH 7.4) supplemented with 0.3 mg/ml lyticase for 1 hour at 30°C to remove the cell wall. Spheroplasts were gently washed once and homogenized in ice-cold SEH buffer (0.6 M sorbitol, 20 mM Hepes-KOH, pH 7.4, 2 mM $MgCl_2$, 1 mM EGTA, and 1mM PMSF) using a Dounce homogenizer applied with 30-40 strokes. Crude mitochondria were further purified by differential centrifugation. Protein concentration was determined using Bradford protein assay (Bio-rad).

Immunoprecipitation

Crude mitochondria extracted from each strain were solubilized in 0.7-0.8% digitonin for 1 hour at 4°C. Cleared mitochondria lysate was mixed with anti-HA antibody conjugated agarose for 2 hours at 4°C. Agarose was washed 5 times for 5 minutes each with the buffer supplemented with 0.1% digitonin. *Laemmli* buffer was added to the agarose to elute protein. Final eluate and 1% of the mitochondria lysate were resolved by 15% SDS-PAGE followed by immunoblot.

Oxygen Consumption Assay

For BY4741 strains, wild-type and *rcf1* mutant strains were diluted 1:100 from a log-phase culture into YP media containing the glucose, lactate and glycerol, and grown to OD_{600} about 0.5. Cells were harvested and resuspended in fresh media at 10^8 cells/ml and rate of oxygen consumption was measure by an oxygen electrode (Hansetech). For the measurement of OCR upon uncoupler treatment, CCCP was added to final concentration of 1 μM to cells in YPD media and OCR was measured as described.

For W303 strain, indicated yeast strains were harvested at early log phase and washed once with ddH_2O. Four OD units of each culture were resuspended in 3% glycerol and oxygen consumption was measured using a 5300A Biological Oxygen Monitor (Yellow Springs Instrument Co.). The rate of consumption was determined using the linear region of the O_2 concentration curve.

Oxygen consumption.

Steady-State Protein Analysis

A certain amount of crude mitochondria were pelleted and resuspended in 1X *Laemmli* buffer to final concentration 1 μg/μl. Samples were incubated at 37°C for 30-60 min and centrifuged at maximum speed using a tabletop microcentrifuge for 2 min. Supernatant was resolved in 12% SDS-PAGE followed by immunoblot.

In-Gel Activity Assay of OXPHOS Complexes

All the assays were performed following a protocol adapted from (Wittig et al., 2007). Gel strips excised from the BN-PAGE were washed once with ddH_2O. For Complex II activity, the gel strip was soaked in assay buffer (50 mM potassium phosphate, pH 7.4, 90 mM succinate, 4.5 mM EDTA, 10 mM KCN) for 10 minutes and activity was stained by 2 mg/ml nitroblue tetrazolium and 0.2 mM phenazine methosulfate. Blue-Purple formazans were formed and the gel strip was scanned. For Complex IV activity, the gel strip was soaked in 50 mM potassium phosphate, pH 7.4 for 10 minutes and overlaid with 1 mg/ml diaminobenzidine and 1 mg/ml cytochrome *c*. Yellow-brown precipitates were produced after incubating gel strips at 30°C for 20 minutes and scanned. For Complex V activity, the gel strip was equilibrated in assay buffer (37 mM Tris, 270 mM Glycine, pH 8.3 and 14 mM $MgSO_4$,) for 10 minutes and overlaid with 8 mM ATP and 0.2 % lead nitrate. White colored precipitates were produced and the gel was scanned under a black background.

Aconitase Activity

Yeast cells grown in SD medium were washed once with ddH_2O and resuspended in lysis buffer (50 mM Tris-HCl, 50 mM KCl, 2 mM sodium citrate dihydrate, 10% glycerol, 1 mM PMSF, and 7 mM β-mercaptoethanol), and stored at –80°C for at least 2 hours. After thawing on ice, cells were homogenized by vortexing with glass beads and cleared lysate was collected by centrifugation. Aconitase activity was measured by coupling with $NADP^+$-dependent isocitrate dehydrogenase activity. 30 µl of crude lysate was mixed with 150 µl of reaction mixture (1 M Tris-Cl pH 8.0, 10 mM $MgCl_2$, 10 mM $NADP^+$, 0.32 units of $NADP^+$-dependent Isocitrate Dehydrogenase), and 10 µl of 50 mM citrate. The reaction mixture was recorded at 340nm for 2 minutes (15 sec intervals). Aconitase - specific activity was calculated by normalizing the activity with the Aconitase protein band intensity.

Hydrogen Peroxide Sensitivity Assay

Overnight cultures of the yeast strains indicated were diluted in fresh SD medium to 0.1 OD and grown for 0.5 day to 1 OD unit. Culture was aliquoted into 3 tubes, mixed with 0, 2.5 or 5 mM H_2O_2 and incubated at 30°C for 2 hours. Cells were harvested, washed once and resuspended in sterilized ddH_2O. Cell intensity was measure at 600nm and 5-fold serial dilutions starting from 0.5 OD was spotted on a SD plate and images were taken after 1 to 2 days of incubation at 30°C.

CCCP Sensitivity Assay

Wild-type and *rcf1* strains of the BY 4741 background were grown to log phase in YPD and harvested. Three hundred cells were plated on YPD plates containing the indicated amount of CCCP and incubated at 30°C. Colonies were counted after 48 hr.

Mammalian Cell Culture

C2C12 myoblasts (ATCC CRL-1772) were maintained in DMEM with 10% FBS, 2 mM Glutamax, and 1% Primocin solution (v/v Invivogen). All knockdowns were performed by treating cells with 20 nM total siRNA, using the Lipofectamine RNAiMax transfection reagent, according to the manufacturer's instructions (Invitrogen). The All-Stars non-targeting siRNA (Qiagen) was used as the control for siRNAs targeting *HIG1A* (NM_019814) and *HIG2A* (NM_025933), which were designed with the Dharmacon siDesign Center tool (http://www.dharmacon.com/designcenter/DesignCenterPage.aspx). Sequences of the sense strands of targeting siRNAs, which include a 3' tt DNA overhang, are as follows. *HIG1A*: (#1) CCAAAUUGUUAGUGACUGAtt and (#2) GGUCUAAGUUUAUUCGGAAtt. *HIG2A*: (#1) CCAGAGGGCUUUAAGGAAAtt, (#2) UCUUAAAGCGCCAUGGAAAtt, (#3) GUGAGGAAGUGGCCGAUUUtt, and (#4) AGGAAAAGUUUAUUCGCAAtt. Cells were subjected to knockdown on day zero, again on day 3, and analyzed on day 6. Total RNA was isolated with the RNeasy Mini Kit (Qiagen) and reverse transcribed to cDNA using the High Capacity cDNA Reverse Transcription Kit

(Applied Biosystems). Quantitative PCR (qPCR) was performed on cDNA with a Roche 480 LightCycler using the LightCycler 480 SYBR Green 1 Master mix.

Supplemental References

1. Boldogh, I.R., and Pon, L.A. (2007). Purification and subfractionation of mitochondria from the yeast Saccharomyces cerevisiae. Methods Cell Biol *80*, 45-64.

2. Wittig, I., Karas, M., and Schagger, H. (2007). High resolution clear native electrophoresis for in-gel functional assays and fluorescence studies of membrane protein complexes. Mol Cell Proteomics *6*, 1215-1225.

Supplemental Figure 1

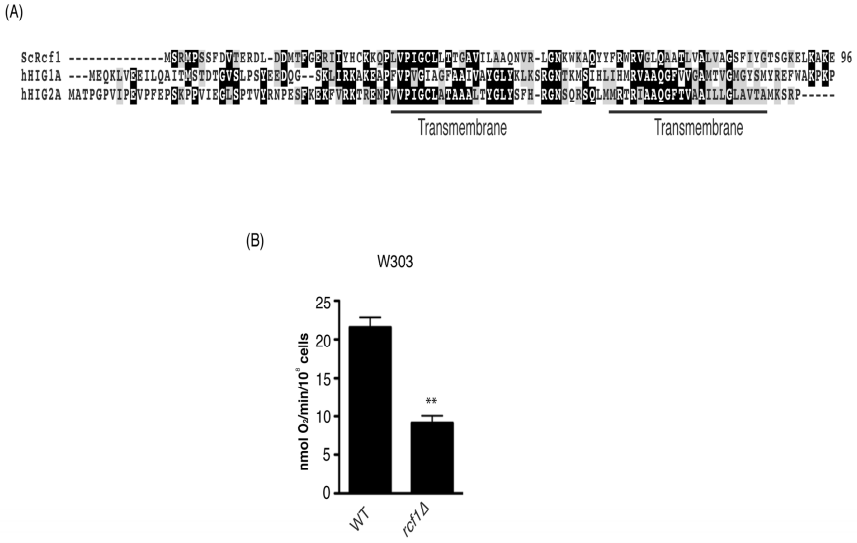

Figure S1. *RCF1* Is Evolutionarily Conserved and Important for Respiration, Related to Figure 1

(A) Protein sequence alignment of the yeast Rcf1 and human Hig1A and Hig2A. Predicted transmembrane domains are indicated. Yeast Rcf1 is depicted only through residue 96 although it has additional C-terminal residues.

(B) Rate of oxygen consumption of the wild-type and *rcf1Δ* mutant strains (W303 background) grown in glucose media was measured. Data shown is representative of three independent experiments and mean + standard deviation (SD) is shown.

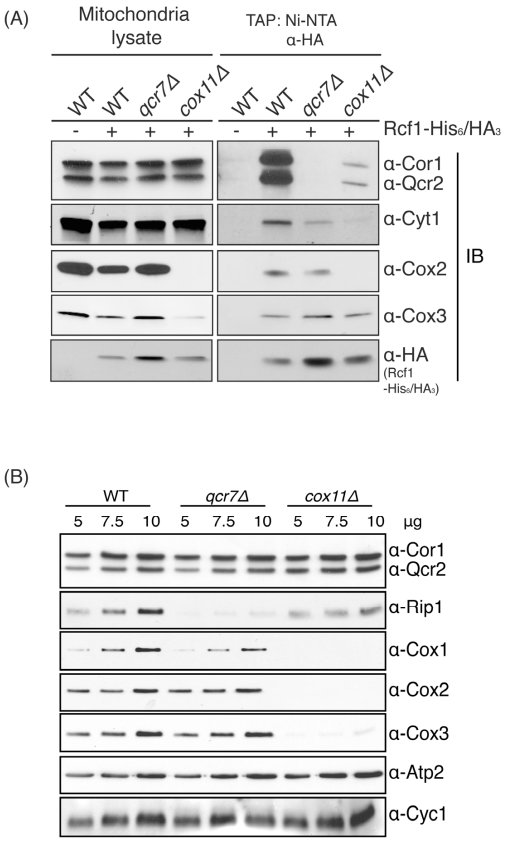
(A)
Mitochondria lysate
TAP: Ni-NTA α-HA
WT
WT
qcr7Δ
cox11Δ
WT
WT
qcr7Δ
cox11Δ
- + + + - + + +
Rcf1-His6/HA3
α-Cor1
α-Qcr2
α-Cyt1
α-Cox2
α-Cox3
α-HA
(Rcf1 -His6/HA3)
IB
(B)
WT
qcr7Δ
cox11Δ
5 7.5 10 5 7.5 10 5 7.5 10 μg
α-Cor1
α-Qcr2
α-Rip1
α-Cox1
α-Cox2
α-Cox3
α-Atp2
α-Cyc1

Figure 2. Rcf1 Interacts Independently with Subunits of Complex III and IV, Related to Figure 3

(A) Rcf1-His_6/HA_3 was subjected to two-step purification by Ni-NTA beads and anti-HA antibody conjugated agarose from wild-type and the indicated mutant strains. Rcf1-His_6/HA_3 was eluted by HA peptide under native conditions and subjected to TCA precipitation. Five percent of crude lysate and the final eluate were immunoblotted by anti-Cor1&Qcr2, Cyt1, Cox2, Cox3 and HA antibodies. (B) Steady-state OXPHOS subunits were detected using mitochondria extracted from the wild-type, *qcr7*Δ and *cox11*Δ mutant strains from (A).

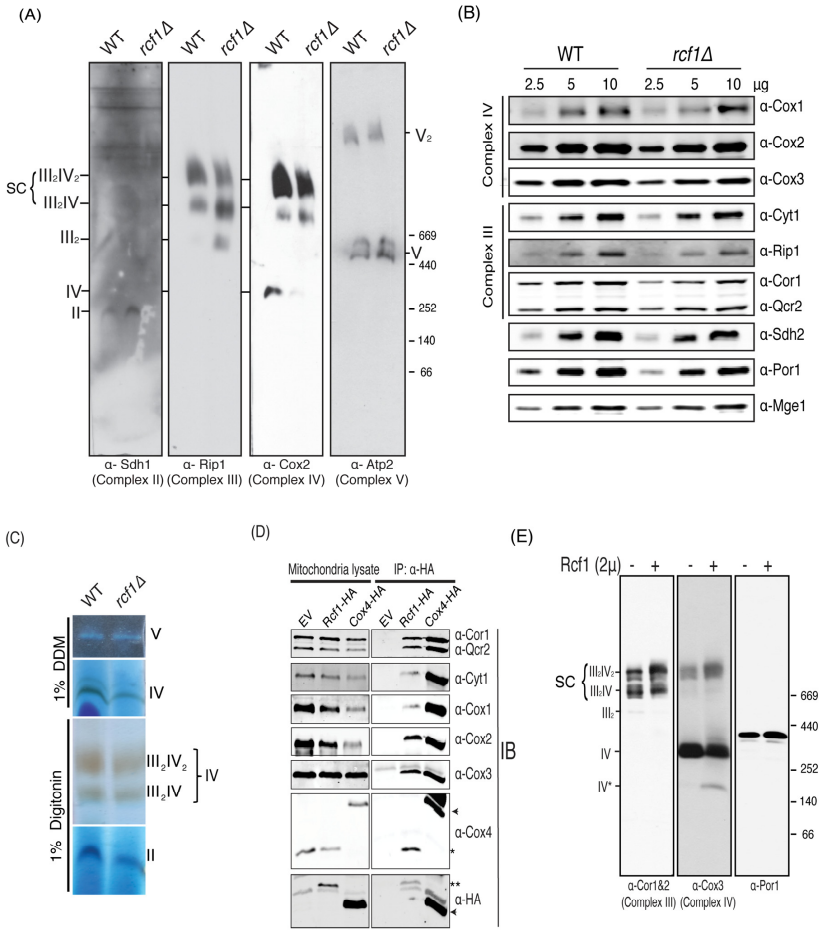
(A)
WT
rcf1Δ
SC
III2IV2
III2IV
III2
IV
II
V2
V
669
440
252
140
66
α- Sdh1 (Complex II)
α- Rip1 (Complex III)
α- Cox2 (Complex IV)
α- Atp2 (Complex V)
(B)
WT
rcf1Δ
2.5 5 10 2.5 5 10 µg
Complex IV
Complex III
α-Cox1
α-Cox2
α-Cox3
α-Cyt1
α-Rip1
α-Cor1
α-Qcr2
α-Sdh2
α-Por1
α-Mge1
(C)
WT
rcf1Δ
1% DDM
1% Digitonin
V
IV
III2IV2
III2IV
IV
II
(D)
Mitochondria lysate
IP: α-HA
EV
Rcf1-HA
Cox4-HA
α-Cor1
α-Qcr2
α-Cyt1
α-Cox1
α-Cox2
α-Cox3
α-Cox4
α-HA
IB
(E)
Rcf1 (2µ) - + - + - +
SC
III2IV2
III2IV
III2
IV
IV*
669
440
252
140
66
α-Cor1&2 (Complex III)
α-Cox3 (Complex IV)
α-Por1

Figure S3. Rcf1 Plays a Role in Maintaining the Integrity of Respiratory Supercomplexes, Related to Figure 4

(A) Mitochondria extracted from the wild-type and *rcf1* Δ mutant grown in 1% dextrose synthetic media to stationary phase were solubilized in 1% digitonin and resolved by BN-PAGE. Complex II, Complex III and Complex IV were immunoblotted by anti-Sdh1, Rip1 and Cox2 antibodies, respectively. Complex V immunoblotted by anti-Atp2 antibody is shown as a loading control.

(B) Crude mitochondria isolated from wild-type and the *rcf1Δ* mutant strains of (A) was resolved on SDS-PAGE and immunoblotted by Complex IV antibodies against Cox1, Cox2 and Cox3; Complex III antibodies against Cor1&Qcr2, Cyt1 and Rip1; and Complex II antibody against Sdh2. Por1 and Mge1 were shown as loading controls.

(C) The enzymatic activities of Complex II, IV, and V (ATP synthase) were assayed by in-gel activity assay of the WT and *rcf1*Δ mitochondria harvested from yeast cells grown in 1% dextrose synthetic media to stationary phase.

(D) Mitochondria from strains expressing EV, Rcf1-HA or Cox4-HA in place of the endogenous gene were solubilized in 0.8% digitonin and immunoprecipitated by anti-HA antibodies. Both 1% mitochondrial lysate and the final eluate were analyzed by immunoblot. Arrowheads indicate HA-tagged Cox4. Asterisk (*) indicates non-tagged Cox4. Double asterisk (**) indicates HA-tagged Rcf1.

(E) Mitochondria harvested from the wild-type strain harboring either EV or a 2μ plasmid overexpressing Rcf1 grown to early stationary phase were solubilized in 1% digitonin and resolved by BN-PAGE. Complex III, Complex IV and porin complex were immunoblotted by anti-Cor1&Qcr2, Cox3 and Por1 antibodies, respectively. IV* indicates a Complex IV intermediate.

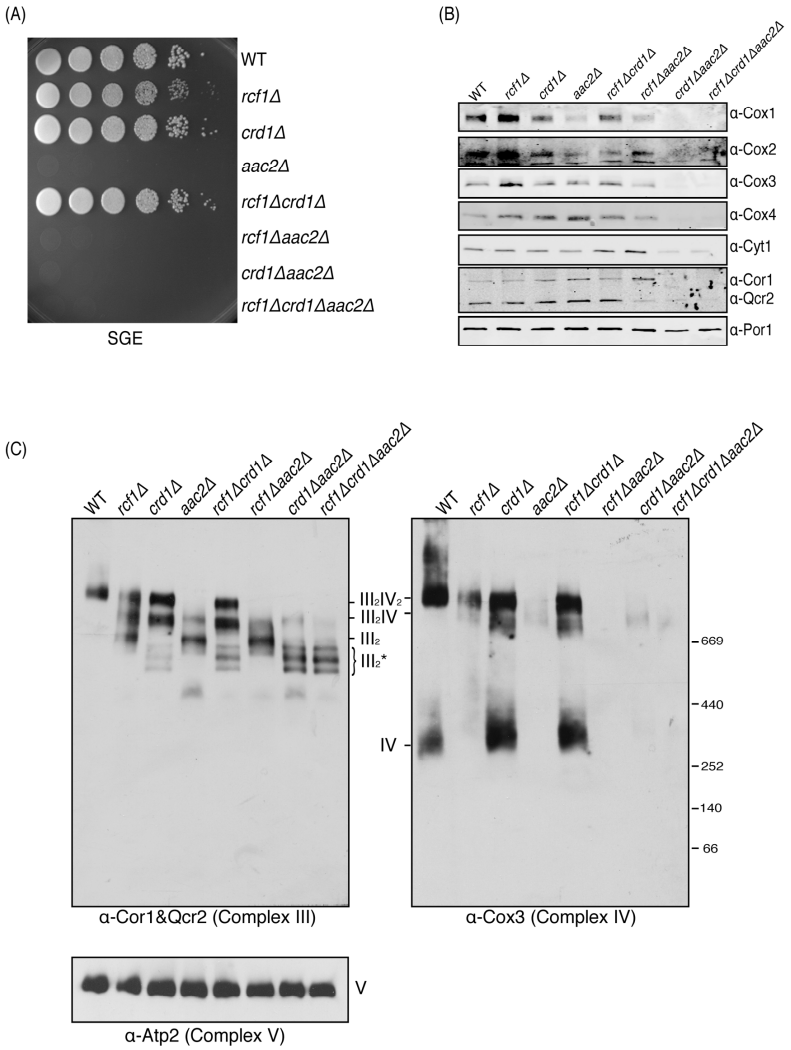
(A)
WT
rcf1Δ
crd1Δ
aac2Δ
rcf1Δcrd1Δ
rcf1Δaac2Δ
crd1Δaac2Δ
rcf1Δcrd1Δaac2Δ
SGE
(B)
WT
rcf1Δ
crd1Δ
aac2Δ
rcf1Δcrd1Δ
rcf1Δaac2Δ
crd1Δaac2Δ
rcf1Δcrd1Δaac2Δ
α-Cox1
α-Cox2
α-Cox3
α-Cox4
α-Cyt1
α-Cor1
α-Qcr2
α-Por1
(C)
III2IV2
III2IV
III2
III2*
IV
669
440
252
140
66
α-Cor1&Qcr2 (Complex III)
α-Cox3 (Complex IV)
V
α-Atp2 (Complex V)

Figure S4. *RCF1* Genetically Interacts with Aac2 to Stabilize Respiratory Supercomplexes, Related to Figure 5

(A) The wild-type and mutant strains were grown in YPAD medium to log phase and 5-fold serial dilutions of each culture were spotted on a synthetic glycerol/ethanol plate and incubated at 30°C for 3 days.

(B) Steady-state OXPHOS subunits were immunodetected from the wild-type and *rcf1*Δ mutant strains grown in synthetic raffinose media as in Figure 5C.

(C) The wild type and mutant strains were grown in YPAD medium for 3 days to reach stationary phase. Purified mitochondria from these strains were solubilized by 1% digitonin and resolved by BN-PAGE. Complex III, Complex IV and Complex V were immunoblotted by anti-Cor1&Qcr2, Cox3 and Atp2 antibodies, respectively. III* indicates Complex III intermediates.

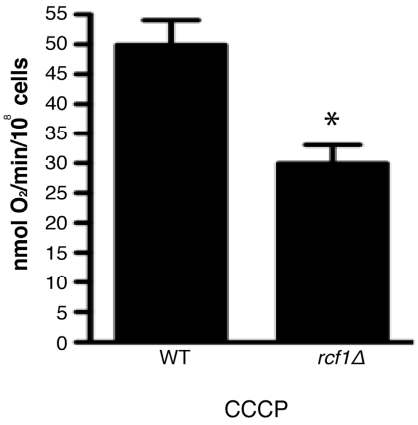
55
50
45
40
35
30
25
20
15
10
5
0
nmol O2/min/10^8 cells
*
WT
rcf1Δ
CCCP

Figure S5. Deletion of *RCF1* Is Susceptible to Oxidative Stress, Related to Figure 6

Rate of oxygen consumption of the wild-type and *rcf1Δ* of the BY4741 background was measure in the presence of 1 μM CCCP. Mean ± SD of three independent cultures is shown. *, P<0.05

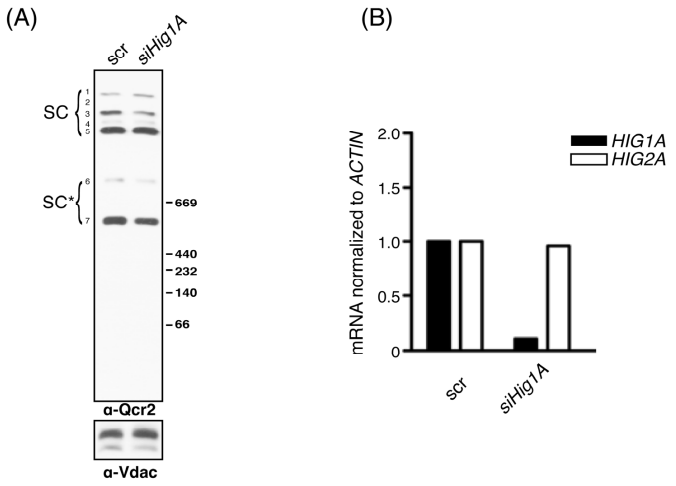
(A)
scr
siHig1A
SC
1
2
3
4
5
SC*
6
7
669
440
232
140
66
α-Qcr2
α-Vdac
(B)
mRNA normalized to ACT1N
2.0
1.5
1.0
0.5
0
HIG1A
HIG2A
scr
siHig1A

Figure S6. Hig2A Is Critical in Maintaining Respiratory Supercomplexes, Related to Figure 7

(A) Mitochondria extracted from C2C12 cells transfected with either scrambled (scr) or *HIG1A*-targeted siRNA were solubilized in 2% digitonin and resolved by BN-PAGE, followed by immunoblotting with anti-Qcr2 to detect Complex III. Respiratory complex species are indicated following the convention of (Acin-Perez et al., 2008), specifically: 1 (I+III+V); 2 (I+II+III+IV); 3 (I+II+III+IV); 4 (I+III+IV); 5 (I+III+V); 6 (III+IV); 7 (III+IV)*. (B) *HIG1A* and *HIG2A* mRNA level normalized to *ACTIN* was measured from cells in (A) using quantitative RT-PCR.

Table S1. Rcf1-Associated Proteins upon Digitonin and DDM Treatment

		Digitonin	DDM
Complex II	Sdh1	Y	Y
	Sdh2	Y	Y
	Sdh3	Y	N.D.
	Sdh4	Y	N.D.
Complex III	Cor1	Y	N.D.
	Qcr2	Y	N.D.
	Cyt1	Y	N.D.
	Rip1	Y	N.D.
	Qcr7	Y	N.D.
	Qcr8	Y	N.D.
	Qcr9	Y	N.D.
	Qcr10	Y	N.D.
Complex IV	Cox1	Y	Y
	Cox2	Y	Y
	Cox4	Y	Y
	Cox5A	Y	Y
	Cox5B	Y	Y
	Cox6	Y	Y
	Cox7	Y	Y
	Cox9	Y	Y
	Cox13	Y	Y
Other	Aac2	Y	N.D.

Table S2. Yeast Strains Used in This Study

Strains	Genotype	Source
WT (W303)	*Mat A his3 leu2 lys2 met15 trp1 ura3*	David Stillman
rcf1Δ	*Mat A his3 leu2 lys2 met15 trp1 ura3 rcf1::kanMX4*	This study
crd1Δ	*Mat A his3 leu2 lys2 met15 trp1 ura3 crd1::kanMX4*	This study
aac2Δ	*Mat A his3 leu2 lys2 met15 trp1 ura3 aac2::natMX4*	This study
rcf1Δcrd1Δ	*Mat A his3 leu2 lys2 met15 trp1 ura3 rcf1::hphMX4 crd1::kanMX4*	This study
rcf1Δaac2Δ	*Mat A his3 leu2 lys2 met15 trp1 ura3 rcf1::hphMX4 aac2::natMX4*	This study
rcf1Δcrd1Δaac2Δ	*Mat A his3 leu2 lys2 met15 trp1 ura3 rcf1::hphMX4 crd1::kanMX4 aac2::natMX4*	This study
qcr7Δ	*Mat A his3 leu2 lys2 met15 trp1 ura3 qcr7::natMX4*	This study
cox11Δ	*Mat A his3 leu2 lys2 met15 trp1 ura3 cox11::kanMX4*	This study
cyt1Δ	*Mat A his3 leu2 lys2 met15 trp1 ura3 cyt1::kanMX4*	This study
pet494Δ	*Mat A his3 leu2 lys2 met15 trp1 ura3 pet494::kanMX4*	This study
mss51Δ	*Mat A his3 leu2 lys2 met15 trp1 ura3 mss51::kanMX4*	This study
cox6Δ	*Mat A his3 leu2 lys2 met15 trp1 ura3 cox6::hphMX4*	Jin-Mi Heo
sod2Δ	*Mat A his3 leu2 lys2 met15 trp1 ura3 sod2::kanMX4*	This study
cox13Δ	*Mat A his3 leu2 lys2 met15 trp1 ura3 cox13::kanMX4*	This study
rcf1 cox13	*Mat A his3 leu2 lys2 met15 trp1 ura3 cox13::kanMX4 rcf1::hphMX4*	This study
cox4Δ	*Mat A his3 leu2 lys2 met15 trp1 ura3 Cox4::kanMX4*	This study
cox7Δ	*Mat A his3 leu2 lys2 met15 trp1 ura3 Cox7::kanMX4*	This study

rcf1Δ pRCF1	*Mat A his3 leu2 lys2 met15 trp1 ura3 rcf1::kanMX4* pRS416-RCF1-GFP, pRS414-mtRFP	This study
rcf1Δ pRCF1	*Mat A his3 leu2 lys2 met15 trp1 ura3 rcf1::kanMX4* pRS416-RCF1-His_6/HA_3	This study
rcf1Δ pRCF1 (2μ)	*Mat A his3 leu2 lys2 met15 trp1 ura3 rcf1::kanMX4* pRS426-RCF1	This study
qcr7Δ pRCF1	*Mat A his3 leu2 lys2 met15 trp1 ura3 qcr7::natMX4* pRS416-RCF1-His_6/HA_3	This study
cox11Δ pRCF1	*Mat A his3 leu2 lys2 met15 trp1 ura3 cox11::kanMX4* pRS416-RCF1-His_6/HA_3	This study
cyt1Δ pRCF1	*Mat A his3 leu2 lys2 met15 trp1 ura3 cyt1::kanMX4* pRS416-RCF1-His_6/HA_3	This study
pet494Δ pRCF1	*Mat A his3 leu2 lys2 met15 trp1 ura3 pet494::kanMX4* pRS416-RCF1-His_6/HA_3	This study
cox7Δ pRCF1	*Mat A his3 leu2 lys2 met15 trp1 ura3 cox7::kanMX4* pRS416-RCF1-His_6/HA_3	This study
cox4Δ pRCF1	*Mat A his3 leu2 lys2 met15 trp1 ura3 cox4::kanMX4* pRS416-RCF1-His_6/HA_3	This study
cox4Δ pCOX4	*Mat A his3 leu2 lys2 met15 trp1 ura3 cox4::kanMX4* pRS416-Cox4-His_6/HA_3	This study
cox13Δ pRCF1	*Mat A his3 leu2 lys2 met15 trp1 ura3 Cox13::kanMX4* pRS416-RCF1-His_6/HA_3	This study
mss51Δ pRCF1	*Mat A his3 leu2 lys2 met15 trp1 ura3 mss51::kanMX4* pRS416-RCF1-His_6/HA_3	This study
cox6Δ pRCF1	*Mat A his3 leu2 lys2 met15 trp1 ura3 cox6::hphMX4* pRS416-RCF1-His_6/HA_3	This study
WT (BY4741)	*Mat A his3 leu2 met15 ura3*	Open Biosystems

rcf1Δ (BY4741)	*Mat A his3 leu2 met15 ura3 rcf1::kanMX4*	Open Biosystems

CHAPTER 3

MSP1/ATAD1 MAINTAINS MITOCHONDRIAL FUNCTION BY FACILITATING THE DEGRADATION OF MISLOCALIZED TAIL-ANCHORED PROTEINS

Yu-Chan Chen, George K. E. Umanah, Noah Dephoure, Shaida A. Andrabi, Steven P. Gygi, Ted M. Dawson, Valina L. Dawson and Jared Rutter

Reprinted from EMBO Press, Vol. 33(14), pp. 1548-1564.

Published online: May 19, 2014

Article

SOURCE DATA | TRANSPARENT PROCESS

THE EMBO JOURNAL

Msp1/ATAD1 maintains mitochondrial function by facilitating the degradation of mislocalized tail-anchored proteins

Yu-Chan Chen[1], George K E Umanah[2,3], Noah Dephoure[4], Shaida A Andrabi[2,3], Steven P Gygi[4], Ted M Dawson[2,3,5,6], Valina L Dawson[2,3,5,7] & Jared Rutter[1,*]

Abstract

The majority of ER-targeted tail-anchored (TA) proteins are inserted into membranes by the Guided Entry of Tail-anchored protein (GET) system. Disruption of this system causes a subset of TA proteins to mislocalize to mitochondria. We show that the AAA+ ATPase Msp1 limits the accumulation of mislocalized TA proteins on mitochondria. Deletion of *MSP1* causes the Pex15 and Gos1 TA proteins to accumulate on mitochondria when the GET system is impaired. Likely as a result of failing to extract mislocalized TA proteins, yeast with combined mutation of the *MSP1* gene and the GET system exhibit strong synergistic growth defects and severe mitochondrial damage, including loss of mitochondrial DNA and protein and aberrant mitochondrial morphology. Like yeast Msp1, human ATAD1 limits the mitochondrial mislocalization of PEX26 and GOS28, orthologs of Pex15 and Gos1, respectively. GOS28 protein level is also increased in *ATAD1*$^{-/-}$ mouse tissues. Therefore, we propose that yeast Msp1 and mammalian ATAD1 are conserved members of the mitochondrial protein quality control system that might promote the extraction and degradation of mislocalized TA proteins to maintain mitochondrial integrity.

Keywords AAA+ ATPase; Guided Entry of Tail-anchored protein; mitochondrial protein quality control; tail-anchored proteins

Subject Categories Membrane & Intracellular Transport; Metabolism

DOI 10.15252/embj.201487943 | Received 19 January 2014 | Revised 22 April 2014 | Accepted 24 April 2014 | Published online 19 May 2014

The EMBO Journal (2014) 33: 1548–1564

See also: **RS Hedge** (July 2014)

Introduction

Tail-anchored (TA) proteins are a distinct subset of membrane proteins, which are uniquely characterized by a single transmembrane domain (TMD) at the C-terminus with the majority of the protein extending into the cytoplasm. They play critical roles in a variety of cellular processes including intracellular trafficking (e.g., all SNARE proteins), protein translocation and maturation (e.g., Sec61β, Tom5, Tom6, Tom7, and Tom22), apoptosis (e.g., Bcl2 family), organelle ultrastructure (e.g., Fis1), and metabolism (e.g., CPT1, Cyb5) (Wattenberg & Lithgow, 2001; Borgese *et al*, 2003). The majority of TA proteins are targeted to two distinct membrane systems: the mitochondrial outer membrane and the ER membrane from where TA proteins can be subsequently sorted to the nuclear envelope, Golgi complex, peroxisome, vacuole/lysosome, and plasma membrane, probably by vesicle-mediated trafficking (Kutay *et al*, 1995).

The topology of TA proteins precludes them from being targeted by the canonical co-translational signal recognition particle pathway that is used by the vast majority of membrane proteins (Kutay *et al*, 1995; Steel *et al*, 2002; Yabal *et al*, 2003; Brambillasca *et al*, 2005). Instead, a post-translational targeting system, GET (Guided Entry of Tail-anchored proteins), or TRC (TMD Recognition Complex) in *Saccharomyces cerevisiae* (yeast) or mammals, respectively, chaperones newly synthesized TA proteins and mediates their insertion into the ER membrane (Stefanovic & Hegde, 2007; Schuldiner *et al*, 2008; Hegde & Keenan, 2011; Denic, 2012). The mechanism whereby TA proteins are targeted and inserted into mitochondria has not yet been determined. In yeast, the GET system starts with capture of the nascent TA protein by the pre-targeting subcomplex composed of Get4, Get5, and Sgt2 (Jonikas *et al*, 2009; Wang *et al*, 2010). Via interaction with Get4, Get3 binds the cargo protein complex and binds the TA protein by directly associating with the TMD (Chartron *et al*, 2010; Wang *et al*, 2010). Through docking of

1 Department of Biochemistry, University of Utah School of Medicine, Salt Lake City, UT, USA
2 Neuroregeneration and Stem Cell Programs, Institute for Cell Engineering, Johns Hopkins University School of Medicine, Baltimore, MD, USA
3 Department of Neurology, Johns Hopkins University School of Medicine, Baltimore, MD, USA
4 Department of Cell Biology, Harvard Medical School, Boston, MA, USA
5 Solomon H. Snyder Department of Neuroscience, Johns Hopkins University School of Medicine, Baltimore, MD, USA
6 Departments of Pharmacology and Molecular Sciences, Johns Hopkins University School of Medicine, Baltimore, MD, USA
7 Department of Physiology, Johns Hopkins University School of Medicine, Baltimore, MD, USA
*Corresponding author. Tel: +1 801 581 3340; Fax: +1 801 581 7959; E-mail: rutter@biochem.utah.edu

Published online: May 19, 2014

Get3 onto the ER membrane receptor, a Get1/Get2 heterodimer, the TA protein is then released and properly inserted (Schuldiner *et al*, 2008; Wang *et al*, 2010; Mariappan *et al*, 2011). However, the fidelity of protein targeting is not perfect, and when it is impaired by mutation (e.g., of the GET system), TA proteins mislocalize to the cytosol or mitochondria (e.g., peroxisomal Pex15 and ER Ubc6) (Schuldiner *et al*, 2008; Jonikas *et al*, 2009). To this end, a protein quality control system has evolved to clear TA protein aggregates from the cytosol (Hessa *et al*, 2011). We hypothesized that a parallel system evolved to clear TA proteins that have mislocalized to the mitochondria and constituted a threat to mitochondrial function.

The mitochondrion is a complex organelle that performs functions that are fundamental to many aspects of cell biology. Therefore, failure or dysregulation of this organelle is associated with many forms of human disease. This includes cancer (Kroemer & Pouyssegur, 2008), diabetes (Patti & Corvera, 2010), neurodegenerative disease (Lessing & Bonini, 2009), and others (Lopez-Armada *et al*, 2013; Lopez-Otin *et al*, 2013). This critical importance necessitates that cells employ a multi-tiered quality control system to maintain the integrity of mitochondria (Rugarli & Langer, 2012). One line of defense consists of intra-mitochondrial proteases that enable the degradation of misfolded or damaged proteins. Among them, two AAA+ (ATPase Associated with various cellular Activities) proteases, *m*-AAA and *i*-AAA, enforce protein quality in the matrix and inter-membrane space compartments, respectively (Gerdes *et al*, 2012; Janska *et al*, 2013). They are characterized by a AAA+ domain that, in most cases, oligomerizes to form a channel to unfold protein substrates using the energy derived from ATP hydrolysis. Unfolded polypeptides are subsequently degraded by an associated proteolytic domain (Sauer & Baker, 2011). Mutations affecting these proteases cause a plethora of phenotypes in yeast, including respiratory deficiency, loss of mitochondrial DNA (mtDNA), altered mitochondrial morphology, and decreased chronological lifespan (Thorsness *et al*, 1993; Campbell *et al*, 1994; Janska *et al*, 2013). Cells employ a related quality control system on the mitochondrial outer membrane, which enables the extraction and proteasomal degradation of proteins exposed to the cytosol (Taylor & Rutter, 2011). This system appears to also utilize the AAA+ ATPase, Cdc48 in yeast or p97 in mammals, for protein extraction prior to engagement of the proteasome (Heo *et al*, 2010; Tanaka *et al*, 2010; Xu *et al*, 2011). When mitochondria depolarize, cells initiate the autophagic degradation of mitochondria or mitophagy as a second line of defense (Youle & Narendra, 2011; Ashrafi & Schwarz, 2013). In animals, neurons seem to be particularly sensitive to the presence of damaged mitochondria. An increasing number of neurodegenerative diseases, including spastic paraplegia, spinocerebellar ataxia, Parkinson's disease, Alzheimer's disease, and peripheral neuropathies, are linked with defective mitochondrial quality control systems (Rugarli & Langer, 2012).

As a result of our ongoing project to functionally annotate the mitochondrial proteome (Hao *et al*, 2009; Heo *et al*, 2010; Bricker *et al*, 2012; Chen *et al*, 2012), we here describe the previously unknown function of Ygr028 (or Msp1) in yeast and ATAD1 (also known as Thorase) in mammals, which are mitochondrial members of the AAA+ family of proteins (Zhang *et al*, 2011). Our data suggest that they are components of the mitochondrial protein quality control system and play a crucial role in degrading TA proteins that escape from the GET system to mislocalize to mitochondria. Depletion of Msp1 in yeast or ATAD1 in human cells and mice leads to ectopic accumulation of a subset of TA proteins that mislocalize to mitochondria. We also showed that Msp1 and ATAD1 physically interact with these same mislocalized TA proteins. Finally, loss of this system causes severe mitochondria damage including respiratory deficiency, loss of mitochondria, and altered mitochondrial morphology. As a result, we hypothesize that Msp1 and ATAD1 are novel mitochondrial protein quality control components that might extract and facilitate the degradation of mislocalized TA proteins from the mitochondria.

Results

Msp1 is an evolutionarily conserved mitochondrial outer membrane protein

Protein sequence alignment and domain prediction of yeast Msp1, fly CG5395, mouse ATAD1, and human ATAD1 suggested that they all contain a transmembrane domain near the N-terminus and a highly conserved AAA+ domain toward the C-terminus (Fig 1A). Because yeast Msp1 was previously annotated as a mitochondrial protein (Nakai *et al*, 1993), we first confirmed its mitochondrial localization. We generated a yeast strain co-expressing a fully functional Msp1-GFP fusion protein from the native *MSP1* promoter and mitochondrial RFP (Mito-RFP) (see Supplementary Fig S2A; the construct fully complements the growth phenotype of the *get3*Δ *msp1*Δ mutant strain, which will be discussed in the next section and Fig 2). As shown in Fig 1B, we observed a nearly complete overlap of RFP and GFP, demonstrating mitochondrial localization of Msp1-GFP. We also observed extra-mitochondrial GFP puncta (marked by arrows), however, which we showed to be peroxisomes based on co-localization with an RFP protein fused with a peroxisomal targeting sequence (SKL) (Supplementary Fig S1A).

To determine in which mitochondrial compartment Msp1 resides, we performed a biochemical fractionation experiment using a strain expressing a fully functional Msp1-His_6-HA_3 fusion protein from the native *MSP1* promoter (see Supplementary Fig S2A). Msp1 was absent from the post-mitochondria supernatant, but present in purified mitochondria. When we subjected intact, hypotonically swollen or Triton X-100 lysed mitochondria to Proteinase K digestion, Msp1 was completely degraded in all three situations, like the mitochondrial outer membrane protein Fzo1 (Fig 1C). Furthermore, similar to Om45 and Por1, both integral mitochondrial membrane proteins, neither high salt nor alkaline carbonate extracted Msp1 from mitochondria, suggesting that it is an integral mitochondrial outer membrane protein (Fig 1D).

To confirm that the mitochondrial localization of this protein family is conserved in higher eukaryotes, we established a number of human cell lines that stably express human ATAD1 (hATAD1) as a C-terminal GFP fusion. As shown in Fig 1E and Supplementary Fig S1B, the GFP signal overlapped with the mitochondrial fluorescent dye, Mitotracker Red. Consistent with yeast Msp1, we also observed that hATAD1-GFP localized to extra-mitochondrial puncta, which were verified to be peroxisomes by co-localization with a peroxisomal RFP marker (Supplementary Fig S1C). We also observed some cytoplasmic localization of ATAD1 (Supplementary Fig S1B and C). Taken together, the aforementioned data indicate

Published online: May 19, 2014
The EMBO Journal Mitochondrial tail-anchored protein removal *Yu-Chan Chen et al*

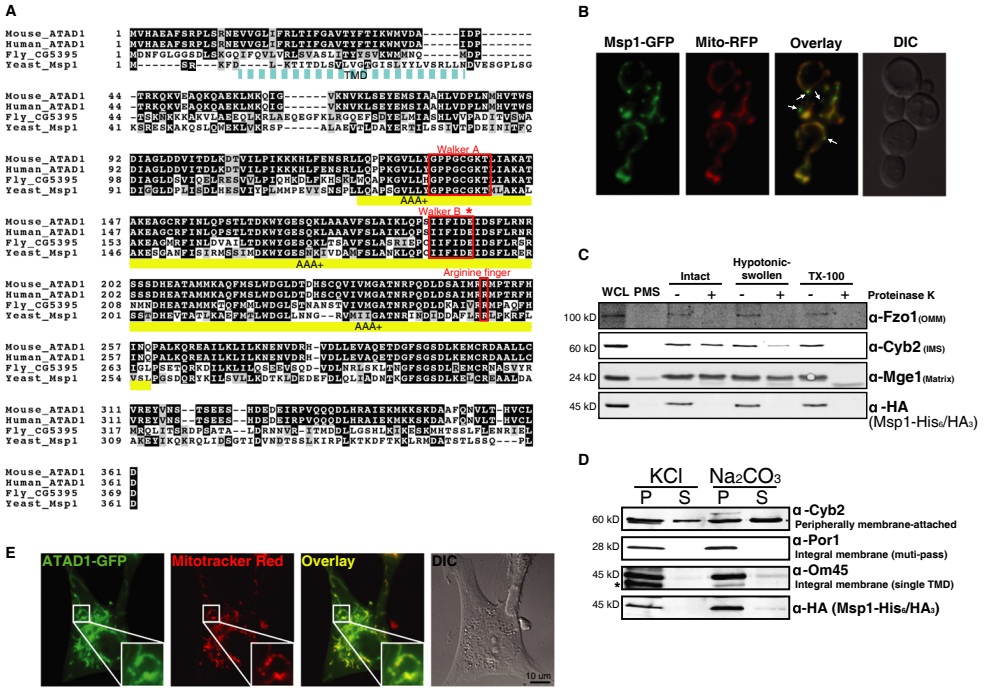

Figure 1. Msp1 is a conserved mitochondrial outer membrane protein.

A Protein sequence alignment and domain prediction of yeast, fly, mouse, and human homologs (SDSC Biology Workbench). The transmembrane domain (TMD) is marked by a dashed cyan box (dashed because the endpoints of the TMD are not clearly defined), and the AAA+ domain is marked by a yellow box. Glutamate 193 is indicated by an asterisk (*).

B Representative images of the *msp1*Δ mutant expressing Msp1-GFP and Mito-RFP. Yeast were grown to early log phase at 30°C in synthetic glucose (SD) medium and visualized by fluorescence microscopy. Peroxisomal Msp1-GFP signal is marked by arrows.

C Intact, hypotonically swollen and Triton X-100-solubilized mitochondria of the *msp1*Δ mutant expressing Msp1-His_6/HA_3 were treated with (+) or without (−) Proteinase K and analyzed by immunoblot with whole-cell lysate (WCL) and post-mitochondrial supernatant (PMS). Mge1, Cyb2, and Fzo1 are matrix, intermembrane space (IMS), and outer membrane proteins (OMM), respectively.

D Soluble (S) and pellet fraction (P) of the KCl- or Na_2CO_3-treated mitochondria purified from the strain described in (C) were analyzed by immunoblot. Cyb2 is a peripherally attached mitochondrial inner membrane protein; Por1 and Om45 are both integral outer membrane proteins. The asterisk (*) indicates a non-specific band.

E Human dermal fibroblasts (HDFs) stably expressing ATAD1-GFP were stained with Mitotracker Red and visualized by florescence microscopy.

Source data are available online for this figure.

that yeast Msp1 and human ATAD1 localize to multiple cellular compartments. Specifically, yeast Msp1 resides on the mitochondrial outer membrane, probably anchored via the N-terminal TMD, with the majority of the protein including the AAA+ domain exposed to cytosol. While Msp1 and hATAD1 might have important peroxisomal (or cytoplasmic for ATAD1) functions, this study will primarily focus on their roles in mitochondria.

The *msp1*Δ mutant exhibits synthetic growth and mitochondrial defects in combination with *GET* mutants

We generated yeast mutants lacking *MSP1*, which did not show any significant growth phenotype in regular laboratory growth conditions (Fig 2A). Two independent synthetic genetic array experiments, however, both suggested that an *msp1*Δ mutant exhibits a strong negative genetic interaction with *get2*Δ or *get3*Δ mutants (lacking critical components of the GET system), indicating that the growth of the double-mutant strain is more severely compromised than predicted from the phenotypes of the single knockouts (Costanzo *et al*, 2010; Hoppins *et al*, 2011). To verify these data, we generated *get2*Δ *msp1*Δ and *get3*Δ *msp1*Δ double-deletion strains and found that both double mutants showed more severe growth phenotypes than the single mutants when grown on glucose at 30°C, which was exacerbated at 37°C (Fig 2A, top panel). Both double mutants completely failed to grow on glycerol medium, which necessitates mitochondrial respiration for growth, whereas

Published online: May 19, 2014

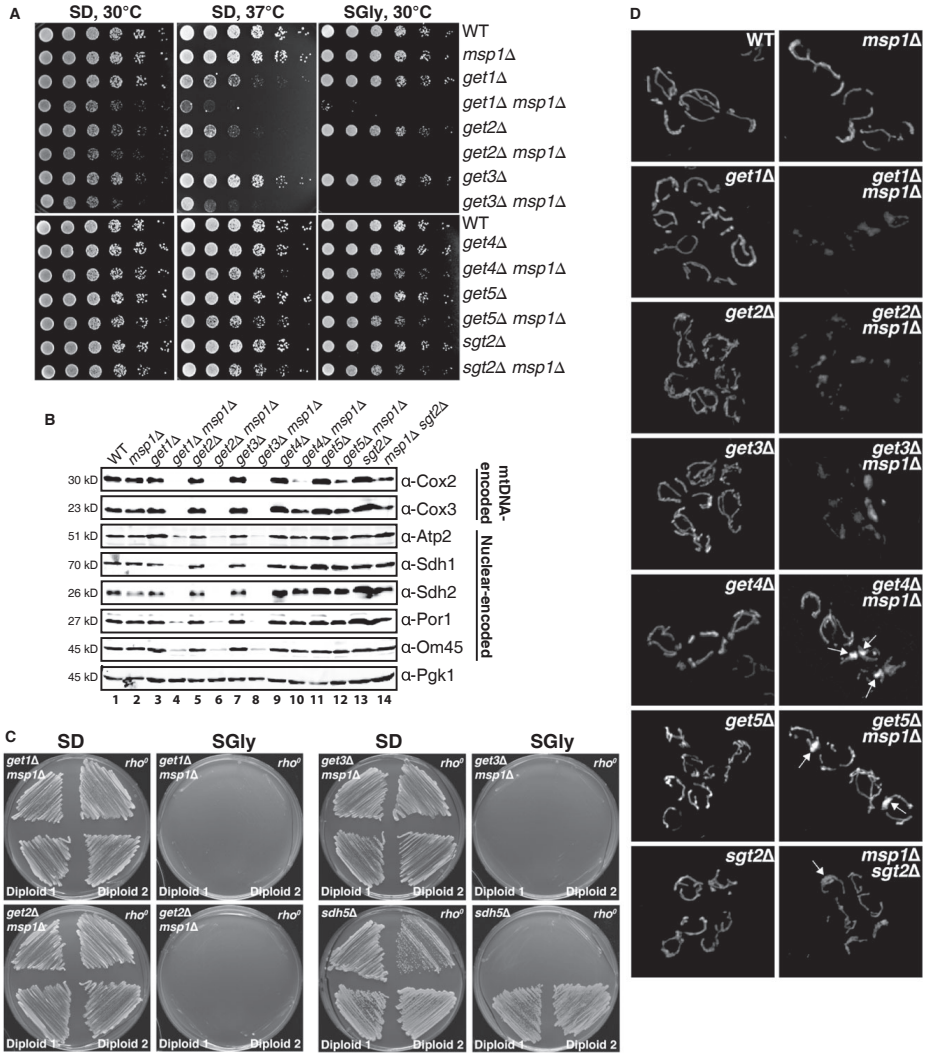

Figure 2. The *msp1Δ* mutant exhibits growth defects and severe mitochondria damage when combined with the *GET* mutants.

A Five-fold dilutions of the indicated yeast strains grown in SD medium were spotted on SD or synthetic glycerol plates (SGly) and incubated at 30 or 37°C.

B Whole-cell lysates of log-phase cultures harvested from synthetic raffinose medium were analyzed by immunoblot. Both mitochondrial and nuclear DNA-encoded mitochondrial proteins were immunoblotted. Pgk1 is a cytoplasmic control protein.

C The parental haploids and two independent diploids were streaked on SD and SGly plates and cultured at 30°C. The *sdh5Δ* strain is a control representing a respiratory deficient *rho*$^+$ strain.

D Representative images of the indicated yeast strains expressing the mito-RFP construct, grown in SD medium to log phase and visualized by fluorescence microscopy. Areas of atypical mitochondrial swelling are indicated by arrows (see also Supplementary Fig S2E). The RFP image intensity was adjusted to be similar for visualization purposes. Unadjusted images from similar exposure times are shown in Supplementary Fig S2F.

Source data are available online for this figure.

Published online: May 19, 2014
The EMBO Journal

all of the single mutants exhibited wild-type growth (Fig 2A, top panel). These growth phenotypes are fully rescued by plasmid expression of the native or C-terminally tagged Msp1 protein, but not by expression of the N-terminally tagged Msp1 protein (which presumably fails to localize to mitochondria) or $Msp1^{E193Q}$, which is predicted to lack ATPase activity (Supplementary Fig S2A and B). In fact, expression of the $Msp1^{E193Q}$ causes dominant-negative growth impairment when expressed in a *get3*Δ mutant (Supplementary Fig S2B). Given the functions of Get2 and Get3, it is reasonable to speculate that *MSP1* might have a similar genetic relationship with other *GET* genes including *GET1*, *GET4*, *GET5*, and *SGT2*. As expected, the synthetic growth phenotype of the *get1*Δ *msp1*Δ mutant is identical to that of the *get2*Δ *msp1*Δ and *get3*Δ *msp1*Δ double mutants (Fig 2A, top panel). The *get4*Δ *msp1*Δ, *get5*Δ *msp1*Δ, and *msp1*Δ *sgt2*Δ mutants exhibited modest synthetic growth defects, particularly on glycerol medium (Fig 2A, bottom panel). This is consistent with the published observations that Get1, Get2, and Get3 are more central players in the GET system, while Get4, Get5, and Sgt2 play a more auxiliary role (Jonikas *et al*, 2009).

The complete failure of *get1*Δ *msp1*Δ, *get2*Δ *msp1*Δ, and *get3*Δ *msp1*Δ mutants to grow on glycerol medium suggested that mitochondrial function might be impaired. To explore a potential mitochondrial phenotype further, we extracted whole-cell lysates from the wild-type (WT) and single and double mutants and immunoblotted for proteins that localize to different mitochondrial compartments (Fig 2B). We observed that the *get1*Δ *msp1*Δ, *get2*Δ *msp1*Δ, and *get3*Δ *msp1*Δ mutants were completely devoid of the mtDNA-encoded proteins, Cox2 and Cox3, and were severely depleted of all nuclear-encoded mitochondrial proteins examined, Atp2, Sdh1, Sdh2, Por1, and Om45 (Lane 4, 6, and 8). The other three double-mutant strains exhibited a partial depletion of some proteins, particularly those encoded by mtDNA (Lane 10, 12 and 14). The respiratory growth defect of the *get1*Δ *msp1*Δ, *get2*Δ *msp1*Δ, and *get3*Δ *msp1*Δ strains was also irreversible as transformation of an Msp1-expressing plasmid failed to restore the growth phenotype (Supplementary Fig S2C). We suspected that these double mutants might have lost their mitochondrial DNA and become rho^0. To directly test this, we employed a classic cross-complementation test and found that the strains lacking *MSP1* and one of the *GET* genes failed to complement the growth phenotype of a rho^0 tester strain on glycerol medium (Fig 2C). These data demonstrate that the *get1*Δ *msp1*Δ, *get2*Δ *msp1*Δ, and *get3*Δ *msp1*Δ strains lack functional mtDNA. While mtDNA depletion could explain the loss of mtDNA-encoded proteins, it causes a much less severe depletion of nuclear-encoded mitochondrial proteins (Supplementary Fig S2D).

Finally, we directly visualized mitochondria by expressing Mito-RFP in the WT and single- and double-mutant strains (Fig 2D). In addition to the expected observation that the mitochondrial RFP signal in the *get1*Δ *msp1*Δ, *get2*Δ *msp1*Δ, and *get3*Δ *msp1*Δ strains was much weaker than WT or the single mutants (Supplementary Fig S2F), we also found that they exhibited severely altered mitochondrial morphology. Again, the severity of the morphological changes cannot be explained by the lack of mtDNA, which has only modest effects on mitochondrial morphology (Supplementary Fig S2E). The *get4*Δ *msp1*Δ, *get5*Δ *msp1*Δ, and *msp1*Δ *sgt2*Δ strains did not have overt morphological changes, but did have some areas of apparent atypical mitochondrial swelling (marked by arrows, Fig 2D and Supplementary Fig S2G). In summary, we have found that the combined impairment of Msp1 and the GET system causes severe mitochondrial damage, including depletion of resident proteins, loss of the mitochondrial genome, and aberrant morphology.

Depletion of mammalian *ATAD1* causes mitochondrial damage

Because a large fraction of human ATAD1 localizes to mitochondria, we wanted to assess whether this mitochondrial function is also conserved in higher eukaryotes. We tested whether depletion of ATAD1 compromises mitochondrial function. First, we performed immunoblots on lysates from brain, which was previously shown to highly express *ATAD1*, of the WT and $ATAD1^{-/-}$ mice (Fig 3A and B) (Zhang *et al*, 2011). We observed a significant decrease of many mitochondrial proteins in the $ATAD1^{-/-}$ brain of both female and male mice. The diminished mitochondrial content is further supported by the decreased basal and mitochondrial respiratory capacity of the mouse embryonic fibroblasts (MEFs) lacking *ATAD1* (Fig 3C). Second, we also directly visualized mitochondrial morphology of $ATAD1^{-/-}$ MEFs. While WT MEFs exhibit tubular mitochondria, we observed that the mitochondria of $ATAD1^{-/-}$ MEFs were severely fragmented (Fig 3D). The same mitochondrial fragmentation was observed in *ATAD1* knockdown HeLa cells (Supplementary Fig S3). Therefore, we conclude that mammalian ATAD1, similar to yeast Msp1, plays an important role in mitochondrial function.

As a complementary test of the conservation of the mitochondrial function of the Msp1 protein family, we expressed human *ATAD1* and *Drosophila melanogaster CG5395* under control of the yeast *ADH1* promoter and found that they either partially or fully rescued the growth phenotype of the *get3*Δ *msp1*Δ mutant, respectively (Fig 3E). The glycerol growth defect was also particularly suppressed, suggesting that the mitochondrial role of this protein family spans across the eukaryotic kingdom.

Msp1/hATAD1 is required to minimize the level of the TA protein Pex15/PEX26 mislocalized to mitochondria

Potential mechanisms that might underlie the severe mitochondrial defects caused by combined loss of Msp1 and the GET system were not clear. One potential connection, however, was the previous observation that disruption of the GET system causes some TA proteins to aggregate in the cytoplasm and others to mislocalize to mitochondria (Schuldiner *et al*, 2008; Jonikas *et al*, 2009). Perhaps, loss of Msp1 causes mitochondria to be particularly sensitive to the damaging effects of TA protein mislocalization to mitochondria found upon impairment of the GET system. Considering that Msp1 is part of the AAA+ protein family that, in most cases, extracts, disassembles, or unfolds protein substrates, we hypothesized that Msp1 might extract TA proteins that mislocalize to mitochondria upon loss of the GET system. We tested this hypothesis for Pex15, a peroxisomal TA protein that mislocalizes to mitochondria upon disruption of the GET system (Schuldiner *et al*, 2008; Jonikas *et al*, 2009). Surprisingly, *msp1*Δ single mutants displayed significant mitochondrial localization of a GFP-Pex15 fusion, nearly identical to previous observations with the *get3*Δ single mutant (Fig 4A) (Schuldiner *et al*, 2008; Jonikas *et al*, 2009). Much of the Pex15

Published online: May 19, 2014

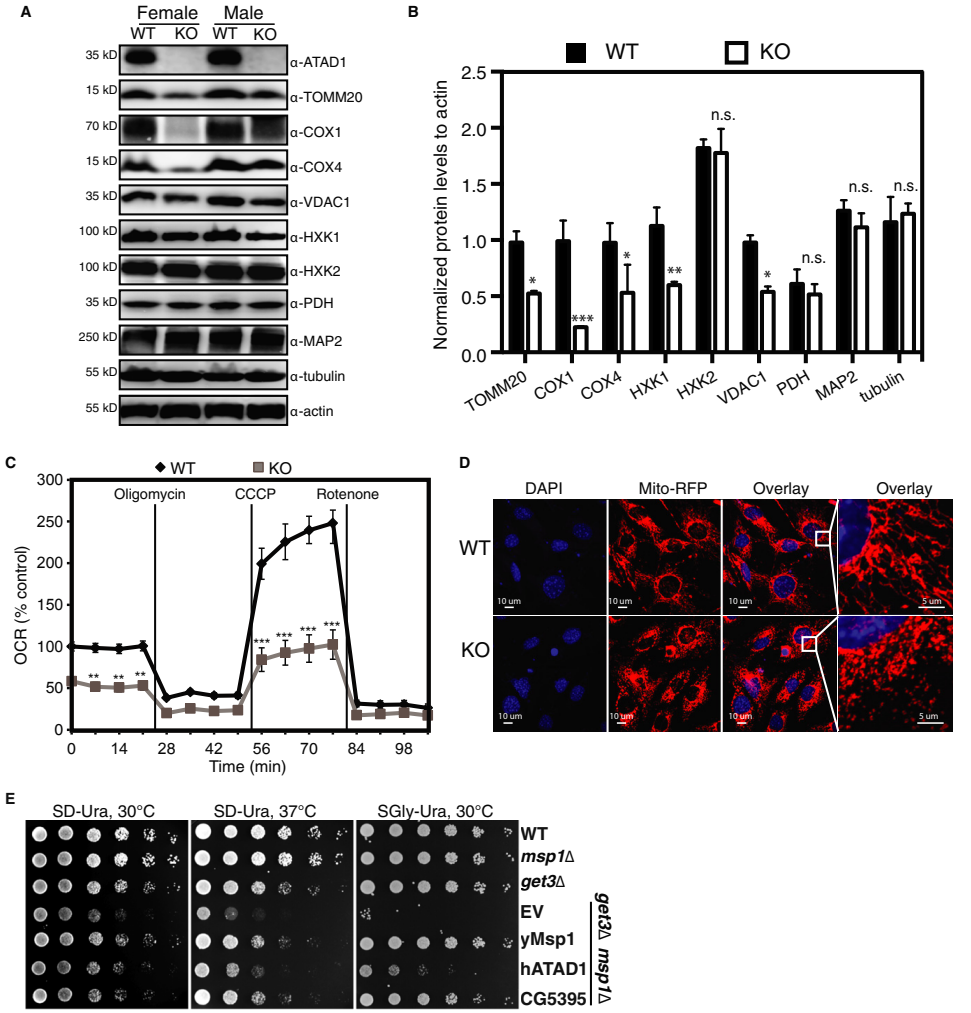

Figure 3. Depletion of *ATAD1* causes decreased mitochondrial protein level and mitochondrial fragmentation in mammals.

A Immunoblots of whole-brain lysates obtained from the wild-type (WT) and *ATAD1*$^{-/-}$ knockout (KO) mice. PDH, pyruvate dehydrogenase; HXK1 and 2, hexokinase 1 and 2.

B The optical densitometry quantification of (A). The values represent the mean ± SEM (n = 3, *P < 0.05, **P < 0.005, ***P < 0.001, one-way ANOVA, Tukey's multiple comparison tests).

C Oxygen consumption rate (OCR) of the WT and *ATAD1*$^{-/-}$ mouse embryonic fibroblasts (MEFs). The data were normalized to the amount of protein in each well and represent % control. **P < 0.005, ***P < 0.001.

D Representative images of the mitochondrial morphology of the WT and *ATAD1*$^{-/-}$ MEFs. The cells were transfected with Mito-RFP (red), stained with DAPI (blue), and visualized.

E Five-fold dilutions of the indicated strains harboring empty vector (EV), yeast Msp1, human ATAD1 or fly CG5395 construct cultured overnight in SD-Ura medium were spotted on SD-Ura or SGly-Ura plates and incubated at 30 or 37°C.

Source data are available online for this figure.

Published online: May 19, 2014
The EMBO Journal

protein continues to be targeted to peroxisomes in the single-mutant strains (Supplementary Fig S4A). In the *get3*Δ *msp1*Δ mutant, we observed more complete co-localization of the GFP and RFP signals, which can only be seen with greatly extended exposure time due to the diminished mitochondrial content in this mutant (Fig 4A; see also Fig 2B and D). We also performed the converse experiment by overexpressing Msp1 in the *get3*Δ mutant expressing GFP-Pex15 and observed complete depletion of mislocalized Pex15 from the mitochondria (Fig 4B).

We tested the possibility that Msp1 binds and perhaps extracts mislocalized Pex15. Given that the wild-type Msp1 protein may associate with substrates transiently, we performed co-immunoprecipitation experiments using yeast strains expressing a 'substrate trap' E193Q mutant (asterisk in Fig 1A), which is predicted to bind substrates but fail to release them efficiently (Weibezahn *et al*, 2003; Hanson & Whiteheart, 2005). Consistent with this notion, exogenous expression of $Msp1^{E193Q}$ was unable to rescue the growth defect of the *get3*Δ *msp1*Δ mutant; moreover, it induced a dominant-negative phenotype in the *get3*Δ single mutant (Supplementary Fig S2B). As shown in Fig 4C, we observed that when Pex15 was overexpressed, it stably interacted with $Msp1^{E193}$ particularly in the *get4*Δ mutant background. Note that we consistently observed higher accumulation of $Msp1^{E193Q}$ in spite of it being expressed under the endogenous *MSP1* promoter. This possibly also contributes to the apparent interaction affinity relative to wild-type Msp1. It is also noteworthy that Pex15 exhibits elevated accumulation in the *get4*Δ mutant expressing the dominant-negative $Msp1^{E193Q}$, possibly related to mislocalization and stabilization on mitochondria (Fig 4C–input panel).

If the severe phenotype of the *get3*Δ *msp1*Δ double mutant is due to accumulation of mislocalized TA proteins in the mitochondrial outer membrane, overexpression of proteins like Pex15 should exacerbate this phenotype. To test this, we compared growth upon overexpression of GFP-Pex15 from the *GAL1* promoter. While the *get3*Δ *msp1*Δ mutant exhibited impaired growth on its own, the *GAL1::PEX15* construct caused a complete loss of growth on galactose medium (Fig 4D). One possible mechanism whereby Msp1 might maintain a low level of mislocalized TA proteins is to extract them and facilitate their degradation. We tested the half-life of GFP-Pex15 utilizing the stringent glucose repression of new transcription from the *GAL1* promoter. We first noticed that the steady-state level of Pex15 was increased in the *msp1*Δ mutant compared to WT (t = 0 min, Supplementary Fig S4B). Furthermore, the time-course of Pex15 degradation was significantly slower in the *msp1*Δ mutant (Supplementary Fig S4B and C) most likely due to impaired extraction and degradation of mitochondrial Pex15. To more rigorously test whether Msp1 limits mitochondrial Pex15 by facilitating its degradation, we measured the half-life of Pex15 in the *get3*Δ mutant expressing either the wild-type Msp1 or mutant $Msp1^{E193Q}$ (Fig 4E, Supplementary Fig S4D and E). Therefore, in both cases, Pex15 is strongly mislocalized to mitochondria (t = 0 min, Supplementary Fig S4D). Pex15 is significantly more stable in the strain expressing $Msp1^{E193Q}$ (Fig 4E and Supplementary Fig S4E). When we visualized the localization of GFP-Pex15 throughout the time-course, we observed that mitochondrial Pex15 was degraded faster in the *get3*Δ mutant expressing the wild-type Msp1 compared to the $Msp1^{E193Q}$, which still retained significant mitochondrial Pex15 after 180 min (Supplementary Fig S4D). Taken together, these results suggest that Msp1 is required to minimize the abundance of the Pex15 TA protein on mitochondria, most likely by promoting its extraction and degradation.

We also tested whether hATAD1 functions similarly to protect mammalian mitochondria from the mislocalization of PEX26, the human ortholog of Pex15. We established a human hepatocellular carcinoma (HepG2) cell line stably expressing GFP-PEX26 and repeatedly observed very modest mitochondrial GFP localization in a minority of cells (Fig 4F-top; marked by arrows). Knockdown of *ATAD1* with three distinct siRNAs (Fig 4G), however, greatly increased the overlap of GFP-PEX26 and Mitotracker Red (Fig 4F). We also observed that the overall intensity of the mitochondrial GFP signal was significantly enhanced, consistent with increased steady-state level of PEX26 in the whole-cell lysates from multiple cell lines (Fig 4F and Supplementary Fig S4F). Taken together, both yeast Msp1 and human ATAD1 protein are important to minimize the mitochondrial mislocalization of the TA proteins, Pex15, and PEX26, respectively.

Figure 4. Yeast Msp1 and human ATAD1 are required to limit the level of mitochondrially mislocalized TA proteins Pex15 and PEX26, respectively.

A Representative images of GFP-Pex15 localization. The indicated yeast strains expressing GFP-Pex15 from the *GAL1* promoter and plasmid-borne Mito-RFP were grown overnight in SD medium, switched to galactose induction medium for 6 h, and visualized by fluorescence microscopy. The *get3*Δ *msp1*Δ images (1,000 ms) were exposed 5 times longer than the WT, *msp1*Δ, and *get3*Δ images (200 ms).

B The WT and *get3*Δ strain expressing GFP-Pex15 from the *GAL1* promoter and the plasmid-borne Mito-RFP were transformed with either EV or a Msp1 overexpressing construct ($Msp1_{(2\mu)}$) and subjected to the same procedure as described in (A).

C Pex15 co-immunoprecipitates with the 'trap mutant' $Msp1^{E193Q}$. Msp1 was immunoprecipitated by anti-HA antibodies from digitonin-solubilized mitochondria that were extracted from the indicated strains overexpressing GFP-Pex15 from the *GAL1* promoter and empty vector (–), wild-type Msp1 (WT) or $Msp1^{E193Q}$ (E193Q). Pex15 expression was induced in galactose medium for 6 h. 4% of the crude lysates, and final eluates were immunoblotted with anti-HA and GFP. Om45 is a mitochondrial outer membrane protein and is used as a loading control.

D Five-fold dilutions of the indicated strains expressing Pex15 from the native *PEX15* promoter or *GAL1* promoter (P_{GAL1}::*GFP–PEX15*) were grown overnight in SD medium, spotted on SD or synthetic galactose (SGal) plates, and cultured at 30°C.

E The *get3*Δ strain co-expressing GFP-Pex15 from the *GAL1* promoter and wild-type Msp1 or $Msp1^{E193Q}$ was pulsed in galactose medium for 5 h to induce GFP-Pex15 accumulation and chased in glucose medium to shut off transcription. Whole-cell lysates were prepared from cells harvested every 45 min and analyzed by immunoblot. Por1 is the loading control.

F HepG2 cells stably expressing GFP-PEX26 were treated with scrambled siRNA (scr) or siRNAs (#1–3) targeting human *ATAD1* for 6 days, stained with Mitotracker Red, and visualized by fluorescence microscopy with equivalent exposure times.

G Whole-cell lysates of cells from (F) were analyzed by immunoblot using the indicated antibodies. QCR2 is a mitochondrial protein and is used as a loading control.

Source data are available online for this figure.

Published online: May 19, 2014

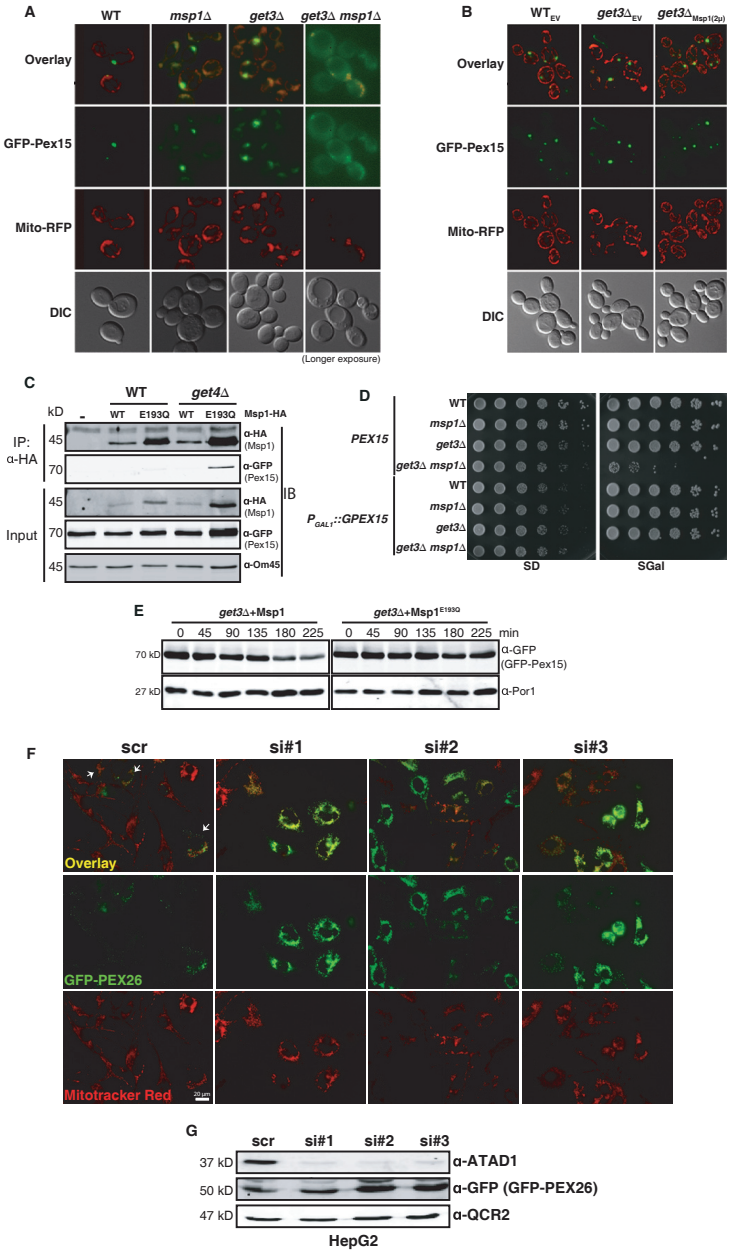

Published online: May 19, 2014
The EMBO Journal

Figure 5. Msp1 physically interacts with the TA protein Gos1 and is required to limit mitochondrial Gos1.

A Gos1 co-immunoprecipitates with the 'trap mutant' Msp1. Msp1 was immunoprecipitated by anti-HA antibody from digotonin-solubilized mitochondria that were extracted from the indicated strains expressing GFP-Gos1 from the native *GOS1* promoter and empty vector (−), wild-type Msp1 (+) or Msp1^{E193Q} (E193Q). 4% of the crude lysates and final eluates were immunoblotted with anti-HA, GFP, and Om45 antibodies. Om45 is a control mitochondrial outer membrane protein.

B The indicated strains expressing GFP-Gos1 from the native promoter and Mito-RFP were grown in SD medium to early log phase and visualized by fluorescence microscopy.

C The *get3*Δ strain expressing GFP-Gos1 from the *GAL1* promoter was transformed with EV or Msp1^{E193Q}, grown in galactose medium for 5 h to induce Gos1 expression and then switched to glucose medium to shut off transcription. Cells were harvested every 30 min thereafter, and the whole-cell lysates were analyzed by immunoblot.

D Representative images of the *GAL1* promoter-based transcriptional shut-off experiment as described in (C) except that the indicated strains were co-transformed with Mito-RFP to visualize mitochondria.

E Five-fold dilutions of the indicated strains harboring either empty vector (−) or Gos1 overexpression 2 μ vector (+) were spotted on SD or SGly plates and incubated at 30 or 37°C.

Source data are available online for this figure.

Msp1/hATAD1 physically interacts with and is required to prevent TA protein Gos1/GOS28 misaccumulation on mitochondria

To identify *bona fide* substrates of Msp1, we performed a two-step purification using a yeast strain expressing Msp1-His$_6$/HA$_3$ tag from the *MSP1* promoter. We expressed the wild-type or E193Q mutant Msp1 in both the WT and *get3*Δ strains and purified Msp1 by two-step purification. In examining potential substrates, we aimed to look for proteins that fulfill two criteria. First, they are purified more efficiently by the 'trap mutant' Msp1^{E193Q} than by the wild-type protein. Second, they exhibit stronger association with Msp1 in the *get3*Δ mutant strain than in the WT strain. As shown in Supplementary Table S1, Gos1 meets both criteria and is one of the most abundant proteins detected by mass spectrometry. Importantly, it is also a TA protein and functions as a v-SNARE in Golgi vesicular trafficking (McNew *et al*, 1998). We first verified this result by conducting a directed co-immunoprecipitation experiment. We expressed GFP-Gos1 and Msp1-HA fusion proteins under their endogenous promoters and performed an anti-HA immunoprecipitation from crude mitochondrial lysate. As seen in Fig 5A, GFP-Gos1 showed a stable association with Msp1^{E193Q}. We also observed a stronger GFP-Gos1 purification with Msp1^{E193Q} in the *get3*Δ and *get4*Δ mutants compared to a strain with a functional GET system (WT). Note that Msp1^{E193Q} consistently accumulated at a higher level compared to the wild-type protein (Fig 5A – input panel; also see Fig 4C – input panel). Similar to Pex15, the steady-state level of Gos1 was higher in the *get3*Δ and *get4*Δ mutant strains expressing the dominant-negative Msp1^{E193Q} mutant (Input panel, Fig 5A). To test Gos1 localization, we expressed GFP-Gos1 under the endogenous *GOS1* promoter and observed a partial overlap of GFP-Gos1 signal with Mito-RFP in both the *get4*Δ *msp1*Δ mutant strain and in the *get3*Δ mutant expressing the dominant-negative Msp1^{E193Q} (Fig 5B and Supplementary Fig S5A).

To test whether Msp1 facilitates the degradation of mislocalized Gos1, we used the *GAL1* promoter-based transcriptional shut-off system to test its half-life. Overexpression of Gos1 from the *GAL1* promoter leads to its mislocalization to the mitochondria of the *get3*Δ mutant (T = 0 min, Fig 5D). The time-course of Gos1 degradation in the *get3*Δ mutant expressing dominant-negative Msp1^{E193Q} is significantly slower than the *get3*Δ mutant, which expresses endogenous wild-type Msp1 (Fig 5C). We also visualized the localization of GFP-Gos1 throughout the time course. We observed that mitochondrial Gos1 was degraded faster in the *get4*Δ mutant compared to the strain expressing Msp1^{E193Q}, which still retained significant mitochondrial Gos1 after 180 min (Fig 5D).

To further address whether misaccumulation of Gos1 contributes to the mitochondrial damage in the *get3*Δ *msp1*Δ mutant, we attempted to delete *GOS1* and test for rescue of the growth phenotype. Unfortunately, loss of Gos1 in our W303-1a strain background causes lethality (Supplementary Fig S5B). Instead, we reasoned that overexpression of Gos1 might overload mitochondria and exacerbate the growth phenotype caused by loss of Msp1 and/or the GET system. As shown in Fig 5E, overexpression of Gos1 either caused or exacerbated growth phenotypes in *get1*Δ, *get2*Δ, and *get3*Δ single mutants. The double mutants containing those deletions combined with an *msp1*Δ mutation already exhibited such severe growth defects that Gos1 had no additional consequence. However, the *get4*Δ *msp1*Δ, *get5*Δ *msp1*Δ, and *msp1*Δ *sgt2*Δ double mutants, which maintained much more mitochondrial function (See Fig 2), were markedly impaired by Gos1 overexpression, particularly in glycerol growth (Fig 5E). The effect of Gos1 overexpression is specific as overexpression of Sbh1, an endoplasmic reticulum TA protein that does not mislocalize to mitochondria, did not exacerbate the growth phenotypes (Supplementary Fig S5C) (Schuldiner *et al*, 2008).

In addition to Gos1, we also observed that Tom5, a native mitochondrial TA protein, was strongly purified by Msp1^{E193Q} in the wild-type and the *get3*Δ mutant strain (Supplementary Table S1). This observation raised the possibility that Msp1 might not only bind to non-native, mislocalized mitochondrial TA proteins but also to native proteins. To test this hypothesis, we tagged Tom5 and all other mitochondrial TA proteins, Tom6, Tom7, Tom22, Fis1, Gem, and Fmp32 with a GFP at their N-termini and performed co-immunoprecipitation experiments (Supplementary Fig S6A). We observed no interaction between Tom5, Tom6, Fis1, Gem1, or Fmp32 and either wild-type Msp1 or the Msp1^{E193Q} mutant. Tom7 and Tom22 showed an interaction, but it was with both the wild-type and mutant Msp1 protein. More importantly, we observed no significant delay in the rate of degradation of any of these native mitochondrial TA proteins in the *msp1*Δ mutant (Supplementary Fig S6B). Furthermore, overexpression of *TOM5*, *TOM6*, or *TOM7* did not exacerbate the growth phenotype of the *msp1*Δ mutant strain (Supplementary Fig S6C). Therefore, it appears that none of the native mitochondrial TA proteins are efficient substrates of Msp1, at least in the conditions in which we conducted these experiments.

Published online: May 19, 2014

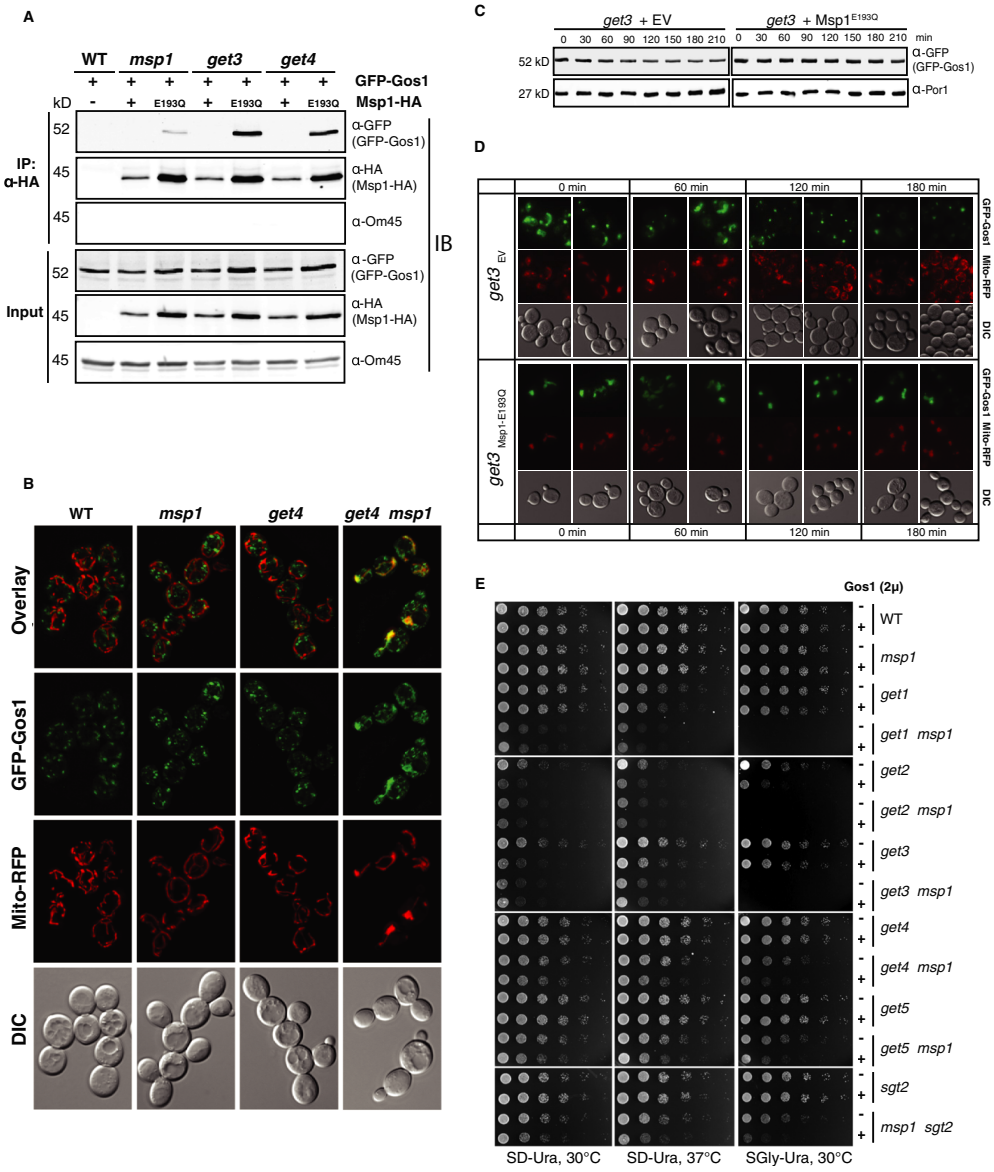

Based on our observations with Gos1, we performed two experiments to test whether GOS28, the mammalian ortholog of yeast Gos1, is subjected to mitochondrial misaccumulation, which is prevented by ATAD1. First, to test whether GOS28 misaccumulates on mitochondria upon ATAD1 depletion, we established a human dermal fibroblast (HDF) cell line stably expressing a GFP-human

Published online: May 19, 2014
The EMBO Journal

GOS28 fusion protein and subjected it to knockdown with control and *ATAD1* siRNAs. In control siRNA (scr)-treated cells or cells treated with si#4 that fails to knockdown *ATAD1* (Fig 6B), the majority of the GFP signal was localized to the peri-nuclear Golgi apparatus and had no overlap with Mitotracker Red (Fig 6A). However, when *ATAD1* was knocked down by si#1, 2, or 3 (Fig 6B), we clearly observed a partial redistribution of GFP-GOS28 to overlap with Mitotracker Red (Fig 6A). Second, to directly test whether GOS28 physically interacts with ATAD1, we assessed co-immunoprecipitation using crude mitochondrial extract from HepG2 cells stably expressing GFP-GOS28 and empty vector, wild-type ATAD1 or a substrate trap mutant ATAD1 ($ATAD1^{E193Q}$). Only the $ATAD1^{E193Q}$ mutant purified detectable amounts of GOS28 (Fig 6C). Note that the steady-state GOS28 level was reproducibly elevated in cells expressing the $ATAD1^{E193Q}$ (Fig 6C, lane 3), which is likely caused by its dominant-negative activity. This is consistent with the observation that expression of $ATAD1^{E193Q}$ causes ectopic accumulation of GFP-GOS28 on the mitochondria (Supplementary Fig S7A). Most importantly, we further observed increased steady-state abundance of endogenous GOS28 in multiple $ATAD1^{-/-}$ mouse tissues, including brain, liver, and heart (Fig 6D and Supplementary Fig S7B). We therefore conclude that Gos1 and GOS28 are *bona fide* substrates of yeast Msp1 and mammalian ATAD1, respectively.

Discussion

Based on the data presented herein, we conclude that yeast Msp1 and human ATAD1 belong to an evolutionarily and functionally conserved protein family. We demonstrate that they play a role in quality control of mitochondrial outer membrane proteins. Specifically, Msp1 or ATAD1 prevents a subset of TA proteins (yeast–Pex15 and Gos1; mammals–PEX26 and GOS28) that escape from the GET or TRC system from inappropriately accumulating on the mitochondria, likely by extracting them and facilitating their cytoplasmic degradation. The physiological consequences of combined impairment of Msp1 and the GET system include loss of mtDNA, loss of mitochondrial resident proteins, and severely altered mitochondrial morphology. The principal evidence supporting this model is enumerated below.

First, we have found that the targeting and insertion systems for TA proteins are quite imprecise. This necessitates quality control systems to manage the burden of TA proteins that are mislocalized to other cellular compartments. In mammals, the cytoplasmic Bag6 protein not only participates in chaperoning TA proteins to the ER for insertion, but also mediates ubiquitination of proteins that are inappropriately released from ribosomes (Mariappan *et al*, 2010; Hessa *et al*, 2011). We suggest that the Msp1 protein family represents a similar protein quality control system for the mitochondria. This system is necessitated by the fact that, even when the GET or TRC system is fully functional, TA proteins can escape and mislocalize to mitochondria. This is demonstrated by our observation that deletion of Msp1 alone caused ectopic accumulation of Pex15 protein on yeast mitochondria (Fig 4A). This is also true for both PEX26 and GOS28 when ATAD1 protein was depleted in multiple human cell lines (Figs 4G and 6A and Supplementary Fig S7A). For reasons that remain unclear, the mitochondrial membrane appears to be a receptive host for TA proteins that fail to target their native membrane. It is possible that this is because the mitochondrial outer membrane appears to be one of the only two organelles where TA proteins are directly targeted and inserted. Previous reports and our data (Fig 4A) clearly show that genetic impairment of the GET system causes mislocalization of a subset of TA proteins on the mitochondria (Schuldiner *et al*, 2008; Jonikas *et al*, 2009). Therefore, we suggest that cells have evolved a protein quality control system residing on mitochondria to handle this burden of mislocalized TA proteins.

Second, Msp1 physically interacts with mislocalized TA proteins. Our two-step purification identified the TA protein Gos1 as a possible genuine substrate of Msp1, which interacts with the substrate trap mutant Msp1 (Supplementary Table S1 and Fig 5A). This Msp1 mutant can also stably bind to overexpressed Pex15, but for unknown reasons, we did not observe Pex15 in the Msp1 co-purification experiment. Presumably, the substrate trap mutant Msp1 stabilizes the physical interaction with substrates, while wild-type Msp1 may bind to them transiently. It is also possible, however, that the enhanced observed binding of mutant Msp1 is simply a function of its elevated accumulation. Beyond Gos1 and Pex15, we expect that additional substrates remain to be discovered. Interestingly, we also identified Tom5 as another potential substrate by Msp1 co-purification; however, we failed to recapitulate this result using directed co-immunoprecipitation experiments (Supplementary Fig S6A). It is possible that the observation of co-purification is an artifact, and Tom5 and Msp1 have no relationship. It is also possible, however, that Tom5 is a *bona fide* substrate of Msp1, but we failed to obtain evidence for this either due to the specific conditions of our experiments or the use of a GFP-Tom5 fusion protein. As a result, we do not firmly conclude that Msp1 cannot recognize native mitochondrial TA proteins as substrates. In addition, it is possible that Msp1 extracts a broader range of protein substrates, including non-TA proteins, which is consistent with our observation of non-TA mitochondrial proteins bound specifically to the Msp1-E193Q mutant in the two-step purification experiment (Supplementary Table S1). In fact, mammalian ATAD1 (possibly the cytoplasmic pool) was shown to extract or disassemble the AMPAR protein complex, which has no TA protein constituents, from the cell surface (Zhang *et al*, 2011). Therefore, while Msp1/ATAD1 clearly functions in the degradation of mitochondrially mislocalized TA proteins, it appears to function in a broader context as well.

Third, Msp1 is required for the normal rate of degradation of mislocalized TA proteins. We repeatedly observed that the steady-state level of Msp1 substrate proteins is higher in Msp1- or ATAD1-depleted cells. Furthermore, we conducted a chase experiment on Pex15 and Gos1 and demonstrated that their half-life is extended in the absence of Msp1 (Fig 4E, Supplementary Figs S4B–E and S5C and D). We speculate that Msp1 unfolds and extracts Pex15 and Gos1 via ATP hydrolysis by the AAA+ domain. However, unlike *m*- or *i*-AAA ATPase, which has an accessory proteolytic domain to digest the unfolded peptide, Msp1 possesses only the AAA+ domain. Therefore, the mechanisms whereby mislocalized TA proteins are degraded in the cytosol remain to be explored. It is known that the cytoplasmic proteasome is engaged to degrade membrane proteins from various organelles, including the ER and mitochondria (Neutzner *et al*, 2007; Karbowski & Youle, 2011; Taylor & Rutter, 2011). Therefore, it seems likely that proteasomes provide the major degradative activity for TA proteins once they are extracted from the mitochondria.

Published online: May 19, 2014

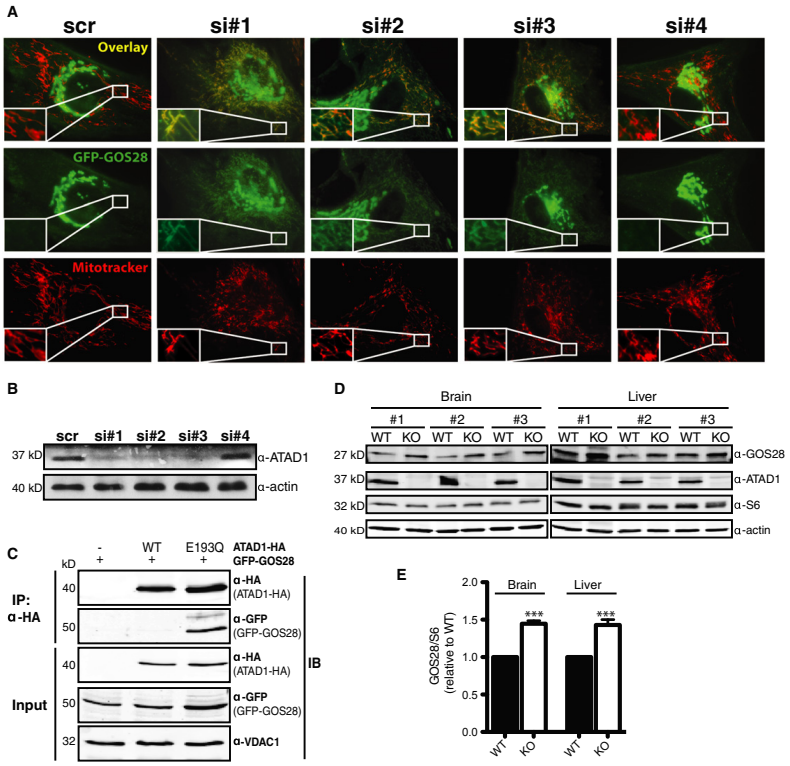

Figure 6. ATAD1 physically interacts with the TA protein, GOS28, and is required to limit the level of mislocalized GOS28 on mitochondria in mammals.

A Human dermal fibroblasts (HDFs) stably expressing GFP-GOS28 were treated with scr or siRNA (#1-4) against h*ATAD1*, stained with Mitotracker Red, and visualized by fluorescence microscopy.

B Whole-cell lysate of cells from (A) were immunoblotted using anti-ATAD1 and actin (loading control) antibodies.

C Crude mitochondria were extracted from HepG2 cells that stably co-express GFP-GOS28 with empty vector (−), HA-tagged wild-type ATAD1 (WT), or ATAD1^{E193Q} mutant. ATAD1 was immunoprecipitated using anti-HA antibody from digitonin-solubilized lysates and 5% of the crude lysates, and eluates were immunoblotted with anti-GFP and HA antibodies.

D Mouse tissue lysates (30 μg protein) from three WT and *ATAD1*$^{-/-}$ mice were analyzed by immunoblot. S6 ribosomal protein and actin are used as loading controls.

E The optical densitometry quantification of (D). The values represent the mean ± SEM (***P < 0.001, one-way ANOVA).

Source data are available online for this figure.

Fourth, the Msp1 and ATAD1 proteins are essential for the maintenance of mitochondria. We observed that loss of both Msp1 and the GET system causes loss of mtDNA and protein, and severe morphological defects (Fig 2). Mammalian cells, however, seem to be more susceptible to the depletion of ATAD1 as mutation of ATAD1 is sufficient to cause significant mitochondrial impairment (Fig 3A–D). Prior to this study, the major connection between the GET system and mitochondria related to TA protein mislocalization to mitochondria upon GET system disruption. Perhaps, the most profound mitochondrial defect observed is the loss of mitochondrial protein content in the *get1*Δ *msp1*Δ, *get2*Δ *msp1*Δ, and *get3*Δ *msp1*Δ mutant strains, which cannot be explained by the loss of mtDNA. Given that the TA proteins Tom5, Tom6, Tom7, and Tom22 are critical components of the TOM complex, perhaps ectopic TA protein accumulation causes defects in TOM complex formation. The ectopic TA proteins could either displace one or more of the tail-anchored components of the TOM complex, rendering it inactive. Alternatively, hyper-accumulation of TA proteins could impair the unknown mitochondrial TA protein import system, leading to decreased import efficiency of Tom5, Tom6, Tom7 and/or Tom22 and therefore impaired mitochondrial protein import. We also observed altered mitochondrial morphology in both *msp1*Δ yeast and *ATAD1* knockdown cells. Intriguingly, before the function of the GET system was determined, Get1 (also known as Mdm39) was

Published online: May 19, 2014
The EMBO Journal

discovered in a genetic screen for genes important for mitochondrial distribution and morphology (Dimmer *et al*, 2002). Perhaps, this observation relates to the effect of mislocalized TA proteins, caused by mutation of *GET1*, to impair mitochondrial morphology. In fact, many mitochondrial shaping factors such as Fis1 (yeast and mammals), Mff (mammals), and Gem1 (yeast) are TA proteins. Therefore, as speculated for the TOM complex above, mitochondrial morphology and dynamics might be susceptible to aberrant accumulation of non-mitochondrial TA proteins. For example, mislocalization of the Gos1 v-SNARE protein might enable promiscuous fusion events with organelles displaying cognate t-SNARE proteins.

Finally, our data suggest that the mitochondrial function of Msp1 protein family is conserved between yeast, flies, and mammals. Both *Drosophila CG5395* and human *ATAD1* suppressed the respiratory growth phenotype of the *get3*Δ *msp1*Δ mutant strains (Fig 3E). In addition, depletion of ATAD1 caused accumulation and mitochondrial localization of PEX26 and GOS28 as well as mitochondrial defects (Figs 3, 4G and 6, and Supplementary Fig S3D). In *Drosophila*, mitochondria undergo dramatic morphological changes during spermatogenesis. At the onion stage, mitochondria form a specialized structure called the nebenkern (Tokuyasu, 1975). Mutation of the fly *MSP1* ortholog *CG5395* (*nmd* mutant, *no mitochondrial derivative*) leads to a much smaller nebenkern and a slight loss of mitochondrial membrane potential (Noguchi *et al*, 2011). While these data do not implicate impaired protein quality control, it demonstrates that this gene is important in mitochondrial morphology and function. Furthermore, *ATAD1* knockout mice exhibit severe neuronal defects, including deficiencies in learning and memory and a seizure-like syndrome (postnatal day 19–25) (Zhang *et al*, 2011). Interestingly, we observed ectopic accumulation of GOS28 in multiple tissues from *ATAD1*$^{-/-}$ mice, particularly the brain (Fig 6D). Some of these neuronal deficits are likely due to the failure of disassembly of the AMPAR receptor, but similar neuronal phenotypes are observed with impaired mitochondrial quality control in mice and humans (Rugarli & Langer, 2012). We speculate that the mitochondrial defects caused by loss of *ATAD1* might partially contribute to the phenotype of the *ATAD1*$^{-/-}$ mice.

In conclusion, we suggest that the Msp1/ATAD1 protein family performs an evolutionarily conserved role in quality control of the mitochondrial outer membrane. This function, while perhaps including additional activities, is likely to extract and promote the degradation of TA proteins that have been mislocalized to mitochondria. The consequences for failure of this activity, particularly under a stress to the GET system, are devastating for mitochondrial morphology and function. Given the critical importance of mitochondrial quality control in human physiology and pathophysiology, we anxiously await a broader and deeper understanding of this protein family in health and disease.

Materials and Methods

Yeast strains and growth conditions

Saccharomyces cerevisiae W303-1a (*MATa, his3 leu2 met15 trp1 ura3*) was used in this study. The standard PCR-based homologous recombination method was used to generate all mutant strains. Briefly, drug selection cassette (KanMX4, hphMX4, or natMX4) flanked with 45-bp fragments upstream and downstream of the gene of interest was PCR amplified and transformed into the wild-type diploid (Goldstein & McCusker, 1999) (Wach *et al*, 1994). The haploid strain was generated by sporulation and tetrad analysis. The strains with chromosomally integrated P_{GAL1}-*GFP-PEX15* were generated as described in (Longtine *et al*, 1998). The genotype of the strain was verified by standard genotyping PCR. The genotypes of all yeast strains used in this study are listed in Supplementary Table S2.

For yeast transformation, the standard lithium acetate procedure was used (Gietz *et al*, 1992). Transformed yeast cells were grown in synthetic complete dextrose (SD) medium lacking the appropriate amino acid(s) for auxotrophic selection purposes at 30°C. Media used in this study include standard YP and synthetic minimal medium supplemented with 2% glucose, 2% raffinose, or 3% glycerol. Solid plates contain 2.2% (w/v) agar.

Plasmid construction

To produce plasmids expressing non-tagged, C-terminal His_6/HA_3 or GFP-tagged Msp1, the *MSP1* ORF flanked with its upstream 500-bp promoter region was PCR amplified from yeast genomic DNA and ligated into the pRS416, pRS426, or pRS416 vector containing either a C-terminal His_6/HA_3 or GFP tag. Msp1^{E193Q} construct was made by site-directed mutagenesis of the Msp1-His_6/HA_3 construct. To generate human *ATAD1* and fly *CG5393* constructs, *ATAD1* and *CG5393* ORF were amplified from HepG2 and fly cDNA, respectively, and ligated into pRS416-based vector containing the *ADH1* promoter (Mumberg *et al*, 1995). N-terminal GFP-tagged Gos1 construct was made by ligating P_{GOS1}, *GFP,* and *GOS1* ORF fragments together using the standard sewing PCR and ligating into the pRS414 vector. The P_{GAL1}::GFP-Gos1 construct was generated by ligating *GOS1* ORF into pRS414-based vector containing the *GAL1* promoter and a N-terminal GFP tag. The Retro-X™Q Vectors (Clontech) were used to generate mammalian constructs. Human *ATAD1* ORF fused with HA or GFP tag at the 3′-end or *PEX26* or *GOS28* ORF fused with GFP at the 5′-end was ligated into pQCXIP or pQCXIZ vector. Site-directed mutagenesis was used to convert ATAD1-HA into ATAD1^{E193Q}-HA. Peroxisomal fluorescent marker construct was made by fusing RFP protein with the peroxisomal targeting sequence (SKL) at the C-terminus.

Isolation of yeast mitochondria

Yeast cells were harvested at mid-log phase (OD_{600} = 2–3) unless indicated otherwise. Preparation of crude and purified mitochondria was as described previously (Boldogh & Pon, 2007). Yeast pellet was washed once with ddH_2O, resuspended, and incubated in TD buffer (100 mM Tris-SO_4, pH 9.4 and 100 mM DTT) for 15 min at 30°C. Spheroplasts were obtained by incubating cells in SP buffer (1.2 M sorbitol and 20 mM potassium phosphate, pH 7.4) supplemented with lyticase (2 mg/g of cell pellet) (Sigma-Aldrich) for 1 h at 30°C to digest the cell wall. Spheroplasts were gently washed once in ice-cold SHE buffer (1.2 M sorbitol, 20 mM HEPES-KOH, pH 7.4, 2 mM $MgCl_2$, 1 mM EGTA, and 1 mM PMSF) and homogenized in ice-cold SHE buffer that contains 0.6 M sorbitol with a Dounce homogenizer applied with 10-20 strokes. The crude mitochondrial fraction was obtained by differential centrifugation. Protein concentration was determined using Bradford protein assay (Bio-Rad).

Published online: May 19, 2014

Continuous Nycodenz gradients were used to purify crude mitochondria. To make a gradient, 2.1 ml of 5, 10, 15, 20, and 25% Nycodenz in SHE buffer was layered in 14 × 89 mm Ultra-Clear centrifuge tubes (Beckman) and the tubes were sat at room temperature for 3–4 h to allow the Nycodenz to diffuse. Crude mitochondria were loaded on top of the chilled gradient and separated at 100,000 × *g* for 1 h at 4°C (SW41 rotor; Beckman). Intact purified mitochondria were recovered from a brown band at around 16% Nycodenz concentration.

Assessment of sub-mitochondrial localization

The experiment was conducted as described previously (Chen *et al*, 2012). Briefly, proteinase-free mitochondria were incubated in the isotonic SH buffer (0.6 M Sorbitol, 20 mM HEPES-KOH) or hypotonic H buffer (20 mM HEPES-KOH) with and without 1% Triton X-100. Proteinase K (10 μg/μl) was then added and incubated on ice for 20–30 min. The digestion was stopped by adding phenylmethylsulfonyl fluoride (PMSF) to 2 mM. The reaction mixtures were denatured in 6× Laemmli buffer and resolved by 12% SDS-PAGE, followed by immunoblot.

The high-salt and alkaline extraction were adapted from a previously described protocol (Boldogh & Pon, 2007). Intact mitochondria were treated with salt (100 mM KCl in SHE buffer without sorbitol) or carbonate (100 mM Na_2CO_3 in SHE buffer) for 30 min on ice and subjected to ultracentrifugation (100,000 × *g* for 20 min) to separate soluble and insoluble proteins. Soluble fractions were precipitated by 15% trichloroacetic acid (TCA) and dissolved in 1× Laemmli buffer. An equal amount of lysate from both the soluble and insoluble fraction was analyzed by immunoblot.

Two-step Msp1-His_6/HA_3 purification

Crude mitochondria isolated from strains grown in synthetic raffinose medium to mid-log phase (OD_{600} = 2.5) were solubilized in lysis buffer (20 mM HEPES, pH 7.4, 10 mM KCl, 1.5 mM $MgCl_2$, 1 mM EDTA, 150 mM NaCl, 10 mM imidazole, 2.1 mg/ml NaF, 10.8 mg/ml 2-glycerolphosphate, 0.5% digitonin and protease inhibitors) for 1 h at 4°C. For the first step of the purification, cleared mitochondria lysates were incubated with equilibrated Ni-NTA beads for 1 h at 4°C. Ni-NTA beads were washed 5 times with wash buffer (compositions are same as lysis buffer except for 20 mM imidazole and 0.05% digitonin). Proteins were eluted three times by 250 mM imidazole under non-denaturing conditions. For the second step of the purification, final eluates of the first purification were combined and mixed with anti-HA antibody-conjugated agarose (A2095; Sigma) for 1 h at 4°C. The agarose was then washed five times, and proteins were eluted five consecutive times by 1 mg/ml HA peptides. Final eluates were precipitated in 15% TCA overnight at 4°C and analyzed by mass spectrometry.

Fluorescence microscopy

Yeast samples were prepared by growing yeast cells to early log phase (OD_{600} = 0.8–1) in synthetic dropout medium with appropriate carbon sources at 30°C. To prepare mammalian cell samples, we cultured cells on Poly-L-Lysine-coated Lab-Tek II chamber slides for a day to allow them to fully attach. They were either visualized directly or stained with 25 nM Mitotracker Red CMXRos (Life Technologies) in FBS-free medium for 5 min at 37°C before imaged. To examine morphological changes in mitochondria from *ATAD1*$^{-/-}$ MEFs, they were transiently transfected with Mito-RFP to label the mitochondria. Transfected cells were fixed for 15 min with 4% PFA + 4% sucrose in PBS without permeabilization. Cells were washed three times with PBS buffer, stained with DAPI, and washed three more times with PBS buffer. Images of the cells were acquired by using a Zeiss LSM 710 laser-scanning confocal microscope using a 40× oil-immersion objective.

Cells were imaged on the Axio Observer. Z1 imaging system (Carl Zeiss) equipped with 40× and 100× objectives (oil-immersion). Digital fluorescence and differential interference contrast (DIC) images were acquired using a monochrome digital camera (AxioCam MRm, Carl Zeiss). *Z*-stacks of 0.35-μm slides were obtained and deconvolved using the AxioVision software (Version 4.8, Carl Zeiss). 2D projection of the *z*-stacks was performed using the ImageJ software. The final images were adjusted and assembled using Adobe Photoshop CS5.1. Brightness and contrast were adjusted only using linear operation on the entire image.

The yeast fluorescent images shown in this study are representative pictures from at least two independent experiments ($n \geq 2$). The images of the mammalian cells are representative of three independent experiments ($n = 3$).

Mass spectrometry

TCA pellets were resuspended in 8 M urea, 50 mM HEPES, and pH 8.8. Proteins were reduced by the addition of dithiothreitol to 5 mM and incubation at room temperature for 30 min. Cysteines were alkylated by adding iodoacetamide to 15 mM and incubating in the dark at room temperature for 60 min. Iodoacetamide was quenched with an additional 10 mM DTT. Samples were digested with lysyl endopeptidase (lysC) at 20 ng/μl overnight at room temperature after diluting the urea to 2 M by adding 3 volumes of 50 mM HEPES, pH 8.8. LysC-digested peptides were subsequently digested with trypsin at 15 ng/μl for 60 min at 37°C. Doubly digested peptides were acidified by adding trifluoroacetic acid to 0.2% and desalted on hand-packed C18 STAGE tips (Rappsilber *et al*, 2007). Peptides were eluted with 70% acetonitrile and 1% formic acid and dried under vacuum. Desalted peptides were resuspended in 5% formic acid, and each sample was analyzed in technical duplicate by reverse-phase liquid chromatography electrospray mass spectrometry on a LTQ Orbitrap Velos Pro (Thermo Fisher Scientific). Peptides were analyzed on a LTQ Orbitrap Velos Pro mass spectrometer (Thermo Fisher Scientific). Nanospray tips were hand-pulled with 100-μm inside diameter fused-silica tubing and packed with 20 cm of Maccel C18AQ resin (3 mm, 200 Å; Nest Group). Peptides were separated with a gradient of 6–30% CH3CN in 0.125% formic acid over 60 min at a flow rate of 300 nl/min. Peptides were detected using a data-dependent Top20 MS2 method. For each cycle, one full MS scan of mass/charge ratio (m/z) = 400–1,200 was acquired in the Orbitrap at a resolution of 60,000 at m/z = 400 with automatic gain control (AGC) target of 1×10^6. Each full scan was followed by the selection of the most intense ions, up to 20, for collision-induced dissociation (CID) and analysis in the linear ion trap. Selected ions were excluded from subsequent selection for 60 s. Ions with a charge of 1 or unassigned were also excluded from MS2 analysis. Maximum ion

Published online: May 19, 2014
The EMBO Journal

accumulation times were 100 ms for both full MS and MS2 scans. Lockmass, with atmospheric polydimethylsiloxane (m/z = 371.1012) as an internal standard, was used for internal mass calibration.

Peptide identification and filtering

MS2 spectra were searched using SEQUEST v.28 (rev. 13) against a composite database containing the translated sequences of all predicted open reading frames of *S. cerevisiae* (http://downloads.yeastgenome.org, downloaded 30 October 2009) and its reversed complement with the following parameters: a precursor mass tolerance of ± 20 parts per million (ppm); 1.0-dalton product ion mass tolerance; combined lysC–trypsin digestion; up to two missed cleavages; a static modification of carbamidomethylation on cysteine (+57.0214); and a dynamic modifications of methionine oxidation (+15.9949). Peptide spectral matches were filtered to 1% FDR using the target-decoy strategy combined with linear discriminant analysis (LDA) using several different parameters including the SEQUEST Xcorr and DCn′ scores, and precursor mass error (Elias & Gygi, 2007; Huttlin *et al*, 2010). The data were further filtered to control protein-level FDRs. Peptides from all fractions in each experiment were combined and assembled into proteins. Protein scores were derived from the product of all LDA peptide probabilities, sorted by rank, and filtered to 1% FDR. The FDR of the remaining peptides fell markedly after protein filtering.

Steady-state protein analysis

Yeast whole-cell lysates were prepared from 1 OD_{600} of yeast cells harvested from raffinose medium at mid-log phase. Yeast pellets were washed with ddH_2O once, resuspended in 200 μl of 20 mM NaOH, incubated at room temperature for 5 min, and pelleted. Laemmli buffer was added to resuspend pellets, and they were denatured at 95°C for 5–10 min (Kushnirov, 2000). Anti-Cox2, Cox3 (MitoSciences), Por1, and Pgk1 (3-phosphoglycerate kinase) (Abcam) were used on immunoblots.

Animal tissue lysates were obtained from brain homogenates of 4- to 5-week-old wild-type and *ATAD1*$^{-/-}$ mice (C57BL/6) (Zhang *et al*, 2011). Freshly isolated whole brains were powderized on dry ice and homogenized in lysis buffer (50 mM HEPES, pH 7.5, 150 mM NaCl, 1 mM DTT, 5% glycerol, 1% Triton X-100) containing protease inhibitors (Sigma-Aldrich). The brain extracts were kept on ice for 1 h and then centrifuged at 15,000 × *g* for 30 min. Protein concentration was determined using the BCA protein assay (Thermo Scientific). Twenty μg of lysates was resolved on 4–20% gradient NuPAGE (Invitrogen) and transferred to PVDF membranes. Immunoblot analyses were performed using ATAD1 antibodies (NeuroMab or abcam) and mitochondrial antibodies, TOMM20, COX1, COX4, hexokinase 1, hexokinase 2, VDAC1, pyruvate dehydrogenase, and S6 ribosomal protein (Cell Signaling Tech.). β-actin, β-tubulin, and MAP2 (SIGMA) antibodies were used for controls. All mouse experiments were performed under approved protocols of the Institutional Animal Care and Use Committee at Johns Hopkins University School of Medicine.

Measurement of oxygen consumption rate

Mitochondrial oxygen consumption rate (OCR) was assessed using WT and *ATAD1* KO MEFs in an XF24 Extracellular Flux Analyzer (Seahorse Bioscience), as described previously (Cooper *et al*, 2012). Culture media of MEF cells plated at a density of ~0.5×10^6 per well in an XF24 cell culture microplates were replaced with XF24 Dulbecco's modified Eagle medium (DMEM) containing 10 mM glucose, 2 mM L-glutamine (Life Technologies), and 2 mM sodium pyruvate (Life Technologies). OCR was measured at 37°C with 1-min mix, 1-min wait, and 5-min measurement protocol. OCR was analyzed after 30 min incubation in a CO_2-free incubator. Oligomycin, carbonilcyanide m-chlorophenylhydrazone (CCCP), and rotenone were sequentially injected into each well to assess basal respiration, coupling of respiratory chain, and mitochondrial respiratory capacity. OCRs were normalized relative to protein concentration in each well, and the data are presented as % change of control.

Co-immunoprecipitation

One milligram of crude mitochondria extracted from each strain was solubilized in 0.5% digitonin for 1 h at 4°C. Cleared mitochondria lysates were mixed with anti-HA antibody-conjugated agarose for 1 h at 4°C. Agarose was washed two times with buffer containing 250 mM NaCl and 0.05% digitonin and three times with buffer containing 600 mM NaCl and 0.05% digitonin. Laemmli buffer without β-ME was added to the agarose to elute proteins. Final eluate and 4–5% of the mitochondria lysate were resolved by 12% SDS-PAGE followed by immunoblot. Results shown in this study are representatives of two independent experiments (n = 2).

Mammalian cell culture

HepG2 (human hepatocellular carcinoma) cells were maintained in DMEM/F12 (Thermo Scientific) with 10% FBS. HEK293T, HDF (human dermal fibroblasts), and HeLa cells were maintained in DMEM (Thermo Scientific) with 10% FBS. Cells were cultured at 37°C with 5% CO_2. To establish stable cell lines, retrovirus was produced in HEK293T cells that were co-transfected with the vector containing the gene of interest, Gag-pol, and VSVG (amount ratio is 3:2:1) using Lipofectamine 2000 (Invitrogen) according to the manufacturer's instructions. Retrovirus was harvested from the medium at 48 h post-transfection and applied to the target cells. After 24 h post-infection, target cells were selected in 4 μg/ml puromycin and/or 150 μg/ml zeocin for 5–7 days. Stable cell lines were maintained in the appropriate medium with 0.5 μg/ml puromycin and/or 20 μg/ml zeocin. All knockdowns were performed by treating cells with 10 nM siRNA, using the Lipofectamine RNAiMax reagent, according to the manufacturer's instructions (Invitrogen). The All-Stars non-targeting siRNA (Qiagen) was used as the control (scr). siRNAs targeting human *ATAD1* (NM_032810.2) were designed with the Dharmacon siDesign Center tool (http://www.thermoscientificbio.com/design-center/). Sequences of the sense strands of targeting siRNAs, which include a 3′ tt DNA overhang, are as follows: (#1) GAAGCAAAUUGGAGUGAAAtt, (#2) GAAUGAAGUUGUUGGUUUAtt, (3) CAUGUUACUUGGAGUGAUAtt and (4) GAUAAGUGGUAUGGAGAAUdtt. Cells were subjected to knockdown on day 0, again on day 3, and analyzed on day 6. Efficacy of *ATAD1* knockdown was verified by immunoblot with mouse monoclonal anti-ATAD1 antibody (1:1,000) (Abcam).

Published online: May 19, 2014

Mouse embryonic fibroblasts (MEFs) were prepared from embryonic day 13 mouse pups as described previously with some modification (Jozefczuk *et al*, 2012). MEFs were isolated from tissues by 0.05% trypsin/EDTA (Gibco, Invitrogen) dissociation. Cells were strained using 40-μm cell strainer (BD Falcon) and resuspended in Dulbecco's modified Eagle's medium (Gibco, Invitrogen), supplemented with 10% fetal bovine serum, 100 μg/ml penicillin, and 100 g/ml streptomycin. Cells were plated on poly-D-lysine-coated cell culture dishes. All mouse experiments were performed under approved protocols of the Institutional Animal Care and Use Committee at Johns Hopkins University School of Medicine.

Supplementary information for this article is available online: http://emboj.embopress.org

Acknowledgements
We thank members of the Rutter laboratory for helpful discussions; Tim Formosa, David Stillman, and Janet Shaw for yeast strains, reagents, antibodies, technical supports, and helpful discussions; Tammy Nguyen for assistance with mammalian live cell imaging; Adam Frost for discussing the MITO-MAP data and critical comments on the manuscript; Adam L. Hughes for critical comments on the manuscript; Dennis Winge for Sdh1 and Sdh2 antibodies. This work was supported by the NIH grant R01GM094232 (to J.R.) and the NIH/NIDA DA000266 (to T.M.D., V.L.D.) and NIH/NINDS 5R01AG029368 (to V.L.D.) American Heart Association 12SDG9310031 (S.A.A.). T.M.D. is the Leonard and Madlyn Abramson Professor in Neurodegenerative Diseases.

Author contributions
Y-CC and JR proposed project hypothesis, designed experiments and prepared manuscript. Y-CC performed and analyzed experiments of Figures 1, 2, 4, 5, 6 and Supplementary Figures 1-7. TMD, VLD, GKEU and SAA designed, performed and analyzed experiments of Figure 3. ND and SG performed mass spectrometry and analyzed the result.

Conflict of interest
The authors declare that they have no conflict of interest.

Note added in proof
In agreement with our conclusions, Okreglak and Walter (2014) independently demonstrated that yeast Msp1 promote the degradation of the mistargeted Pex15 tail-anchored protein on the mitochondrial outer membrane.

Okreglak V, Walter P (2014) The conserved AAA-ATPase Msp1 confers organelle specificity to tail-anchored proteins. *Proc Natl Acad Sci U S A*, in press

References

Ashrafi G, Schwarz TL (2013) The pathways of mitophagy for quality control and clearance of mitochondria. *Cell Death Differ* 20: 31 – 42

Boldogh IR, Pon LA (2007) Purification and subfractionation of mitochondria from the yeast *Saccharomyces cerevisiae*. *Methods Cell Biol* 80: 45 – 64

Borgese N, Colombo S, Pedrazzini E (2003) The tale of tail-anchored proteins: coming from the cytosol and looking for a membrane. *J Cell Biol* 161: 1013 – 1019

Brambillasca S, Yabal M, Soffientini P, Stefanovic S, Makarow M, Hegde RS, Borgese N (2005) Transmembrane topogenesis of a tail-anchored protein is modulated by membrane lipid composition. *EMBO J* 24: 2533 – 2542

Bricker DK, Taylor EB, Schell JC, Orsak T, Boutron A, Chen YC, Cox JE, Cardon CM, Van Vranken JG, Dephoure N, Redin C, Boudina S, Gygi SP, Brivet M, Thummel CS, Rutter J (2012) A mitochondrial pyruvate carrier required for pyruvate uptake in yeast, *Drosophila*, and humans. *Science* 337: 96 – 100

Campbell CL, Tanaka N, White KH, Thorsness PE (1994) Mitochondrial morphological and functional defects in yeast caused by yme1 are suppressed by mutation of a 26S protease subunit homologue. *Mol Biol Cell* 5: 899 – 905

Chartron JW, Suloway CJ, Zaslaver M, Clemons WM Jr (2010) Structural characterization of the Get4/Get5 complex and its interaction with Get3. *Proc Natl Acad Sci USA* 107: 12127 – 12132

Chen YC, Taylor EB, Dephoure N, Heo JM, Tonhato A, Papandreou I, Nath N, Denko NC, Gygi SP, Rutter J (2012) Identification of a protein mediating respiratory supercomplex stability. *Cell Metab* 15: 348 – 360

Cooper O, Seo H, Andrabi S, Guardia-Laguarta C, Graziotto J, Sundberg M, McLean JR, Carrillo-Reid L, Xie Z, Osborn T, Hargus G, Deleidi M, Lawson T, Bogetofte H, Perez-Torres E, Clark L, Moskowitz C, Mazzulli J, Chen L, Volpicelli-Daley L *et al* (2012) Pharmacological rescue of mitochondrial deficits in iPSC-derived neural cells from patients with familial Parkinson's disease. *Sci Transl Med* 4: 141ra190

Costanzo M, Baryshnikova A, Bellay J, Kim Y, Spear ED, Sevier CS, Ding H, Koh JL, Toufighi K, Mostafavi S, Prinz J, St Onge RP, VanderSluis B, Makhnevych T, Vizeacoumar FJ, Alizadeh S, Bahr S, Brost RL, Chen Y, Cokol M *et al* (2010) The genetic landscape of a cell. *Science* 327: 425 – 431

Denic V (2012) A portrait of the GET pathway as a surprisingly complicated young man. *Trends Biochem Sci* 37: 411 – 417

Dimmer KS, Fritz S, Fuchs F, Messerschmitt M, Weinbach N, Neupert W, Westermann B (2002) Genetic basis of mitochondrial function and morphology in *Saccharomyces cerevisiae*. *Mol Biol Cell* 13: 847 – 853

Elias JE, Gygi SP (2007) Target-decoy search strategy for increased confidence in large-scale protein identifications by mass spectrometry. *Nat Methods* 4: 207 – 214

Gerdes F, Tatsuta T, Langer T (2012) Mitochondrial AAA proteases–towards a molecular understanding of membrane-bound proteolytic machines. *Biochim Biophys Acta* 1823: 49 – 55

Gietz D, St Jean A, Woods RA, Schiestl RH (1992) Improved method for high efficiency transformation of intact yeast cells. *Nucleic Acids Res* 20: 1425

Goldstein AL, McCusker JH (1999) Three new dominant drug resistance cassettes for gene disruption in *Saccharomyces cerevisiae*. *Yeast* 15: 1541 – 1553

Hanson PI, Whiteheart SW (2005) AAA+ proteins: have engine, will work. *Nat Rev Mol Cell Biol* 6: 519 – 529

Hao HX, Khalimonchuk O, Schraders M, Dephoure N, Bayley JP, Kunst H, Devilee P, Cremers CW, Schiffman JD, Bentz BG, Gygi SP, Winge DR, Kremer H, Rutter J (2009) SDH5, a gene required for flavination of succinate dehydrogenase, is mutated in paraganglioma. *Science* 325: 1139 – 1142

Hegde RS, Keenan RJ (2011) Tail-anchored membrane protein insertion into the endoplasmic reticulum. *Nat Rev Mol Cell Biol* 12: 787 – 798

Heo JM, Livnat-Levanon N, Taylor EB, Jones KT, Dephoure N, Ring J, Xie J, Brodsky JL, Madeo F, Gygi SP, Ashrafi K, Glickman MH, Rutter J (2010) A stress-responsive system for mitochondrial protein degradation. *Mol Cell* 40: 465 – 480

Hessa T, Sharma A, Mariappan M, Eshleman HD, Gutierrez E, Hegde RS (2011) Protein targeting and degradation are coupled for elimination of mislocalized proteins. *Nature* 475: 394 – 397

Hoppins S, Collins SR, Cassidy-Stone A, Hummel E, Devay RM, Lackner LL, Westermann B, Schuldiner M, Weissman JS, Nunnari J (2011) A

Published online: May 19, 2014
The EMBO Journal Mitochondrial tail-anchored protein removal *Yu-Chan Chen et al*

mitochondrial-focused genetic interaction map reveals a scaffold-like complex required for inner membrane organization in mitochondria. *J Cell Biol* 195: 323 – 340

Huttlin EL, Jedrychowski MP, Elias JE, Goswami T, Rad R, Beausoleil SA, Villen J, Haas W, Sowa ME, Gygi SP (2010) A tissue-specific atlas of mouse protein phosphorylation and expression. *Cell* 143: 1174 – 1189

Janska H, Kwasniak M, Szczepanowska J (2013) Protein quality control in organelles – AAA/FtsH story. *Biochim Biophys Acta* 1833: 381 – 387

Jonikas MC, Collins SR, Denic V, Oh E, Quan EM, Schmid V, Weibezahn J, Schwappach B, Walter P, Weissman JS, Schuldiner M (2009) Comprehensive characterization of genes required for protein folding in the endoplasmic reticulum. *Science* 323: 1693 – 1697

Jozefczuk J, Drews K, Adjaye J (2012) Preparation of mouse embryonic fibroblast cells suitable for culturing human embryonic and induced pluripotent stem cells. *J Vis Exp* 3854

Karbowski M, Youle RJ (2011) Regulating mitochondrial outer membrane proteins by ubiquitination and proteasomal degradation. *Curr Opin Cell Biol* 23: 476 – 482

Kroemer G, Pouyssegur J (2008) Tumor cell metabolism: cancer's Achilles' heel. *Cancer Cell* 13: 472 – 482

Kushnirov VV (2000) Rapid and reliable protein extraction from yeast. *Yeast* 16: 857 – 860

Kutay U, Ahnert-Hilger G, Hartmann E, Wiedenmann B, Rapoport TA (1995) Transport route for synaptobrevin via a novel pathway of insertion into the endoplasmic reticulum membrane. *EMBO J* 14: 217 – 223

Lessing D, Bonini NM (2009) Maintaining the brain: insight into human neurodegeneration from *Drosophila melanogaster* mutants. *Nat Rev Genet* 10: 359 – 370

Longtine MS, McKenzie A III, Demarini DJ, Shah NG, Wach A, Brachat A, Philippsen P, Pringle JR (1998) Additional modules for versatile and economical PCR-based gene deletion and modification in *Saccharomyces cerevisiae*. *Yeast* 14: 953 – 961

Lopez-Armada MJ, Riveiro-Naveira RR, Vaamonde-Garcia C, Valcarcel-Ares MN (2013) Mitochondrial dysfunction and the inflammatory response. *Mitochondrion* 13: 106 – 118

Lopez-Otin C, Blasco MA, Partridge L, Serrano M, Kroemer G (2013) The hallmarks of aging. *Cell* 153: 1194 – 1217

Mariappan M, Li X, Stefanovic S, Sharma A, Mateja A, Keenan RJ, Hegde RS (2010) A ribosome-associating factor chaperones tail-anchored membrane proteins. *Nature* 466: 1120 – 1124

Mariappan M, Mateja A, Dobosz M, Bove E, Hegde RS, Keenan RJ (2011) The mechanism of membrane-associated steps in tail-anchored protein insertion. *Nature* 477: 61 – 66

McNew JA, Coe JG, Sogaard M, Zemelman BV, Wimmer C, Hong W, Sollner TH (1998) Gos1p, a *Saccharomyces cerevisiae* SNARE protein involved in Golgi transport. *FEBS Lett* 435: 89 – 95

Mumberg D, Muller R, Funk M (1995) Yeast vectors for the controlled expression of heterologous proteins in different genetic backgrounds. *Gene* 156: 119 – 122

Nakai M, Endo T, Hase T, Matsubara H (1993) Intramitochondrial protein sorting. Isolation and characterization of the yeast MSP1 gene which belongs to a novel family of putative ATPases. *J Biol Chem* 268: 24262 – 24269

Neutzner A, Youle RJ, Karbowski M (2007) Outer mitochondrial membrane protein degradation by the proteasome. *Novartis Found Symp* 287: 4 – 14; discussion 14-20

Noguchi T, Koizumi M, Hayashi S (2011) Sustained elongation of sperm tail promoted by local remodeling of giant mitochondria in *Drosophila*. *Curr Biol* 21: 805 – 814

Patti ME, Corvera S (2010) The role of mitochondria in the pathogenesis of type 2 diabetes. *Endocr Rev* 31: 364 – 395

Rappsilber J, Mann M, Ishihama Y (2007) Protocol for micro-purification, enrichment, pre-fractionation and storage of peptides for proteomics using StageTips. *Nat Protoc* 2: 1896 – 1906

Rugarli EI, Langer T (2012) Mitochondrial quality control: a matter of life and death for neurons. *EMBO J* 31: 1336 – 1349

Sauer RT, Baker TA (2011) AAA+ proteases: ATP-fueled machines of protein destruction. *Annu Rev Biochem* 80: 587 – 612

Schuldiner M, Metz J, Schmid V, Denic V, Rakwalska M, Schmitt HD, Schwappach B, Weissman JS (2008) The GET complex mediates insertion of tail-anchored proteins into the ER membrane. *Cell* 134: 634 – 645

Steel GJ, Brownsword J, Stirling CJ (2002) Tail-anchored protein insertion into yeast ER requires a novel posttranslational mechanism which is independent of the SEC machinery. *Biochemistry* 41: 11914 – 11920

Stefanovic S, Hegde RS (2007) Identification of a targeting factor for posttranslational membrane protein insertion into the ER. *Cell* 128: 1147 – 1159

Tanaka A, Cleland MM, Xu S, Narendra DP, Suen DF, Karbowski M, Youle RJ (2010) Proteasome and p97 mediate mitophagy and degradation of mitofusins induced by Parkin. *J Cell Biol* 191: 1367 – 1380

Taylor EB, Rutter J (2011) Mitochondrial quality control by the ubiquitin-proteasome system. *Biochem Soc Trans* 39: 1509 – 1513

Thorsness PE, White KH, Fox TD (1993) Inactivation of YME1, a member of the ftsH-SEC18-PAS1-CDC48 family of putative ATPase-encoding genes, causes increased escape of DNA from mitochondria in *Saccharomyces cerevisiae*. *Mol Cell Biol* 13: 5418 – 5426

Tokuyasu KT (1975) Dynamics of spermiogenesis in *Drosophila melanogaster*. VI. Significance of "onion" nebenkern formation. *J Ultrastruct Res* 53: 93 – 112

Wach A, Brachat A, Pohlmann R, Philippsen P (1994) New heterologous modules for classical or PCR-based gene disruptions in *Saccharomyces cerevisiae*. *Yeast* 10: 1793 – 1808

Wang F, Brown EC, Mak G, Zhuang J, Denic V (2010) A chaperone cascade sorts proteins for posttranslational membrane insertion into the endoplasmic reticulum. *Mol Cell* 40: 159 – 171

Wattenberg B, Lithgow T (2001) Targeting of C-terminal (tail)-anchored proteins: understanding how cytoplasmic activities are anchored to intracellular membranes. *Traffic* 2: 66 – 71

Weibezahn J, Schlieker C, Bukau B, Mogk A (2003) Characterization of a trap mutant of the AAA+ chaperone ClpB. *J Biol Chem* 278: 32608 – 32617

Xu S, Peng G, Wang Y, Fang S, Karbowski M (2011) The AAA-ATPase p97 is essential for outer mitochondrial membrane protein turnover. *Mol Biol Cell* 22: 291 – 300

Yabal M, Brambillasca S, Soffientini P, Pedrazzini E, Borgese N, Makarow M (2003) Translocation of the C terminus of a tail-anchored protein across the endoplasmic reticulum membrane in yeast mutants defective in signal peptide-driven translocation. *J Biol Chem* 278: 3489 – 3496

Youle RJ, Narendra DP (2011) Mechanisms of mitophagy. *Nat Rev Mol Cell Biol* 12: 9 – 14

Zhang J, Wang Y, Chi Z, Keuss MJ, Pai YM, Kang HC, Shin JH, Bugayenko A, Wang H, Xiong Y, Pletnikov MV, Mattson MP, Dawson TM, Dawson VL (2011) The AAA+ ATPase Thorase regulates AMPA receptor-dependent synaptic plasticity and behavior. *Cell* 145: 284 – 299

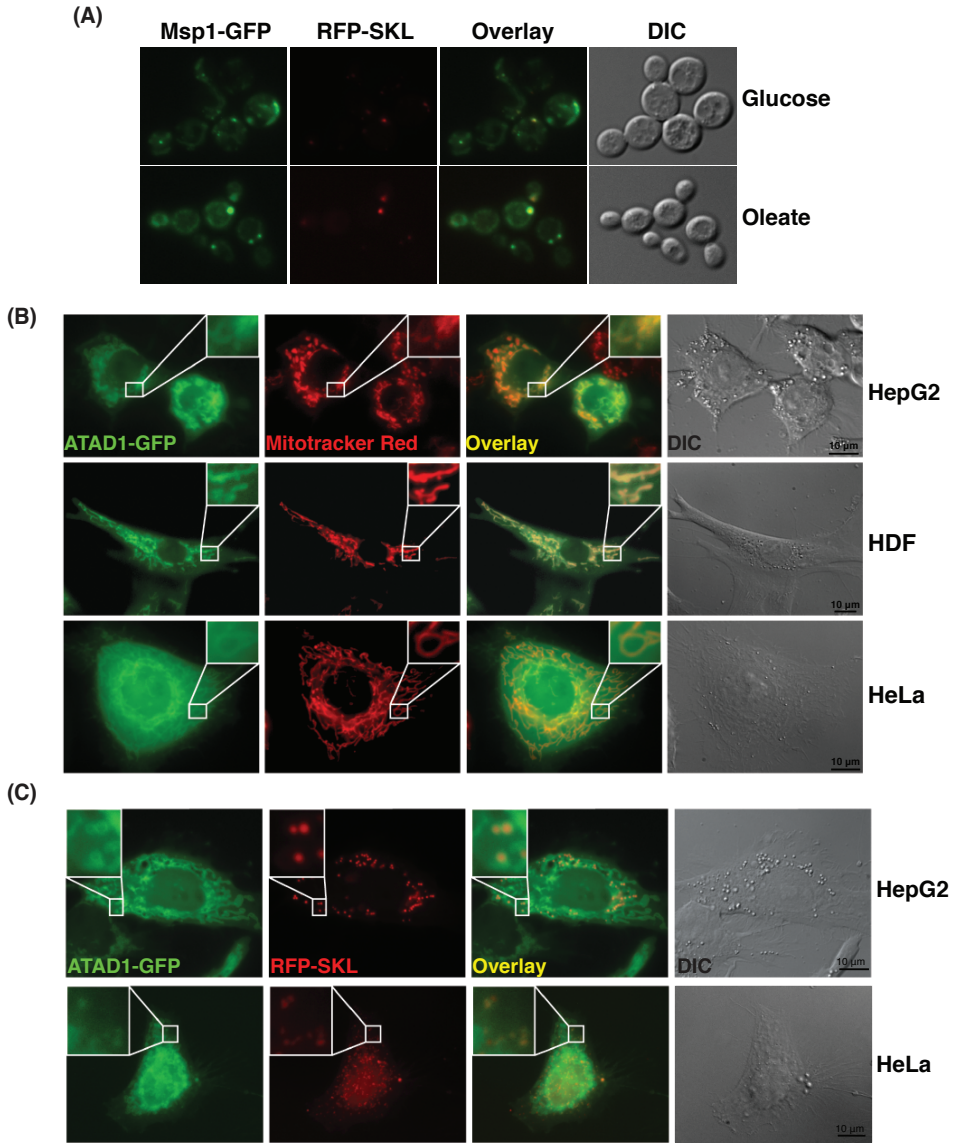

Supplementary Figure 1. Yeast Msp1 and human ATAD1 localize to both mitochondria and peroxisomes. (Related to Figure 1)

(A) The *msp1*Δ strain transformed with plasmids expressing Msp1-GFP and peroxisomal RFP (RFP-SKL) was grown in SD or synthetic oleate medium for 10 hr, fixed in 4% formaldehyde and visualized by fluorescence microscopy. (B) Human hepatocelluar liver carcinoma (HepG2), HDF or HeLa cells that stably express the ATAD1-GFP fusion were stained with Mitotracker Red and visualized by fluorescence microscopy. (C) HepG2 or HeLa cells stably expressing the ATAD1-GFP fusion and the peroxisomal RFP marker (RFP-SKL) were examined by fluorescence microscopy.

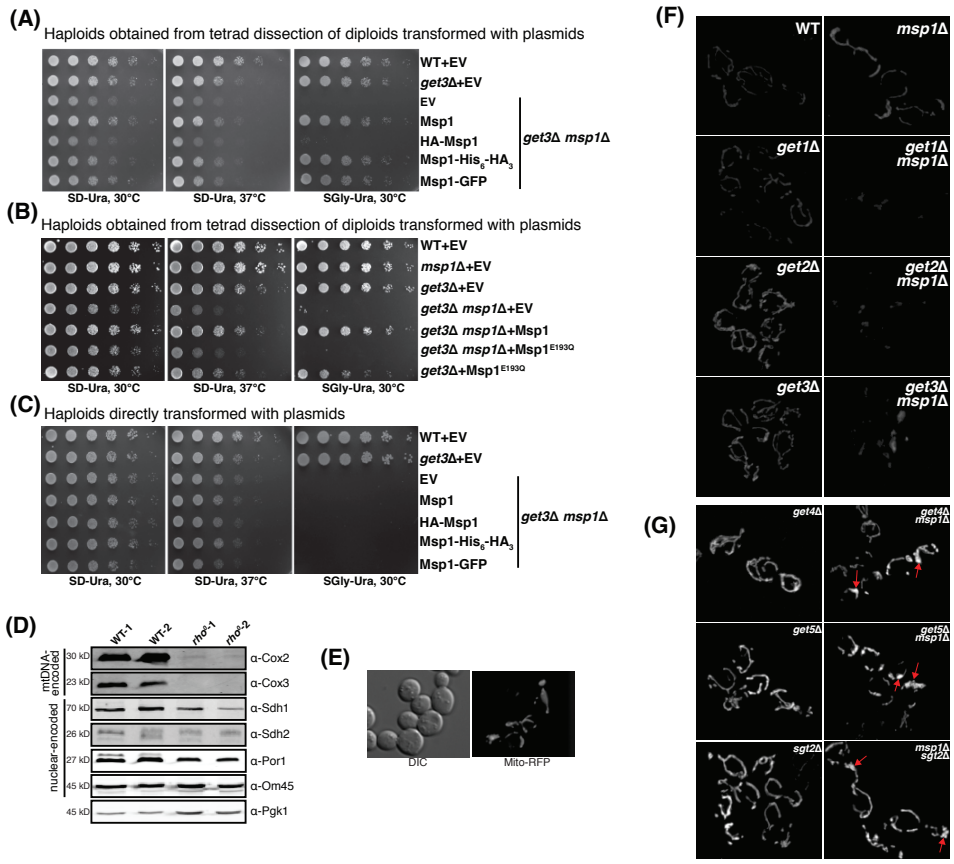

Supplementary Figure 2. The *msp1*Δ mutant exhibits growth defects and severe mitochondria damage when combined with GET mutants. (Related to Figure 2)

(A) The heterozygous *get3*Δ/*GET3 msp1*Δ/*MSP1* diploid strain was transformed with EV, wild-type, N-terminal HA tagged (HA-Msp1), or C-terminal GFP (Msp1-GFP) or His_6-HA_3 (Msp1-His_6-HA_3) tagged Msp1 construct, was sporulated and tetrads were dissected. The obtained haploid strains harboring different vectors as well as the wild-type (WT) and the *get3*Δ strains that were transformed with EV were spotted on SD-Ura or SGly-Ura plates and cultured at 30 or 37°C. (B) The *get3*Δ *msp1*Δ haploid strains harboring the indicated constructs were prepared as in (A). Five-fold dilutions of these strains and the WT, *msp1*Δ or *get3*Δ strain transformed with EV or $Msp1^{E193Q}$ construct were spotted on SD-Ura or SGly-Ura plates and incubated at 30 or 37°C. (C) The indicated strains were transformed with EV, wild-type or the tagged Msp1 construct, and five-fold dilutions were spotted on SD-Ura or SGly-Ura plates and incubated at 30 or 37°C. (D) Whole-cell lysates extracted from the WT and the *rho*^{0} strain were immunoblotted for mitochondrial proteins and the Pgk1 cytoplasmic protein. (E) The *rho*^{0} strain expressing a Mito-RFP was visualized by fluorescence microscopy. (F) Images of cells from Figure 2D, but more similar exposure time images are shown here. Even still, the images of the *get1*Δ *msp1*Δ, *get2*Δ *msp1*Δ and *get3*Δ *msp1*Δ strains were exposed 2X longer (400 ms) than the WT and single mutant strains (200 ms). When we image the *get1*Δ *msp1*Δ, *get2*Δ *msp1*Δ and *get3*Δ *msp1*Δ strains with 200 ms exposure times, we see no or very dim RFP signal. (G) Another set of images showing the atypical mitochondrial swelling (indicated by arrows) observed in the *get4*Δ *msp1*Δ, *get5*Δ *msp1*Δ and *msp1*Δ *sgt2*Δ strains (also see Figure 2D).

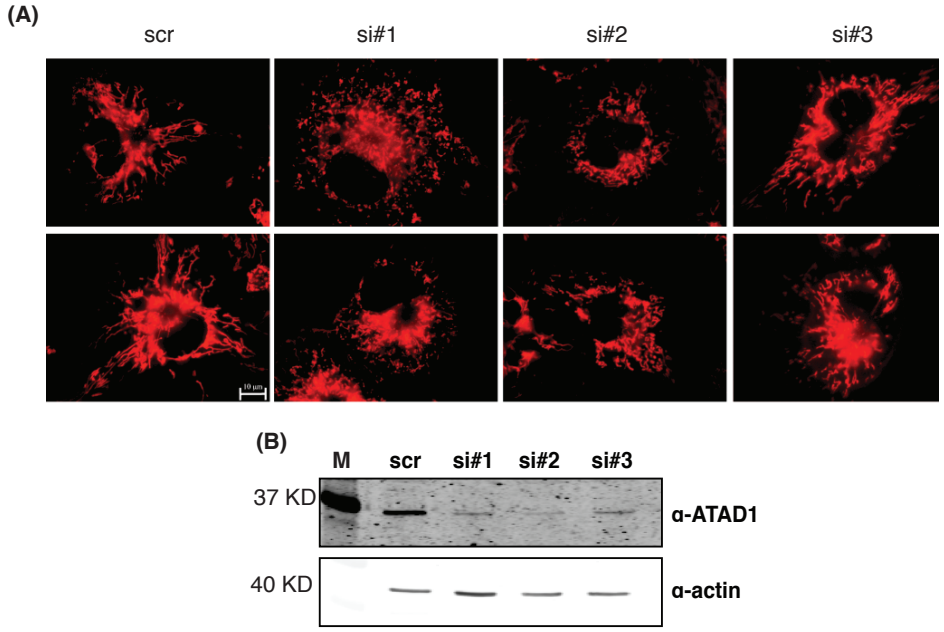

Supplementary Figure 3. Depletion of human *ATAD1* causes mitochondrial fragmentation in HeLa cells. (Related to Figure 3)
(A) HeLa cells were treated with the control siRNA (scr) or siRNAs (#1-#3) targeting human *ATAD1* for 6 days and stained with Mitotracker Red for fluorescence microscopic imaging. (B) The knockdown efficacy was evaluated by immunoblot. M, molecular weight maker.

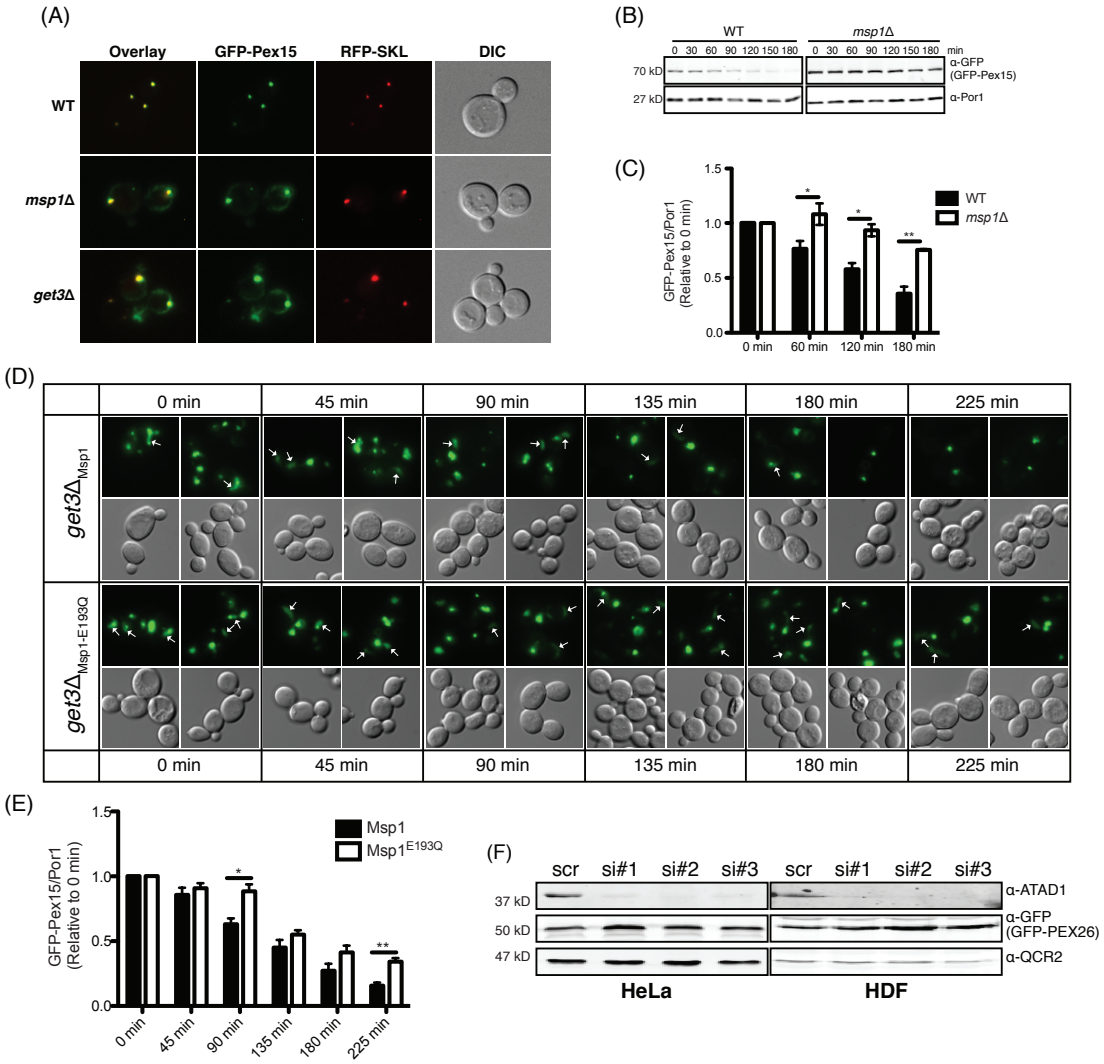

Supplementary Figure 4. Msp1 and ATAD1 facilitate the turnover of Pex15 and Pex26, respectively. (Related to Figure 4)

(A)The indicated strains co-expressing GFP-Pex15 from the *GAL1* promoter and RFP-SKL were cultured in galactose medium for 6 hr and imaged by fluorescence microscopy. (B)The wild-type and *msp1*Δ strain expressing GFP-Pex15 from the *GAL1* promoter were grown in SGal medium for 5-6 hr to induce GFP-Pex15 accumulation and then pulsed in glucose medium. Whole-cell lysates were prepared from cells harvested every 30 min and analyzed by immunoblot. Por1 is the loading control. (C) The optical densitometry quantification of (B). The values represent mean ± SEM (n=3, * p<0.05, **<0.01, t-test, two-tail). (D) Representative images of the galactose promoter-based shut-off experiment shown in Figure 4E. Arrows mark the area of mitochondria. (E)The optical densitometry quantification of Figure 4E. The values represent mean ± SEM (n=3, * p<0.05, **<0.01, t-test, two-tail). (F) HeLa cells and HDFs stably expressing GFP-PEX26 protein were treated with the control siRNA (scr) or the siRNAs (#1-#3) against human *ATAD1* for 6 days. Whole-cell lysates were harvested and immunoblotted with anti-ATAD1, GFP and QCR2 antibodies. QCR2 is a mitochondrial protein used as a loading control.

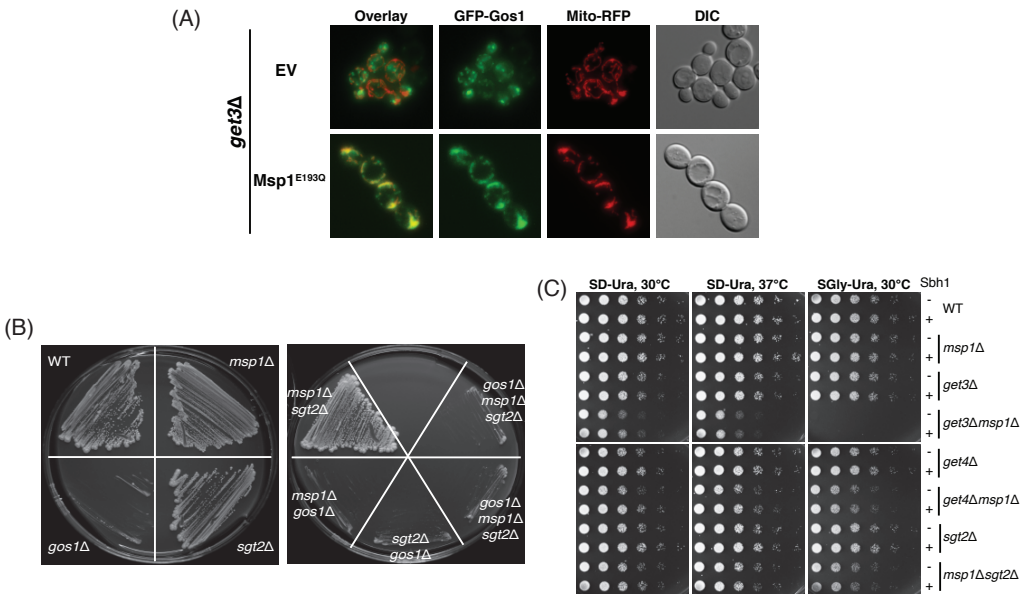

Supplementary Figure 5. Msp1 physically interacts with the TA protein Gos1 and is required to limit the level of mislocalized Gos1 on mitochondria. (Related to Figure 5)
(A) Representative images of the *get3*Δ mutant strain expressing GFP-Gos1 with Msp1^{E193Q} or without Msp1^{E193Q} (EV). Cells were grown in SD medium to log-phase and imaged by fluorescence microscopy. (B)The *gos1*Δ/*GOS1 msp1*Δ/*MSP1 sgt2*Δ/SGT2 diploid strain transformed with a wild-type Gos1 construct (pRS416-based) was sporulated and tetrad analyzed. The indicated haploid strains harboring the plasmid were streaked on SD plates containing 5-FOA and incubated at 30°C for 3-4 days. (C) The indicated strains with or without overexpression of the Sbh1 protein from the *TEF1* promoter were serial-diluted, spotted on SD-Ura or SGly medium and cultured at 30 or 37°C.

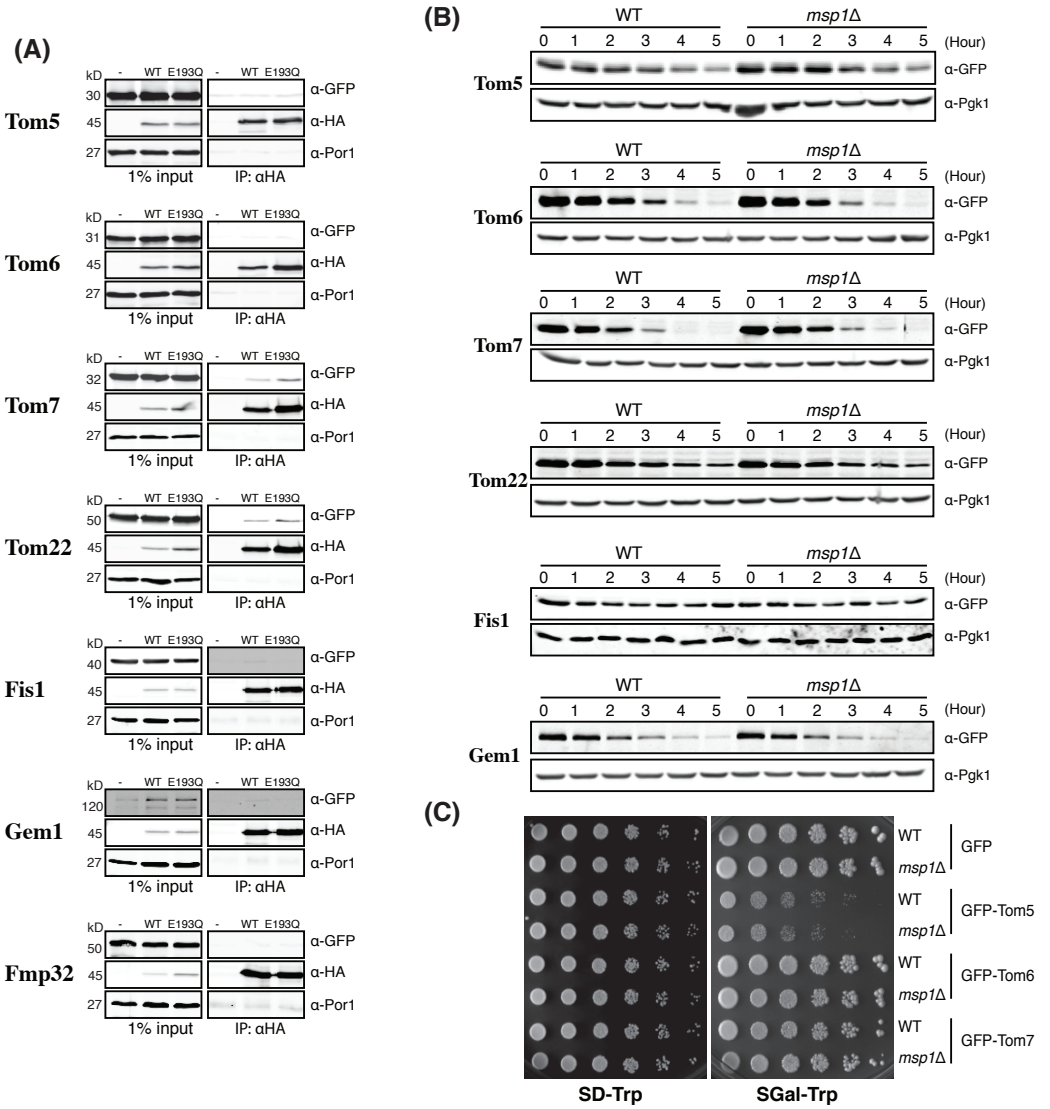

Supplementary Figure 6. Mitochondrial TA proteins are poor substrates of yeast Msp1.
(A) The wild-type strain harboring the N-terminally GFP tagged mitochondrial TA proteins (Tom5, Tom6, Tom7, Tom22, Fis1, Gem1 and Fmp32) expressed from the *GAL1* promoter and empty vector (-), Msp1-His_6-HA_3 or $Msp1^{E193Q}$-His_6-HA_3 fusion were cultured in galactose medium for 6 hours and subjected to co-immunoprecipitation. Both 1% whole-cell lysates and anti-HA antibody-precipitated final eluates were analyzed and immunoblotted with anti-HA, GFP and Por1 antibodies. (B) Both the wild-type (WT) and *msp1*Δ mutant strains expressing the indicated GFP-tagged mitochondrial TA proteins from the *GAL1* promoter were cultured in galactose medium for 6 hours to induce protein expression and switched back to glucose medium. Whole-cell lysates were harvested every hour post-induction and analyzed by immunoblot. Pgk1 is a cytoplasmic protein used a loading control. (C) The indicated strains were five-fold diluted, spotted on glucose or galactose plates and incubated at 30°C.

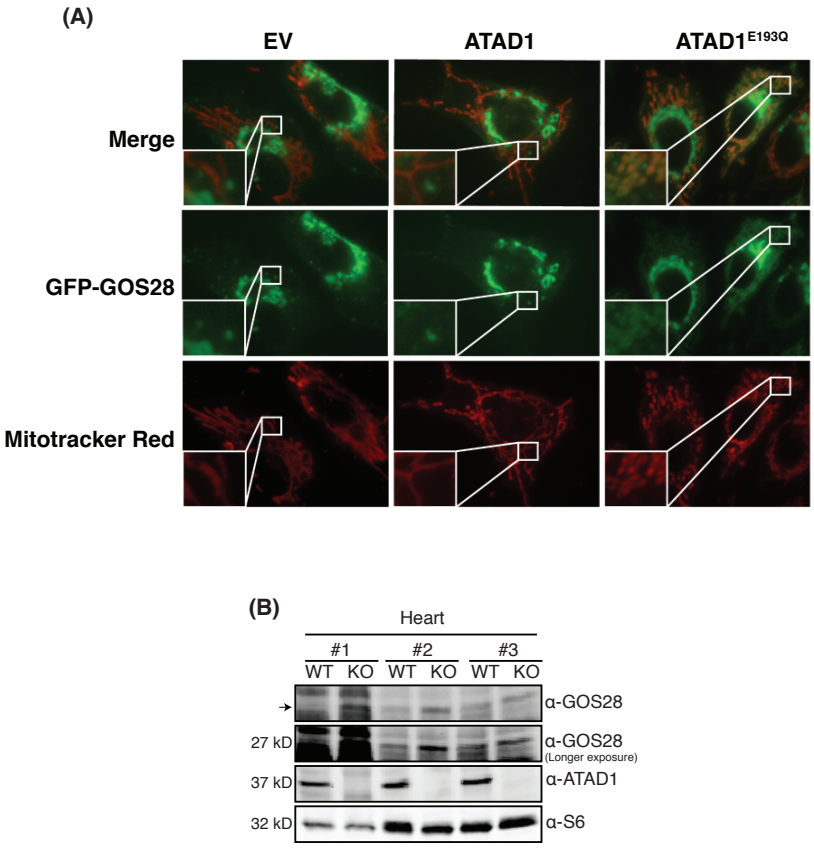

Supplementary Figure 7. Expression of the dominant-negative mutant ATAD1-E193Q causes mislocalization of GOS28 to the mitochondria. (Related to Figure 6)
HepG2 cells stably expressing the GFP-GOS28 fusion protein and empty vector (EV), wild-type ATAD1 or mutant ATAD1 (ATAD1^{E193Q}) protein were stained with Mitotracker Red and visualized by fluorescence microscopy. (B) WT and *ATAD1*$^{-/-}$ mouse heart were homogenized and analyzed by immunoblot. S6 ribosomal protein is the loading control. GOS28 is indicated by the arrow.

Supplementary Table S1. List of proteins identified by mass spectrometry

Legend	
Identified proteins shown in this table	NSAF>100
WT EV	wild-type strain harboring empty vector
WT Msp1	wild-type strain harboring Msp1-6His-3HA construct
WT Msp1-E193Q	wild-type strain harboring Msp1(E193Q)-6His-3HA construct
get3Δ Msp1-E193Q	get3 null mutant harboriing Msp1(E193Q)-6His-3HA construct
Reference	sgd ORF name
Gene Symbol	sgd gene symbol
description	sgd gene description
prot_len	# amino acids in predicted ORF
NSAF	NSAF = normalized spectral abundance factor, a crude quantitative measure that is simply the fraction of total psms assigned to this protein normalized to the length of the protein

				Peptide Counts		Normalize to protein length	
	Reference	Gene symbol	SeqLen	control	WT Msp1	ctl NSAF	WT Msp1_NSAF
	YGR028W	*MSP1*	362	0	191	0	**1416**
	YNL055C	*POR1*	283	1	50	17	**474**
	YCL057C-A	*YCL057C-A*	97	0	16	0	**443**
	YOR354C	*MSC6*	692	0	69	0	**268**
	YDR481C	*PHO8*	566	5	52	43	**247**
	YDL174C	*DLD1*	587	0	47	0	**215**
	YMR209C	*YMR209C*	457	0	36	0	**211**
	YER086W	*ILV1*	576	1	42	8	**196**
	YGR132C	*PHB1*	287	1	20	17	**187**
	YOR317W	*FAA1*	700	3	47	21	**180**
	YOR125C	*CAT5*	233	0	14	0	**161**
WT EV v.s. WT Msp1	YKL212W	*SAC1*	623	0	37	0	**159**
	YPL218W	*SAR1*	190	1	11	26	**155**
	YCR003W	*MRPL32*	183	1	10	27	**147**
	YGL037C	*PNC1*	216	1	11	22	**137**
	YHR190W	*ERG9*	444	0	22	0	**133**
	YGR157W	*CHO2*	869	0	43	0	**133**
	YMR089C	*YTA12*	825	4	40	24	**130**
	YMR129W	*POM152*	1337	0	64	0	**128**
	YER017C	*AFG3*	761	2	34	13	**120**
	YBR106W	*PHO88*	188	0	8	0	**114**
	YDR513W	*GRX2*	143	0	6	0	**113**
	YNL111C	*CYB5*	120	0	5	0	**112**
	YAL042W	*ERV46*	415	0	16	0	**103**

	Reference	Gene symbol	SeqLen	control	get3Δ Msp ctl NSAF	get3Δ Msp1_NSAF	
	YGR028W	*MSP1*	362	0	676	0	**4248**
	YDR231C	*COX20*	205	0	44	0	**488**
	YNL055C	*POR1*	283	1	58	17	**466**
	YDL067C	*COX9*	59	0	11	0	**424**
	YCR003W	*MRPL32*	183	1	28	27	**348**
	YPR133W-A	*TOM5*	50	0	7	0	**318**
	YPL249C-A	*RPL36B*	100	1	14	49	**318**
	YJL189W	*RPL39*	51	0	7	0	**312**
	YPR010C-A	*YPR010C-A*	72	0	8	0	**253**
	YMR194W	*RPL36A*	100	1	11	49	**250**
	YML030W	*AIM31*	159	0	15	0	**215**
	YLR167W	*RPS31*	152	1	14	32	**210**
	YKR094C	*RPL40B*	128	1	11	38	**195**
	YIL148W	*RPL40A*	128	1	11	38	**195**
	YMR193W	*MRPL24*	258	0	18	0	**159**
WT EV v.s. WT Msp1-E193Q	YJR094W-A	*RPL43B*	92	0	6	0	**148**
	YPR043W	*RPL43A*	92	0	6	0	**148**
	YGL037C	*PNC1*	216	1	14	22	**147**
	YBL068W-A	*YBL068W-A*	78	0	5	0	**146**
	YPL218W	*SAR1*	190	1	11	26	**132**
	YIL083C	*CAB2*	365	0	20	0	**125**
	YDL174C	*DLD1*	587	0	31	0	**120**
	YBL026W	*LSM2*	95	0	5	0	**120**
	YCL057C-A	*YCL057C-A*	97	0	5	0	**117**
	YOR317W	*FAA1*	700	3	35	21	**114**
	YMR203W	*TOM40*	387	0	19	0	**112**
	YDR513W	*GRX2*	143	0	7	0	**111**
	YIL136W	*OM45*	393	0	19	0	**110**
	YCR046C	*IMG1*	169	0	8	0	**108**
	YBL030C	*PET9*	318	0	15	0	**107**
	YGL191W	*COX13*	129	0	6	0	**106**
	YCR031C	*RPS14A*	137	0	6	0	**100**

	Reference	Gene symbol	SeqLen	control	get3Δ_Msp	ctl_NSAF	get3Δ_Msp1-E193Q_NSAF
	YGR028W	*MSP1*	362	0	512	0	**3065**
	YNL055C	*POR1*	283	1	67	17	**513**
	YHL031C	*GOS1*	223	0	36	0	**350**
	YPR133W-A	*TOM5*	50	0	8	0	**347**
	YCL057C-A	*YCL057C-A*	97	0	15	0	**335**
	YDL067C	*COX9*	59	0	9	0	**331**
	YDR231C	*COX20*	205	0	29	0	**307**
	YMR203W	*TOM40*	387	0	44	0	**246**
	YDL174C	*DLD1*	587	0	61	0	**225**
	YPR010C-A	*YPR010C-A*	72	0	7	0	**211**
	YML030W	*AIM31*	159	0	15	0	**204**
	YJL062W-A	*YJL062W-A*	85	0	8	0	**204**
	YBL030C	*PET9*	318	0	29	0	**198**
	YJR085C	*YJR085C*	105	0	9	0	**186**
	YDR513W	*GRX2*	143	0	12	0	**182**
	YGR132C	*PHB1*	287	1	23	17	**174**
	YLR142W	*PUT1*	476	0	38	0	**173**
	YIL083C	*CAB2*	365	0	29	0	**172**
	YMR209C	*YMR209C*	457	0	36	0	**171**
WT EV v.s. get3Δ Msp1-E193Q	YER120W	*SCS2*	244	0	19	0	**169**
	YGR174C	*CBP4*	170	0	13	0	**166**
	YGL231C	*EMC4*	190	0	14	0	**160**
	YMR029C	*FAR8*	523	0	37	0	**153**
	YJL066C	*MPM1*	252	0	17	0	**146**
	YMR052W	*FAR3*	204	0	12	0	**127**
	YNL111C	*CYB5*	120	0	7	0	**126**
	YOR065W	*CYT1*	309	0	18	0	**126**
	YER141W	*COX15*	486	0	27	0	**120**
	YDR079W	*PET100*	111	0	6	0	**117**
	YNL131W	*TOM22*	152	0	8	0	**114**
	YCR031C	*RPS14A*	137	0	7	0	**111**
	YJL191W	*RPS14B*	138	0	7	0	**110**
	YMR129W	*POM152*	1337	0	66	0	**107**
	YMR264W	*CUE1*	203	0	10	0	**107**
	YMR110C	*HFD1*	532	0	26	0	**106**
	YML120C	*NDI1*	513	0	25	0	**106**
	YER086W	*ILV1*	576	1	28	8	**105**
	YDR292C	*SRP101*	621	0	30	0	**105**
	YPL224C	*MMT2*	449	0	21	0	**101**
	YKL212W	*SAC1*	623	0	29	0	**101**

Supplementary Table S2. List of yeast strains used in this study

Number	Strains	Genotype	Source
JRY245	WT (W303)	*MAT***a** *his3 leu2 lys2 met15 trp1 ura3*	David Stillman
JRY1816	*msp1*Δ	*MAT***a** *his3 leu2 lys2 met15 trp1 ura3 msp1::kanMX4*	This study
JRY2352	*get1*Δ	*MAT***a** *his3 leu2 lys2 met15 trp1 ura3 get1::hphMX4*	This study
JRY2082	*get2*Δ	*MAT***a** *his3 leu2 lys2 met15 trp1 ura3 get2::hphMX4*	This study
JRY1815	*get3*Δ	*MAT***a** *his3 leu2 lys2 met15 trp1 ura3 get3::hphMX4*	This study
JRY2337	*get4*Δ	*MAT***a** *his3 leu2 lys2 met15 trp1 ura3 get4::hphMX4*	This study
JRY2357	*get5*Δ	*MAT***a** *his3 leu2 lys2 met15 trp1 ura3 get5::hphMX4*	This study
JRY2502	*sgt2*Δ	*MAT***a** *his3 leu2 lys2 met15 trp1 ura3 sgt2::hphMX4*	This study
JRY2348	*get1*Δ *msp1*Δ	*MAT***a** *his3 leu2 lys2 met15 trp1 ura3 get1::hphMX4 msp1::kanMX4*	This study
JRY2098	*get2*Δ *msp1*Δ	*MAT***a** *his3 leu2 lys2 met15 trp1 ura3 get2::hphMX4 msp1::kanMX4*	This study
JRY1814	*get3*Δ *msp1*Δ	*MAT***a** *his3 leu2 lys2 met15 trp1 ura3 get3::hphMX4 msp1::kanMX4*	This study
JRY2339	*get4*Δ *msp1*Δ	*MAT***a** *his3 leu2 lys2 met15 trp1 ura3 get4::hphMX4 msp1::kanMX4*	This study
JRY2358	*get5*Δ *msp1*Δ	*MAT***a** *his3 leu2 lys2 met15 trp1 ura3 get5::hphMX4 msp1::kanMX4*	This study
JRY2504	*msp1*Δ *sgt2*Δ	*MAT***a** *his3 leu2 lys2 met15 trp1 ura3 msp1::kanMX4 sgt2::hphMX4*	This study
JRY490	rho^0	*MAT***a** *his3 leu2 lys2 met15 trp1 ura3* ρ^-	Jared Rutter
JRY2285	*sdh5*Δ	*MAT***a** *his3 leu2 lys2 met15 trp1 ura3 sdh5::NatMX4*	Jonathan Van Vranken
JRY1862a	WT *GAL1::GFP-Pex15*	*MAT***a** *his3 leu2 lys2 met15 trp1 ura3 His3MX6-GAL1::GFP-PEX15*	This study
JRY1862c	*msp1*Δ *GAL1::GFP-Pex15*	*MAT***a** *his3 leu2 lys2 met15 trp1 ura3 His3MX6-GAL1::GFP-PEX15 msp1::KanMX4*	This study
JRY1862e	*get3*Δ *GAL1::GFP-Pex15*	*MAT***a** *his3 leu2 lys2 met15 trp1 ura3 His3MX6-GAL1::GFP-PEX15 get3::hphMX4*	This study
JRY1862g	*get3*Δ*msp1*Δ *GAL1::GFP-Pex15*	*MAT***a** *his3 leu2 lys2 met15 trp1 ura3 His3MX6-GAL1::GFP-PEX15 msp1::KanMX4 get3::hphMX4*	This study

CHAPTER 4

MSP1/ATAD1 PARTICIPATES IN MITOCHONDRIA-TO-PEROXISOME TRAFFICKING AND PEROXISOME FUNCTION

Introduction

Peroxisomes are single membrane organelles that are known for their conserved functions in the metabolism of fatty acids and scavenging of reactive oxygen species. They are present in virtually all eukaryotes. In spite of these common functions, peroxisomes also possess diverse and specialized functions according to the cell type and organism (Smith and Aitchison, 2013). The mammalian peroxisome is involved in the biosynthesis of many biomolecules, including plasmalogen, the precursor used for making myelin for neurons, bile acids, purine and fatty acids. This organelle also serves as an antiviral signaling platform that is activated upon infection by a peroxisome-localized antiviral protein (Dixit et al., 2010; Lodhi and Semenkovich, 2014). The plant peroxisome is specialized for photorespiration and the glyoxylate cycle, particularly during seed germination (Hu et al., 2012). The fungal peroxisome synthesizes antibiotics and pathogenic toxins (van der Klei and Veenhuis, 2013). The majority of peroxisomal reactions occur inside the organelle, into which more than 50 enzymes are imported. On the membrane, peroxisomal membrane proteins (PMPs) comprise primarily metabolite transporters and peroxins (Theodoulou et al., 2013). Peroxins are peroxisome biogenesis factors that participate in different aspects of peroxisomal biogenesis ranging from protein import, inheritance, and division. Peroxisome biogenesis disorders (PBDs) are severe inherited metabolic and neuropathic diseases that often lead to early childhood death. Mutations affecting almost all peroxins are linked to PBD with various degrees of severity (Delille et al., 2006). PBDs include Zellweger syndrome (ZS), neonatal adrenoleukodystrophy and infatile Refsum disease. ZS is among the most severe presentations of the PDBs, with clinical features of dysmorphia, neonatal seizures,

hematomegaly, renal cysts, skeletal abnormalities and impaired hearing (Crane, 2014).

Like mitochondria, peroxisomes have been postulated to be autonomous organelles because peroxisomal proteins are synthesized on free polyribosome and post-translationally incorporated into the pre-existing peroxisomes and they can multiply by division (Lazarow and Fujiki, 1985). However, this idea has been challenged by the observations that peroxins localize to ER in mutants lacking peroxisomes and peroxisomes can be formed *de novo* from ER upon complementation (South and Gould, 1999). A subset of peroxins (*e.g.*, Pex3 in yeast and PEX16 in mammals) were shown to traffic from ER to peroxisomes in both yeast and mammalian cells. The peroxins are targeted to ER after being translated and sorted into ER subdomains (Hoepfner et al., 2005). Subsequently, the pre-peroxisomal vesicles carrying different peroxin cargoes bud off from the ER and eventually fuse to form mature and import-competent peroxisomes in the cytoplasm (van der Zand et al., 2012).

Apparently, in spite of coupling with ER, peroxisomes and mitochondria are functionally and physically engaged based on several observations (Schrader and Yoon, 2007). First, mammalian β-oxidation is shared between the two organelles. Peroxisomes break down long chain fatty acids, leukotrienes and prostaglandins, and the shortened fatty acids can be transported into mitochondria for further oxidation into acetyl-coA, which is then fed into the TCA cycle (Poirier et al., 2006). How fatty acids are transported from peroxisomes to mitochondria is still under debate. Second, several studies suggest that mitochondria and peroxisomes might be physically adjacent to each other (Cohen et al., 2014). Third, they share the same set of fission machinery. Both peroxisomes and mitochondria can multiply by fission of preexisting organelles. The

peroxin, Pex11, first works on membrane elongation and deformation and then the components of the classical mitochondrial fission machinery are recruited to the peroxisomes (Opalinski et al., 2011). This includes the adaptor proteins, FIS1 and MFF in mammals; Fis1, Caf4 and Mdv1 in yeast; the large GTPase, DLP1/DRP1 in mammals; and Dnm1 in yeast, which performs the terminal membrane scission reaction (Schrader et al., 2012). Last but not least, recent research indicates that there are vesicles trafficking from mitochondria to peroxisomes (Braschi et al., 2010; Mohanty and McBride, 2013; Neuspiel et al., 2008). Mitochondria-derived vesicles (MDVs), by which a cargo protein, mitochondrial anchored protein ligase MAPL, is trafficked from mitochondria to peroxisomes were first discovered several years ago. MAPL was shown to localize to both mitochondria and a subpopulation of peroxisomes. Live-cell imaging showed that MAPL-decorated vesicles bud off from mitochondria and eventually fuse with a subset of peroxisomes (Neuspiel et al., 2008). The formation of MAPL decorated-MDVs appears to depend on the retromer complex, a critical component for vesicle transport (Braschi et al., 2010). The function of MAPL or MDVs has not yet been determined but a few ideas have been proposed, including peroxisomal biogenesis and metabolite shuttling (Mohanty and McBride, 2013).

Yeast Msp1 and mammalian ATAD1 (also known as Thorase) belong to the AAA+ (ATPase associated with various cellular activities) ATPase protein family. We previously described this protein in facilitating the extraction and degradation of mis-localized tail-anchored proteins from mitochondria (Chen et al., 2014). Since Msp1/ATAD1 localizes to mitochondria and peroxisomes and perhaps the plasma membrane, we believe that it must perform multiple tasks in the cell (Chen et al., 2014;

Zhang et al., 2011). Most AAA+ ATPases oligomerize to form a channel that translocates and unfolds protein complexes using the energy derived from ATP hydrolysis (Hanson and Whiteheart, 2005). It is known that a subset of AAA+ ATPases play a specialized role in membrane dynamics and trafficking (*e.g.*, VPS4 in multivesicular body budding; NSF in disassembly of SNARE proteins; Torsin in budding of large ribonucleiprotein granules at the nuclear envelope) (Babst, 2005; Jokhi et al., 2013; Littleton et al., 2001). Intriguingly, mammalian ATAD1 was shown to participate in the disassembly of α-amino-3-hydroxy-5-methylisoxazole-4-proprionic acid receptor (AMPAR) complex on the synaptic membrane, which determines the rate of endocytosis of AMPAR receptor (Zhang et al., 2011). This result suggests that members of the Msp1/ATAD1 protein family likely also play a role in membrane internalization and vesicle trafficking.

In this study, we provide evidence that Msp1/ATAD1 participates in mitochondria-to-peroxisome trafficking *via* small vesicles. These data include: first, the AAA+ ATPase domain on Msp1 is sufficient for Msp1 localization to peroxisomes. Second, pulse-chase experiments indicate that Msp1 first localizes to mitochondria and then traffics to peroxisomes. Third, in a mutant yeast strain lacking peroxisomes, Msp1 colocalizes to vesicle-like structures. Fourth, we show that the mitochondrial fusion protein, Fzo1 (fuzzy onion 1) is crucial for Msp1 localization to peroxisomes. Last, we show that Msp1 plays a crucial role in maintaining peroxisome morphology and peroxin localization as depletion of Msp1 causes peroxisome fragmentation and peroxin localization to mitochondria. Overexpression of ATAD1, however, sequesters peroxins to vesicle-like structures from the mitochondria in mammalian cells. Therefore, we

hypothesize that Msp1/ATAD1 plays a role in sorting peroxins from mitochondria to peroxisomes *via* a novel vesicular trafficking pathway.

Results

The AAA+ ATPase domain is necessary and sufficient for Msp1 localization to peroxisomes

We previously showed that Msp1/ATAD1 localizes to both mitochondria and peroxisomes (Chen et al., 2014). We wanted to know how this dual localization is achieved. As both proteins share a highly conserved AAA+ domain at the C-terminus and a semiconserved TMD at the N-terminus, we hypothesized that one of these elements should contribute to this unique localization pattern. First, to test if ATPase activity of the AAA+ domain is required for the dual localization, we co-expressed GFP-tagged wild-type- (Msp1-GFP) or ATPase-inactive Msp1 (Msp1^{E193Q}-GFP) and mitochondria- or peroxisome-targeted red fluorescent protein (mito-RFP or RFP-SKL) in the *msp1*Δ strain. As shown in Figure 4-1A, Msp1-GFP signal overlapped with mito-RFP signal with extra-mitochondrial puncta, which were demonstrated to be peroxisomes based on co-localization with RFP-SKL. However, Msp1^{E193Q}-GFP, despite colocalizing normally with mito-RFP, did not exhibit any extra-mitochondrial signal. We then confirmed that Msp1^{E193Q} had lost the ability to localize to peroxisomes, because Msp1^{E193Q}-GFP showed almost no colocalization with RFP-SKL **(**Figure 4-1A, middle panel). The loss of peroxisome localization of the Msp1^{E193Q} mutant was also observed when these same strains were cultured in oleic acid medium to induce peroxisome biogenesis (Figure 4-1A, right panel). Mutations of other conserved residues in the AAA+ domain also

Figure 4-1. The Msp1 AAA+ domain is necessary and sufficient for the peroxisomal localization

(A) Representative images of the *msp1*Δ mutant co-expressing Msp1-GFP or Msp1^{E193Q}-GFP and mito-RFP or RFP-SKL. Overnight yeast cultures were diluted and grown to early log-phase at 30°C in synthetic glucose medium for 6 hr or oleate medium for 10 hr, and visualized by fluorescence microscopy. (B) Representative images of the *msp1*Δ mutant co-expressing Msp1-GFP, Msp1^{K139A}-GFP, Msp1^{R248E}-GFP or Msp1$^{W166G/Y167D}$-GFP and mito-RFP or RFP-SKL. (C) Representative images of the *msp1*Δ mutant co-expressing TOM70^{TMD}-Msp1-GFP, TOM70^{TMD}-Msp1^{E193Q}-GFP, OM45^{TMD}-Msp1-GFP or OM45^{TMD}-Msp1^{E193Q}-GFP and mito-RFP or RFP-SKL. (D) Plasmid borne-wild-type Msp1, TOM70^{TMD}-Msp1-GFP, TOM70^{TMD}-Msp1^{E193Q}-GFP, OM45^{TMD}-Msp1-GFP or OM45^{TMD}-Msp1^{E193Q}-GFP was shuffled into *get3*Δ *msp1*Δ strain. Five-fold dilutions of the indicated yeast strains were spotted on synthetic glucose (SD) or synthetic glycerol plates (SGly), and incubated at 30 or 37°C, respectively (E) Representative images of the *msp1*Δ mutant co-expressing Msp1^{TMD}-Tom70-GFP or TOM70-GFP and mito-RFP or RFP-SKL. Overnight cultured yeast strains in (B), (C) and (E) were diluted and grown to early log-phase at 30°C in synthetic glucose medium for 6 hr and visualized by fluorescence microscopy.

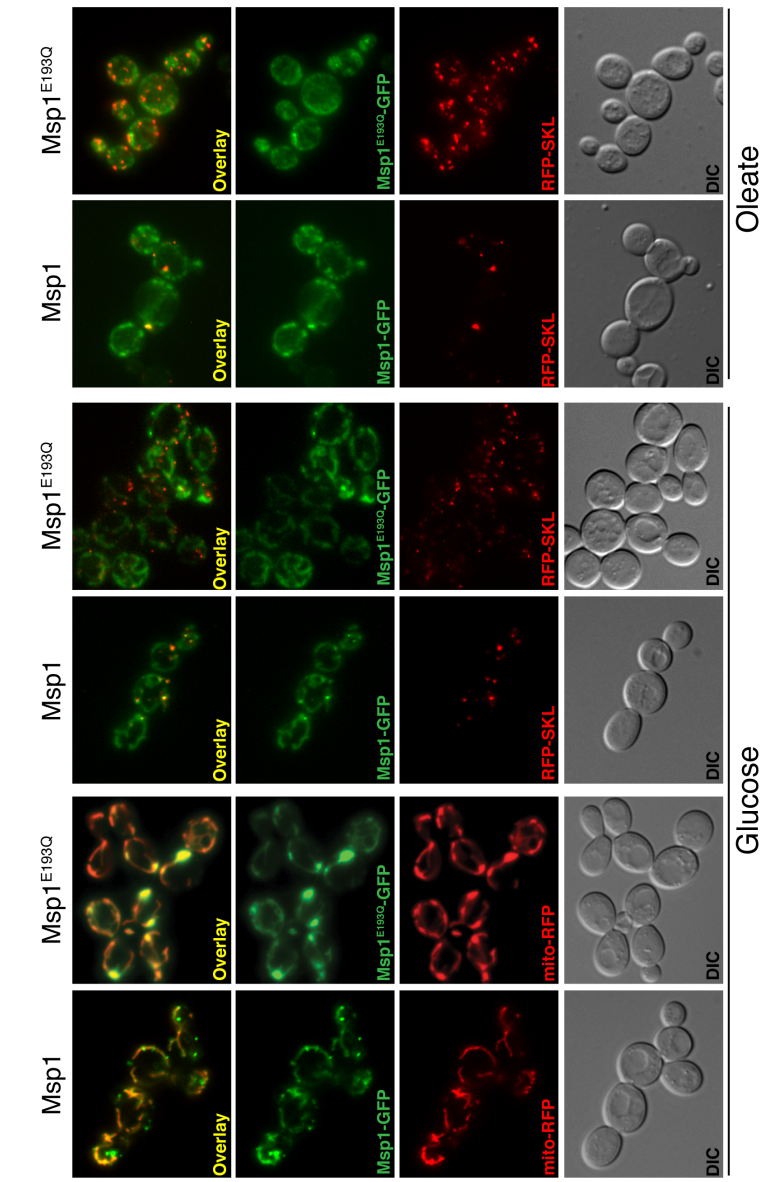
(A)
Msp1
Msp1E193Q
Msp1
Msp1E193Q
Msp1
Msp1E193Q
Overlay
Msp1-GFP
Msp1E193Q-GFP
mito-RFP
RFP-SKL
DIC
Glucose
Oleate

(B)

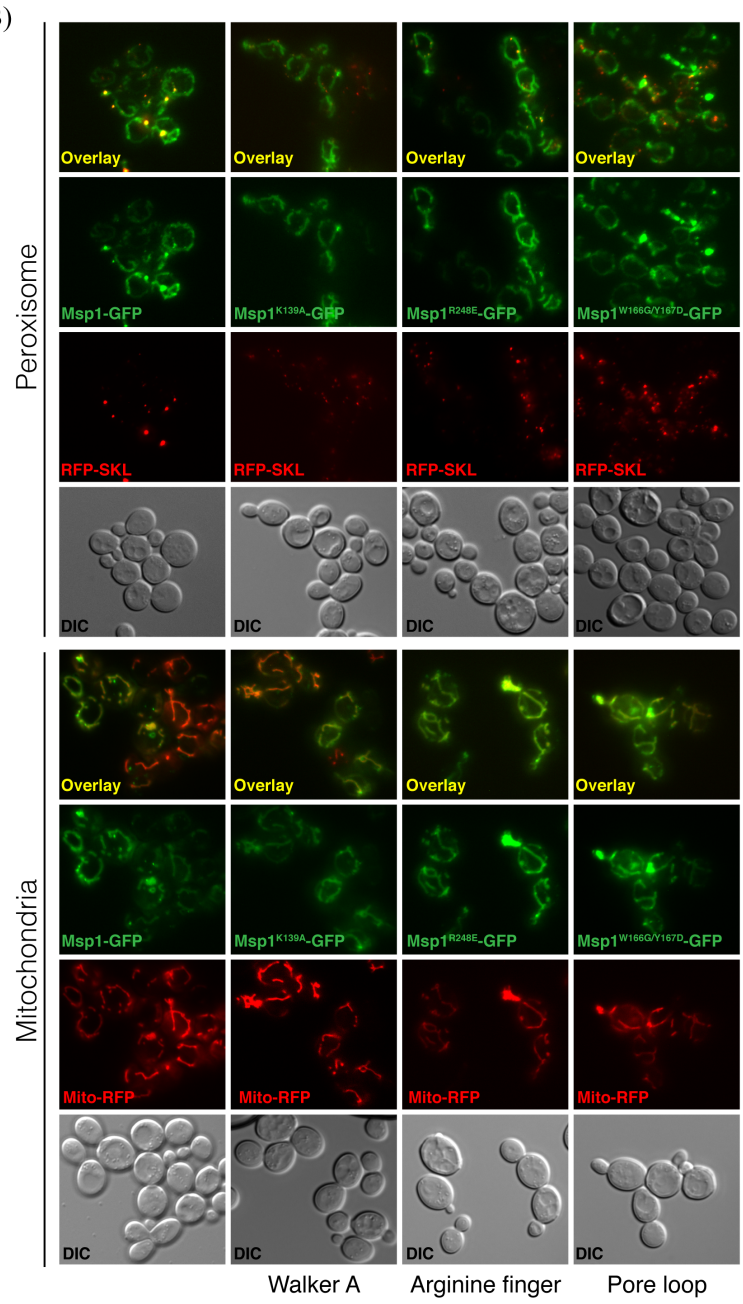
Peroxisome
Mitochondria
Overlay
Msp1-GFP
Msp1K139A-GFP
Msp1R248E-GFP
Msp1W166G/Y167D-GFP
RFP-SKL
Mito-RFP
DIC
Walker A
Arginine finger
Pore loop

(C)

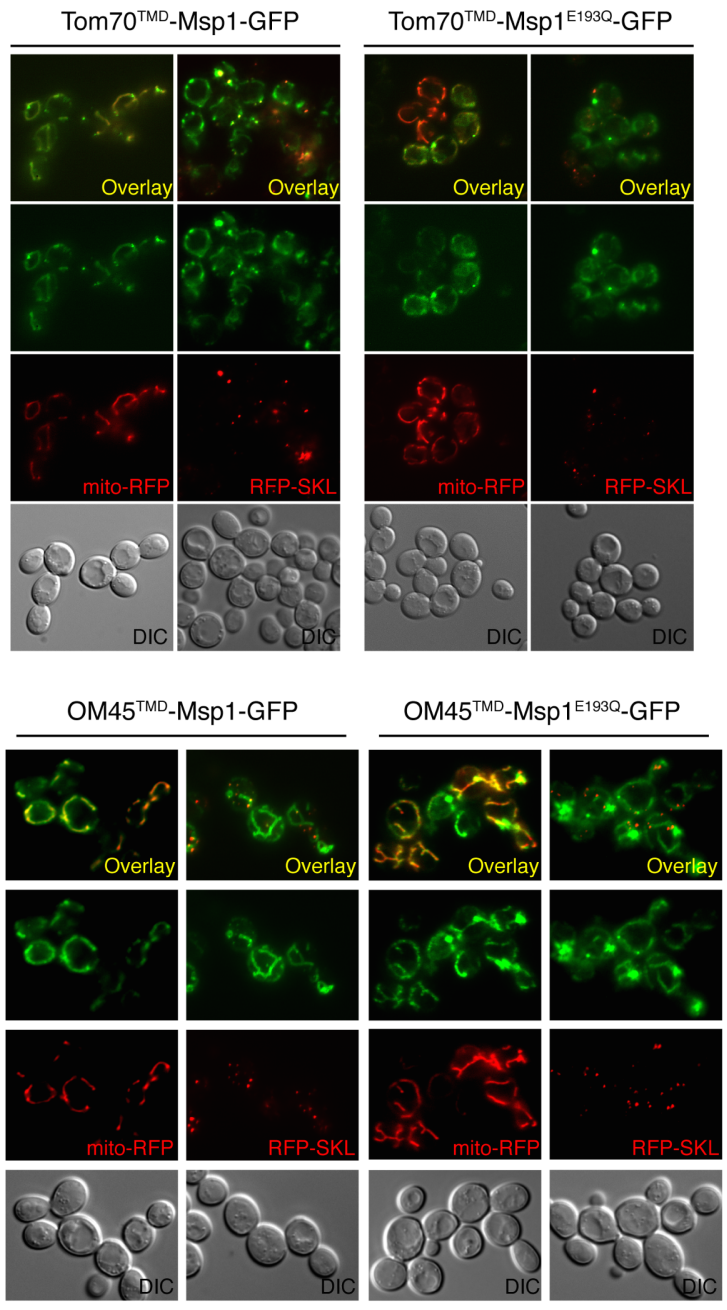
Tom70TMD-Msp1-GFP
Tom70TMD-Msp1E193Q-GFP
Overlay
mito-RFP
RFP-SKL
DIC
OM45TMD-Msp1-GFP
OM45TMD-Msp1E193Q-GFP

(D)

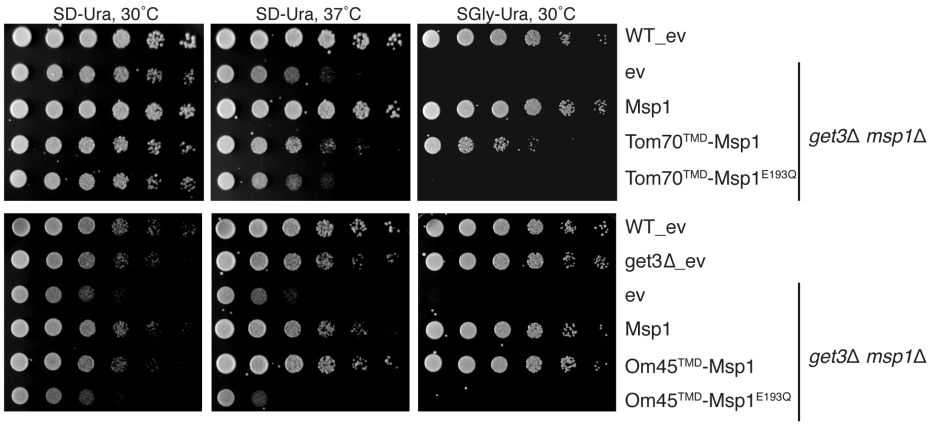
SD-Ura, 30˚C
SD-Ura, 37˚C
SGly-Ura, 30˚C
WT_ev
ev
Msp1
Tom70TMD-Msp1
Tom70TMD-Msp1E193Q
get3Δ msp1Δ
WT_ev
get3Δ_ev
ev
Msp1
Om45TMD-Msp1
Om45TMD-Msp1E193Q
get3Δ msp1Δ

(E)

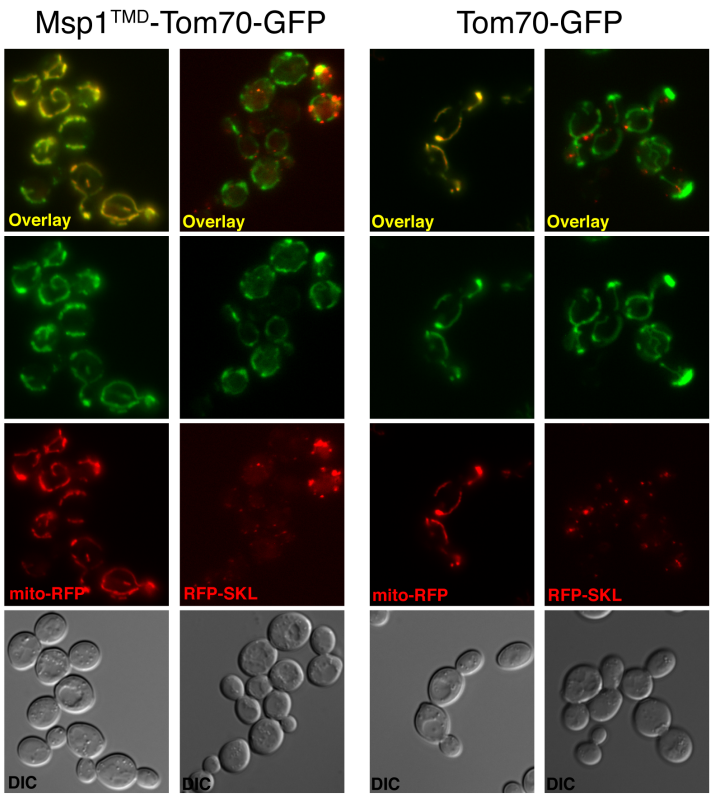
Msp1TMD-Tom70-GFP
Tom70-GFP
Overlay
Overlay
Overlay
Overlay
mito-RFP
RFP-SKL
mito-RFP
RFP-SKL
DIC
DIC
DIC
DIC

drastically diminished peroxisomal localization of Msp1, but did not affect mitochondrial localization (Figure 4-1B). These data demonstrate that activity of the AAA+ domain is crucial for Msp1 localizing to peroxisomes but not to mitochondria.

To further test if the C-terminal region that contains primarily the AAA+ domain is sufficient for Msp1 to localize to peroxisomes, we fused the Msp1 C-terminal fragment (lacking the N-terminal TMD) with Tom70 TMD (Tom70^{TMD}-Msp1-GFP) or OM45 TMD (OM45^{TMD}-Msp1-GFP) and assessed the localization. Tom70 and OM45 are two mitochondrial membrane proteins that are anchored to the OMM by their N-terminal TMD. Neither of them has ever been shown to localize to peroxisomes (see Figure 4-1E, right panel and data not shown). As shown in Figure 4-1C, the subcellular localization of Tom70^{TMD}-Msp1 and OM45^{TMD}-Msp1 resembles that of the wild-type Msp1. The *msp1*Δ strain co-expressing Tom70^{TMD}-Msp1-GFP or OM45^{TMD}-Msp1-GFP and mito-RFP exhibits a complete overlap of the GFP and RFP signal, and extra-mitochondrial puncta that were confirmed to be peroxisomes based on colocalization with the RFP-SKL marker (Figure 4-1C, left panel). Similar to intact Msp1, a mutation that impairs the ATPase activity of the AAA+ domain of the chimeric proteins (Tom70^{TMD}-Msp1 ^{E193Q}-GFP or OM45^{TMD}-Msp1^{E193Q}-GFP) abolished the peroxisomal localization (Figure 4-1C, right panel). Both chimeric proteins were functional as they can completely or partially rescue the growth defect of the *get3*Δ*msp1*Δ on a nonfermentable carbon source, whereas the AAA+ inactive proteins failed to do so (Figure 4-1D) (Chen et al., 2014). These data demonstrate that the AAA+ domain of Msp1 is not only necessary but also sufficient for Msp1 to localize to peroxisome.

Next, to determine the role of the N-terminal TMD for the dual localization pattern of Msp1, we replaced the N-terminal TMD of Tom70 protein with Msp1 TMD (Msp1^{TMD}-Tom70) and observed its localization. Similar to the wild-type Tom70, GFP-tagged Msp1^{TMD}-Tom70 shows complete colocalization with mito-RFP and appears to not colocalize with RFP-SKL (Figure 4-1E). Hence, the peroxisomal localization of Msp1 is unlikely the result of direct protein import and insertion posttranslationally. In conclusion, these data suggest that the peroxisomal localization of Msp1 depends primarily on the ATPase activity of the AAA+ domain instead of the TMD domain. We speculate that perhaps Msp1 is imported into mitochondria, from where it is transported to peroxisomes in an ATPase activity-dependent manner.

Msp1 traffics from mitochondria to peroxisomes *via* vesicles

Similar to MAPL, Msp1 localizes to both mitochondria and peroxisomes, the latter of which appears to depend on the AAA+ domain. Previously, we hypothesized that Msp1 is imported to mitochondria and then transported to peroxisomes. Furthermore, members of the AAA+ proteins (*e.g.*, VPS4, Torsin and NSF) are known to play a crucial role in membrane dynamics and vesicle trafficking (Babst, 2005; Jokhi et al., 2013; Littleton et al., 2001; Rabouille et al., 1995; Woodman, 2003). Therefore, it is tempting to speculate that Msp1 traffics from mitochondria to peroxisomes through a vesicular trafficking pathway. To tackle this question, we generated a GFP-tagged Msp1 expressed from the inducible *GAL1* promoter and performed galactose pulse-chase experiments. The *msp1*Δ mutant co-expressing Msp1-GFP and mito-RFP or RFP-SKL was cultured in galactose medium to induce overexpression of Msp1 and then switched to glucose

medium to stop transcription. We observed that Msp1 localized primarily to mitochondria starting at 1 hr of induction, and then to both mitochondria and peroxisomes at 1.5 hr of induction (data not shown). Thirty minutes after the induction was pulsed, we started observing that the GFP signal localized to small puncta, which was maximal at about 90 min, as shown in Figure 4-2A, top panel. Neither mitochondrial nor peroxisomal RFP overlapped with the small puncta (indicated by arrows). The diameter of the puncta is smaller than that of peroxisomes. When we induced overexpression of the AAA+ ATPase inactive Msp1 ($Msp1^{E193Q}$), we did not observe that Msp1-GFP localized to these small puncta (Figure 4-2A, bottom panel). Instead, in spite of fully colocalizing with the mitochondrial RFP, we observed that the GFP signal was accumulated massively on subdomains of the mitochondria (indicated by arrows). This unusual mitochondrial localization was also observed when we expressed the AAA+ ATPase inactive Msp1 constructs from the *MSP1* promoter (Figure 4-1A-C). It appears that upon overexpression, Msp1 localizes to small puncta and the AAA+ domain is required for this localization. We speculated that these puncta are likely vesicles that bud from mitochondria. When the ATPase activity is impaired, however, the vesicles fail to bud off, which results in over-accumulation of Msp1 on the mitochondria.

We reasoned if these puncta represent vesicles derived from mitochondria, they might only exist transiently as they rapidly traffic to and fuse with peroxisomes. In fact, we have never observed that Msp1 localizes to small puncta when it is expressed from the native *MSP1* promoter. Therefore, in order to trap these vesicle-like puncta, we expressed Msp1-GFP from the native promoter in the *pex19*Δ mutant that lacks peroxisomes. Pex19 plays a crucial role in peroxisome biogenesis. It binds newly

Figure 4-2 Msp1 localizes to vesicle-like puncta

(A) Representative images of the *msp1*Δ mutant co-expressing Msp1-GFP or Msp1^{E193Q}-GFP expressed from the *GAL1* promoter and mito-RFP or RFP-SKL. Overnight yeast cultures grown in synthetic glucose medium were harvested, incubated in the galactose medium for 1.5 hr and switched to glucose medium to pulse the expression of Msp1 protein. Cells were harvested at 90 min after being grown in glucose medium and examined by fluorescence microscopy. Arrows in the upper panel indicate extra-mitochondrial and peroxisomal puncta and arrows in the lower panel indicate unusual mitochondrial accumulation of Msp1. (B) Representative images of the wild-type and *pex19*Δ mutant co-expressing Msp1-GFP and mito-RFP. Overnight cultures of the wild-type and *pex19*Δ mutant harboring Msp1-GFP and mito-RFP were diluted in synthetic glucose medium and cultured for 6 hr to early log-phase. Cells were examined by fluorescence microscopy. Arrows indicate extra-mitochondrial puncta.

(A)

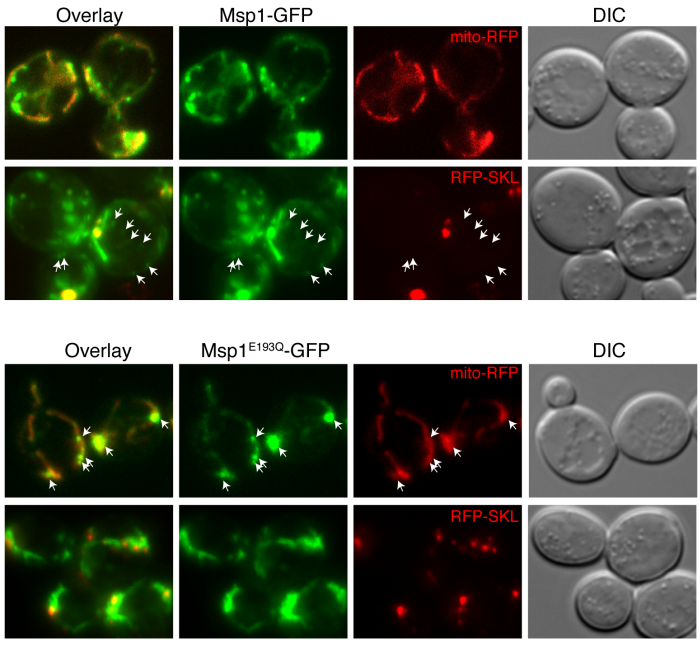
Overlay
Msp1-GFP
mito-RFP
DIC
RFP-SKL
Overlay
Msp1E193Q-GFP
mito-RFP
DIC
RFP-SKL

(B)

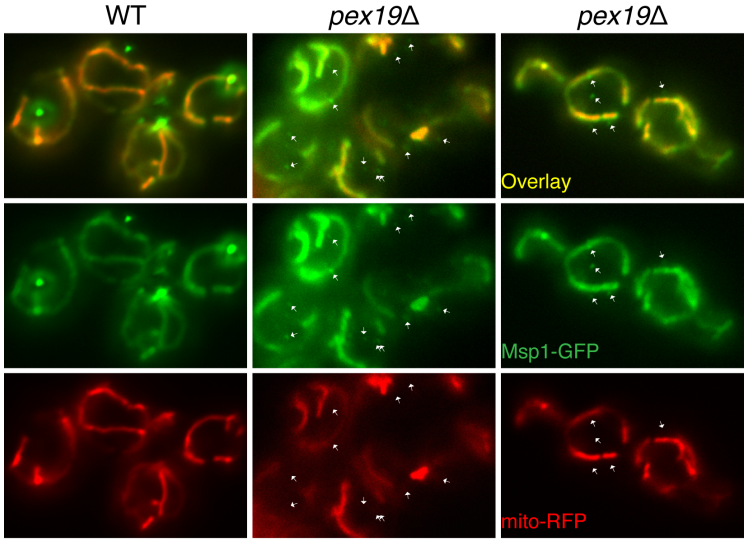
WT
pex19Δ
pex19Δ
Overlay
Msp1-GFP
mito-RFP

synthesized PMPs in the cytoplasm and delivers them to peroxisomes for insertion into the peroxisomal membrane. Thus, deletion of *PEX19* completely abolishes peroxisome biogenesis (Heiland and Erdmann, 2005; Hettema et al., 2000). When we expressed Msp1-GFP in the *pex19*Δ mutant as shown in Figure 4-2B, we observed that the Msp1-GFP signal localized to extra-mitochondrial small puncta (indicated by arrows). Similar to the puncta shown in Figure 4-2A, they are also significantly smaller than peroxisomes that are observed as extra-mitochondrial puncta in the wild-type strain. Hence, we hypothesized that the Msp1-decorated puncta might be vesicles that have budded from mitochondria in an AAA+ domain-dependent manner and are destined to eventually fuse with peroxisomes in wild-type cells.

To directly test whether Msp1 traffics from mitochondria to peroxisomes, we utilized the galactose pulse-chase system previously described. We induced the expression of Msp1-GFP for the minimal time (1.25 hr), and found that the majority of the protein only localized to mitochondria rather than to both peroxisomes and mitochondria. The time-course distribution of the Msp1-GFP signal was examined after yeast were switched to glucose medium to turn off Msp1-GFP expression (Figure 4-3). We observed that yeast co-expressing Msp1-GFP and RFP-SKL showed a minimal co-localization of the GFP and RFP signal at 0 min postinduction. At 60 and 150 min, there was an increased colocalization of GFP and RFP-SKL **(**Figure 4-3, left panel). Concomitantly, we saw a slight decrease of the mitochondrial Msp1 signal through the time-course in the strain co-expressing Msp1-GFP and mito-RFP (Figure 4-3, right panel). Taken together, these data are suggestive that Msp1 might traffic from mitochondria to peroxisomes through an unknown vesicular trafficking pathway.

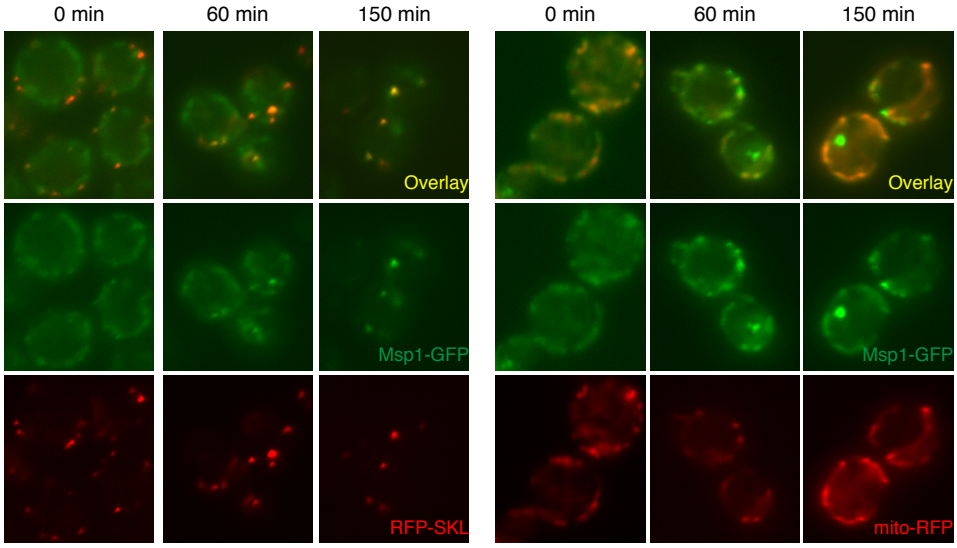

Figure 4-3. Msp1 traffics from mitochondria to peroxisomes

Representative images of the galactose shut-off experiment. Overnight cultures of the *msp1*Δ mutant co-expressing Msp1-GFP from the *GAL1* promoter and mito-RFP or RFP-SKL were harvested, incubated in the galactose induction medium for 1.25 hr and switched to glucose medium to pulse the expression of Msp1 protein. Cells were harvested at 0, 60 and 150 min after being incubated in glucose medium and examined by fluorescence microscopy.

Fzo1 is required for Msp1 peroxisomal localization

To determine if the formation of vesicle-like Msp1 puncta requires the shared mitochondrial/peroxisomal fission machinery, we assessed the localization of Msp1 in various fission mutants including *fis1*Δ, *mdv1*Δ and *dnm1*Δ (Figure 4-4A). By co-expressing Msp1-GFP and RFP-SKL (top panel) or mito-RFP (bottom panel) in the wild-type and mutant strains, we showed that Msp1-GFP colocalized with both mitochondrial and peroxisomal RFP signal in each of these mutant strains. Thus, the conventional fission machinery appears to be dispensable for Msp1 localization to peroxisomes. Unlike the fission machinery, the mitochondrial fusion machinery has never been reported to function on peroxisomes. To our surprise, however, when we assessed Msp1 localization in the *fzo1*Δ mitochondrial fusion mutant, we observed that Msp1 no longer colocalized to peroxisomes but its mitochondrial localization was unaffected (Figure 4-4B). As depletion of *FZO1* progressively leads to loss of mitochondria DNA, which impacts many aspects of mitochondrial function, this loss of peroxisomal localization could be an artifact of mitochondrial impairment (Hermann et al., 1998; Rapaport et al., 1998). To further test the Fzo1 requirement for Msp1 peroxisomal localization, we utilized the *fzo1-1* temperature-sensitive mutant to acutely deplete *FZO1* and assessed Msp1 localization (Hermann et al., 1998; Rapaport et al., 1998). When we cultured the *fzo1-1* mutant harboring Msp1-GFP and mitochondrial or peroxisomal RFP under the restrictive temperature at 37°C for 15 min as suggested in the literature, we still observed that Msp1 localized to both organelles (data not shown). We suspected that 15 min was likely too short to observe decay of peroxisomal Msp1. Thus, we decided to increase the incubation time of the *fzo1-1* mutant to 6 and 12 hr but at a moderately restrictive

Figure 4-4. Peroxisomal localization of Msp1 is dependent on Fzo1

(A) Representative images of the wild-type, *fis1*Δ, *mdv1*Δ, *dnm1*Δ and mdm30Δ and rho^0 strain co-expressing Msp1-GFP and mito-RFP or RFP-SKL. (B) Representative images of the wild-type and *fzo1*Δ strain co-expressing Msp1-GFP and mito-RFP or RFP-SKL. Overnight culture of the yeast strains indicated in (A) and (B) was diluted in synthetic glucose medium and examined by fluorescence microscopy. (C) Representative images of the *fzo1*-1 strain co-expressing Msp1-GFP and mito-RFP or RFP-SKL. Overnight yeast culture grown at 25 °C was diluted in synthetic glucose medium, incubated at 25 for 6 hr and 30 °C for 6 and 12 hr, respectively and examined by fluorescence microscopy

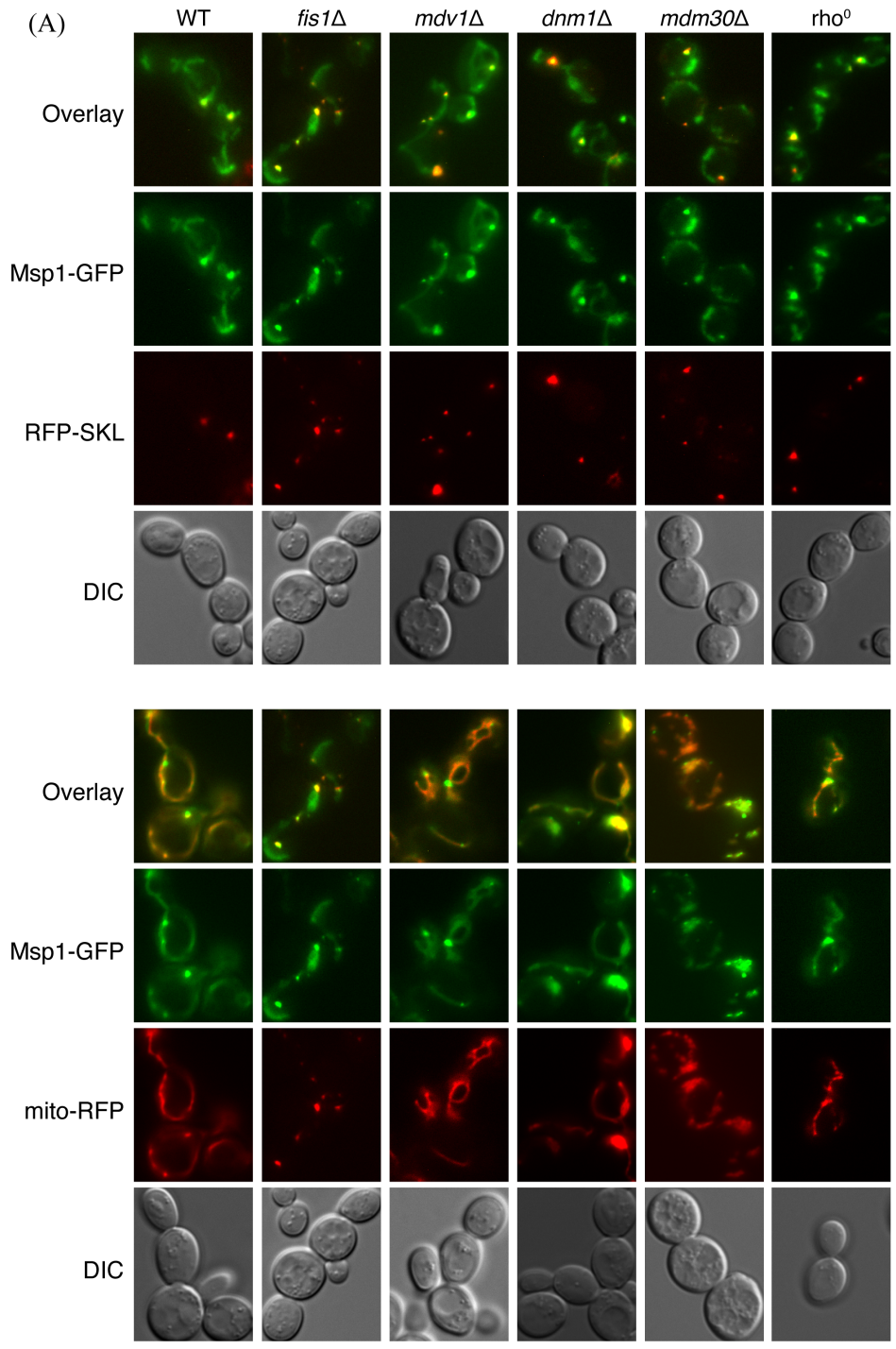
(A)
WT
fis1Δ
mdv1Δ
dnm1Δ
mdm30Δ
rho0
Overlay
Msp1-GFP
RFP-SKL
DIC
Overlay
Msp1-GFP
mito-RFP
DIC

(B)

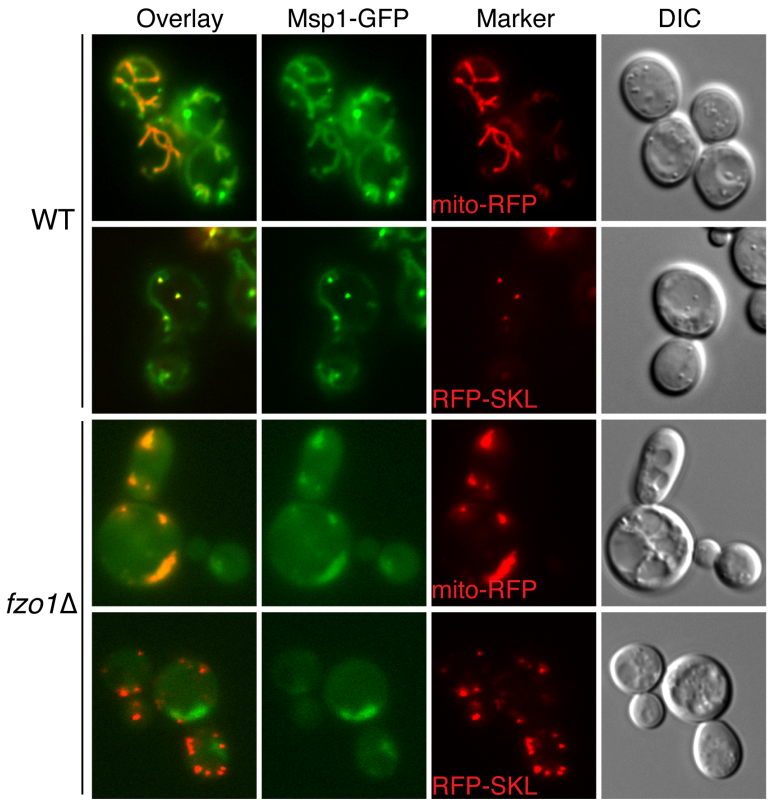
Overlay
Msp1-GFP
Marker
DIC
WT
mito-RFP
RFP-SKL
fzo1Δ
mito-RFP
RFP-SKL

(C)

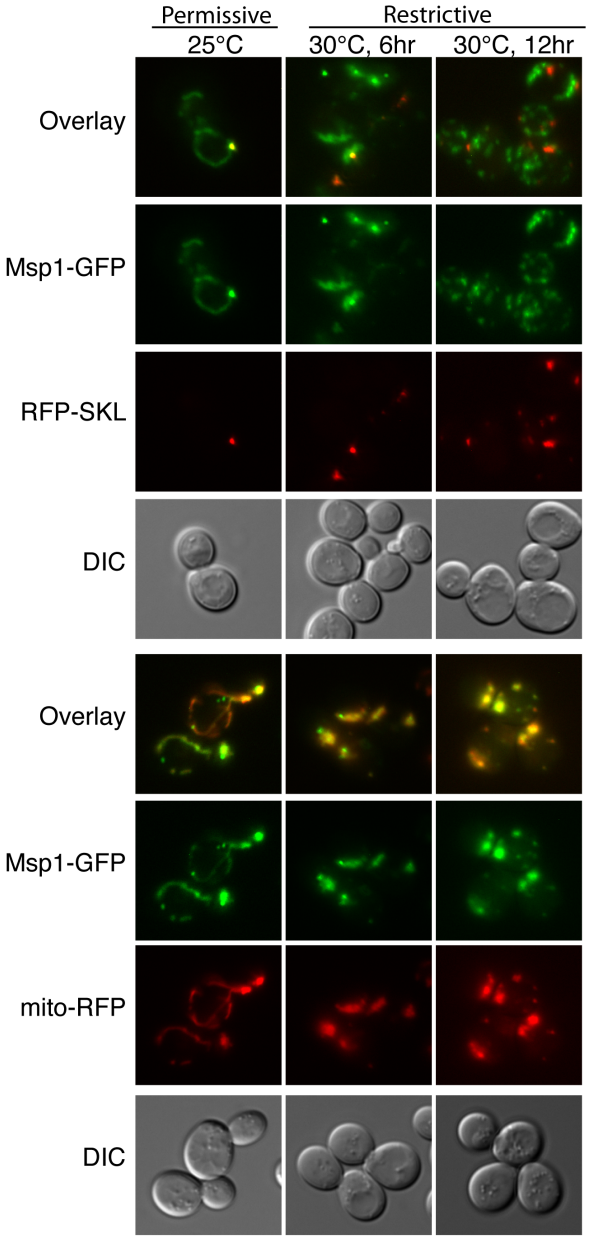
Permissive
25°C
Restrictive
30°C, 6hr
30°C, 12hr
Overlay
Msp1-GFP
RFP-SKL
DIC
Overlay
Msp1-GFP
mito-RFP
DIC

temperature, 30°C. As shown in Figure 4-4C, in comparison to cells grown at 25°C (permissive temperature), we observed that at 6 hr after temperature shift, there was some colocalization of Msp1-GFP with RFP-SKL. After 12 hr, however, Msp1 no longer localized to peroxisomes, but localized normally to the mitochondria, which were fragmented under these conditions. To verify that mitochondrial dysfunction is not sufficient to prevent Msp1 localization to peroxisomes, we also tested the localization of Msp1 in a strain that was treated with ethidium bromide to deplete mitochondrial DNA (rho^0). We observed that Msp1 localized to both mitochondria and peroxisomes similar to wild-type cells (Figure 4-4A). Thus, we confirmed that loss of peroxisomal localization of Msp1 is an Fzo1-specific phenomenon. On the other hand, hyperaccumulation of Fzo1 caused by mutating Mdm30, a ubiquitin E3 ligase that promotes Fzo1 degradation, does not affect Msp1 localization (Figure 4-4A). Taken together, these results demonstrate that the peroxisomal localization of Msp1 is dependent on Fzo1 but independent of the fission machinery. We are currently investigating the mechanism of Fzo1-mediated localization of Msp1 on peroxisomes.

Msp1/ATAD1 is crucial to maintain peroxisome morphology

Because Msp1 localizes to peroxisomes, we asked whether it is important for peroxisomal function. As one of the major functions of yeast peroxisomes is to catalyze β-oxidation of lipids, we first tested whether deletion of *MSP1* affected the ability of cells to utilize oleic acid as the sole carbon source to survive and grow. We cultured both the wild-type and the *msp1*Δ mutant in liquid oleate medium and recorded their growth curve. We did not observe any growth difference between the two strains (Figure 4-5A).

Figure 4-5. Msp1/ATAD1 plays a role in maintaining peroxisomal morphology

(A) Growth curve of the wild-type and *msp1*Δ mutant in oleate medium. The yeast strains were grown overnight in YPD medium and diluted into fresh oleate medium. Cell density was measured by OD600 every 2-3 hr. (B) Representative images of the peroxisome in the wild-type and *msp1*Δ mutant. Overnight cultures of the wild-type and *msp1*Δ mutant harboring RFP-SKL were diluted in synthetic glucose medium and cultured for 6 hr until early log-phase. Cells were examined by fluorescence microscopy. (C) Representative images of the peroxisome in the wild-type and *atad*$^{-/-}$ mouse embryonic fibroblasts (MEFs). MEFs were immunostained with anti-PMP70 antibody followed by Alexa flour-546 antibody and imaged by fluorescence microscopy.

(A)

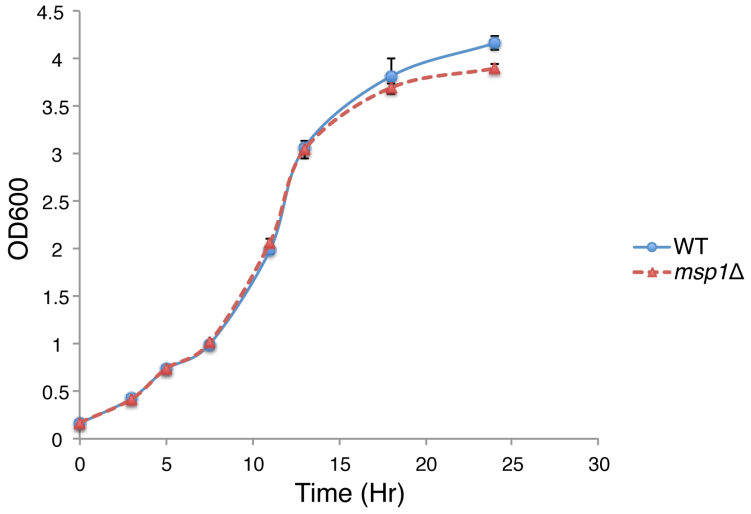
4.5
4
3.5
3
2.5
2
1.5
1
0.5
0
OD600
0
5
10
15
20
25
30
Time (Hr)
WT
msp1Δ

(B)

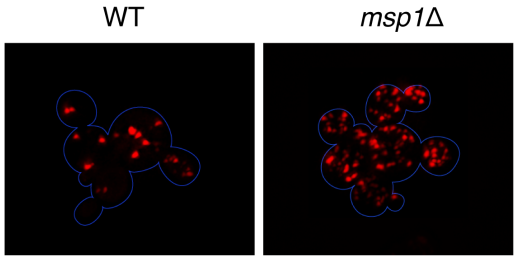
WT
msp1Δ

(C)

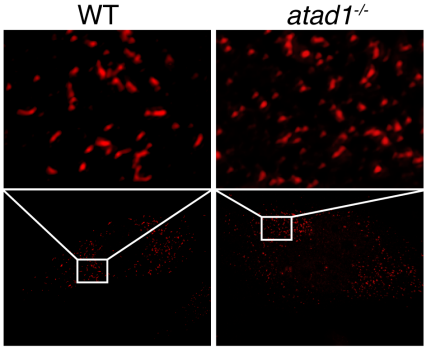
WT
atad1-/-

As peroxisomes perform other functions in addition to β-oxidation, we believed that this growth assay is probably not sufficient to reveal the functionality of every aspect of this organelle. Next, we directly visualized the morphology of peroxisomes with fluorescence microscopy by labeling peroxisomes with RFP-SKL. In the wild-type strain, there were an average of 3-8 large peroxisomes per cell, whereas the *msp1*Δ strain exhibited a larger number of smaller peroxisomes (Figure 4-5B). We also confirmed the same phenotype in mammalian cells by immunostaining peroxisomes in the wild-type and *atad1*$^{-/-}$ mouse embryonic fibroblasts (MEFs), as shown in Figure 4-5C. The wild-type cells contained a mixture of tubular and punctate peroxisomes but *atad1*$^{-/-}$ MEFs only exhibited punctate peroxisomes. It seems that deletion of *MSP1* in yeast and *ATAD1* in mammalian cells both cause similar fragmentation of peroxisomes, implying that they perform a conserved function that is required for normal peroxisome morphology, but we do not yet know the nature of this function.

Msp1/ATAD1 participates in sorting peroxins from mitochondria into vesicles

Peroxisomes can be formed *de novo* from the ER according to the observation that in mutant cells lacking peroxisomes, some peroxins were shown to localize to ER (Nagotu et al., 2010; Smith and Aitchison, 2013). These peroxins, after being synthesized, are incorporated into ER and sorted into vesicles, which then bud out from ER (Hoepfner et al., 2005; van der Zand et al., 2012). Intriguingly, a subset of peroxins were observed to "mislocalize" to mitochondria in cells from Zellweger syndrome patients or peroxin mutant mammalian cells (Sacksteder et al., 2000; South et al., 2000;

Toro et al., 2009). These results have to been thought to be artifacts, because it has been assumed that there is no way out for those "mislocalized" peroxins. Given our results described above, we are interested in exploring the possibility that mitochondria-derived vesicles contribute to peroxisome biogenesis. Therefore, these peroxins, instead of being mislocalized, might be targeted mitochondria as part of their normal trafficking pathway. As localization of peroxins to mitochondria has never been observed in yeast before, we tried to recapitulate this phenomenon in a peroxisomal biogenesis defective mutant strain. We generated RFP-tagged peroxins including Pex1, Pex3, Pex10, Pex11, Pex12, Pex13, Pex14, Pex15, Pex16, Pex18 and Pex22 and examined their localization in a *pex19*Δ mutant that also co-expressed a mitochondrial GFP marker (mito-GFP). We observed that, similar to the peroxisome biogenesis-defective mammalian cells, a subset of these peroxins (Pex1l, Pex13 and Pex22) colocalized to mitochondria in the *pex19*Δ strain when expressed from their endogenous promoters (Figure 4-6A, top panel). Furthermore, when we deleted *MSP1* in the *pex19*Δ strain, Pex1, Pex10 and Pex12 also localized to mitochondria in addition to the three peroxins mentioned above (Figure 4-6A, bottom panel). It also appears that deletion of *MSP1* further increased the amount of each of these peroxins localizing to mitochondria, as compared to the *pex19*Δ single mutant strain. One potential explanation for the mitochondrial localization of peroxins caused by Msp1 mutation is that, like tail-anchored proteins, they are direct substrates of Msp1. Msp1 can directly interact with them and facilitate their extraction and degradation. Thus, our hypothesis is that *MSP1* could cause the accumulation of peroxins on the mitochondria. To test that, we performed co-immunoprecipitation experiments. As shown in Figure 4-6B**,** both wild-type Msp1 and substrate trap Msp1 ($Msp1^{E193Q}$) failed

Figure 4-6. Msp1/ATAD1 is required for peroxin localization

(A) Representative images of the *pex19*Δ and *msp1*Δ *pex19*Δ co-expressing Pex11-RFP, Pex10-RFP, Pex13-RFP, Pex22-RFP, Pex1-RFP or Pex12-RFP with mito-GFP. Overnight cultures of the indicated strain were diluted in synthetic glucose medium and cultured for 6 hr until early log-phase and examined by fluorescence microscopy. (B) Co-immunoprecipitation of Msp1 with peroxins. Crude mitochondria extracted from the *msp1*Δ *pex19*Δ strain expressing Pex1-RFP, Pex12-RFP, Pex13-RFP or Pex22-RFP and empty vector (EV), Msp1-HA (Msp1) or Msp1^{E193Q}-HA (E193Q) were solubilized in 0.5% digitonin and subjected to anti-HA antibody agarose pull-down. (C) Representative images of peroxin localization in the ZS patient fibroblasts (*pex16* mutant) upon ATAD1 overexpression. Both the wild-type and the ZS patient fibroblasts stably expressing PEX10 or PEX13 were infected with empty vector (EV) or ATAD1 and examined by fluorescence microscopy.

(A)

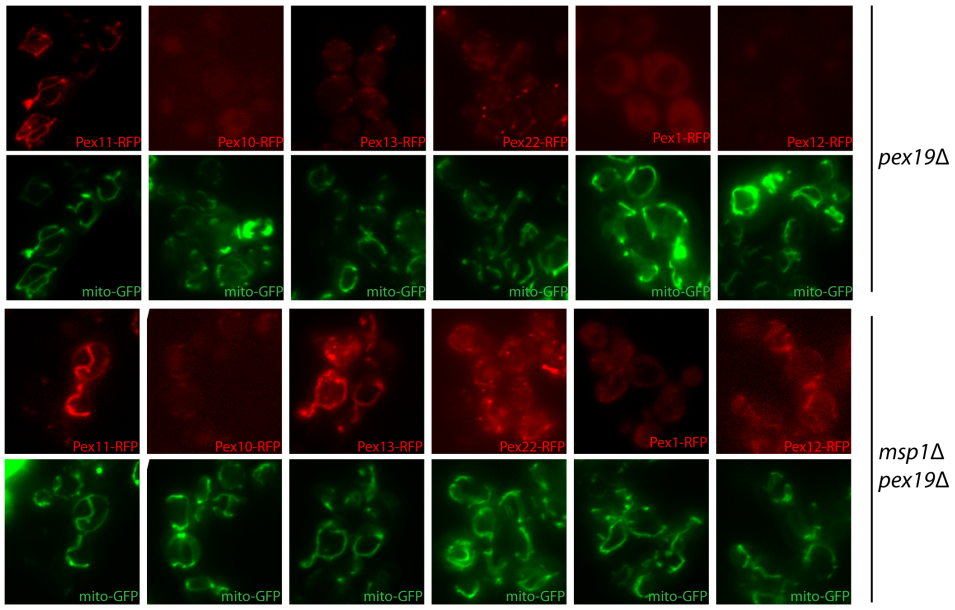
Pex11-RFP
Pex10-RFP
Pex13-RFP
Pex22-RFP
Pex1-RFP
Pex12-RFP
mito-GFP
pex19Δ
msp1Δ
pex19Δ

(B)

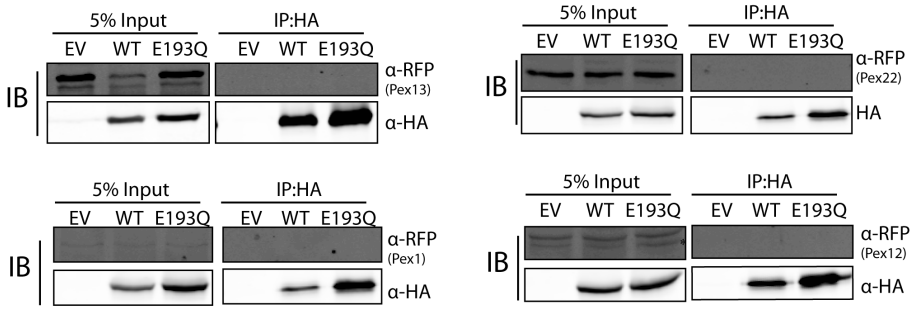
5% Input
IP:HA
EV
WT
E193Q
IB
α-RFP
(Pex13)
α-HA
α-RFP
(Pex22)
HA
α-RFP
(Pex1)
α-RFP
(Pex12)

(C)

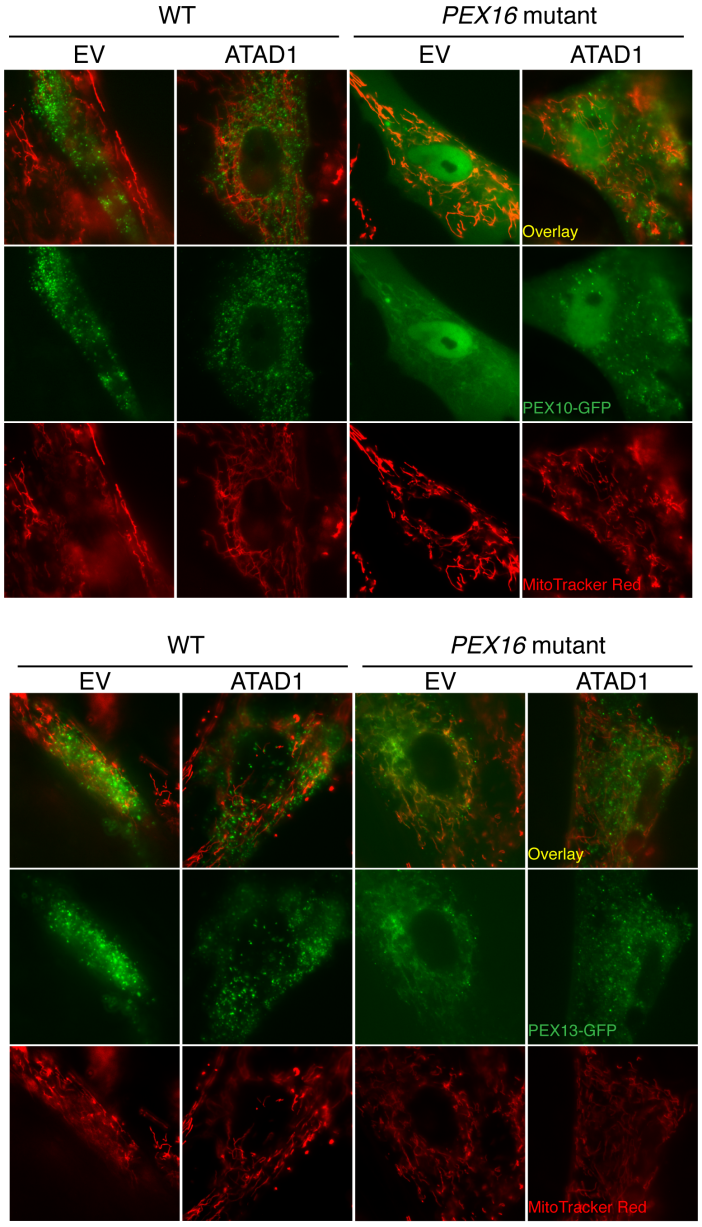
WT
PEX16 mutant
EV
ATAD1
EV
ATAD1
Overlay
PEX10-GFP
MitoTracker Red
WT
PEX16 mutant
EV
ATAD1
EV
ATAD1
Overlay
PEX13-GFP
MitoTracker Red

to co-immunoprecipitate any of these peroxins under conditions that were identical to those where we saw strong interaction with tail-anchored proteins, demonstrating that the mitochondria-localized peroxins are probably not direct substrates of Msp1.

As yeast Msp1 traffics from mitochondria to peroxisomes, we next speculated that Msp1/ATAD1, instead of functioning in protein quality control on peroxisomes, participates in sorting peroxins from mitochondria to peroxisomes *via* vesicles. We stably expressed GFP-tagged PEX10 and PEX13 in both wild-type and Zellweger syndrome patient (*PEX16* mutation) fibroblasts. Figure 4-6C shows that both proteins partially colocalized to mitochondria in the patient fibroblasts in addition to exhibiting strong cytoplasmic accumulation. In the wild-type cells, however, they both localized to puncta that are presumably peroxisomes (but this awaits verification) and showed little or no mitochondrial colocalization. The most important question is whether ATAD1 expression has any effect on this mitochondrial localization and whether perhaps ATAD1 overexpression is capable of sorting these peroxins into vesicles. We overexpressed *ATAD1* in both the wild-type and *PEX16* mutant fibroblasts and found that ectopic expression of *ATAD1* promoted the removal of both PEX10 and PEX13 from mitochondria (Figure 4-6C). Interestingly, the GFP signal now also began to localize to extra-mitochondrial puncta. We speculate that these puncta are perhaps the vesicles that are formed from the mitochondria *via* the assistance of ATAD1, their nature and content requires further characterization. To summarize, we show evidence suggesting that Msp1/ATAD1 plays a critical role in mediating the sorting of peroxins from mitochondria into vesicles. Whether these puncta eventually fuse with peroxisomes needs to be addressed rigorously in the future.

Discussion

Based on the data presented herein, we conclude that Msp1/ATAD1 participates in a novel vesicular trafficking pathway, which is likely crucial for sorting peroxins from mitochondria to peroxisomes. We show that yeast Msp1 traffics from mitochondria to peroxisomes, probably in small vesicles, in an AAA+ domain-dependent manner. To our surprise, the Fzo1 mitochondria fusion protein is required for the peroxisomal localization of Msp1 *via* a mechanism that remains unknown. The consequences of loss of Msp1/ATAD1 include peroxisome fragmentation and peroxin localization to mitochondria. Finally, we show that overexpression of mammalian *ATAD1* in Zellweger syndrome patient cells facilitates the removal of peroxins from mitochondria, which then accumulate in vesicle-like structures, suggesting that Msp1/ATAD1 functions in sorting peroxins from mitochondria into vesicles. Several additional interesting observations related to this study are discussed below.

First, it has been a matter of debate whether vesicles bud out of mitochondria. In the past few years, two types of MDVs *en route* to distinct destinations have been described (Braschi et al., 2010; Neuspiel et al., 2008; Soubannier et al., 2012; Sugiura et al., 2014). One of these vesicle systems, which carries only one known protein, MAPL, is trafficked to and fused with peroxisomes (Braschi et al., 2010; Neuspiel et al., 2008). In this study, we appear to have identified peroxisome-targeted MDVs that contains Msp1. Like MAPL, Msp1/ATAD1 localizes to both mitochondria and peroxisomes (see Figure 4-1A and (Chen et al., 2014), raising the question whether the Msp1-decorated and MAPL-decorated MDVs are the same objects. Unfortunately, we do not yet know enough about either system to answer this question. We do know, however, that the

mitochondrial fission machinery is dispensable for trafficking Msp1 to peroxisomes in yeast and is also dispensable for the formation of MAPL-decorated vesicles in mammalian cells (Figure 4-4A and Neuspiel et al., 2008). Nonetheless, to address this question directly, double labeling of MAPL and ATAD1 in mammalian cells is required. Another interesting question is what proteins or protein complexes participate in the Msp1/ATAD1 vesicular trafficking pathway. The retromer complex was shown to be important for MAPL trafficking; we will first test whether it is also crucial for ATAD1 trafficking (Braschi et al., 2010). Second, we previously performed a two-step tandem affinity purification to identify the binding partners of Msp1 and found some components of the COPII vesicle trafficking pathway (data not shown). Although there is not yet any evidence indicating that the COPII pathway is involved in mitochondrial vesicle formation, we suspect that some players in this pathway might play a role on mitochondria. Future work is needed to verify the interaction between the COPII components and Msp1 and, more importantly, to test whether they are required for Msp1 vesicle formation.

The functional role of Msp1 in vesiculation is also of interest. AAA+ proteins are crucial for membrane dynamics and vesicle trafficking and we have shown that the AAA+ domain of Msp1 is required for Msp1 localization to vesicle-like punta and to peroxisomes (Figure 4-1C and 4-2A). Intriguingly, when we expressed the ATPase-inactive Msp1, we observed an unusual accumulation of Msp1 on subdomains of mitochondria (Figure 4-1A-C and Figure 4-2A). We speculate that this phenomenon is likely caused by the Msp1-decorated vesicles that stall in the scission step on the mitochondrial membrane. Similar to the Msp1 protein, Torsin is another AAA+ ATPase

that has a N-terminal TMD and a C-terminal AAA+ domain. It appears to be involved in formation of vesicels that bud from the inner nuclear membrane into the internuclear space, perhaps helping to mediate the terminal fission step. These vesicles carry large ribonucleoproteins (MegaRNPs) and help viral cores from the nucleus into the cytoplasm. Mutation of the AAA+ domain causes Torsin to accumulate on the necks of the enveloped MegaRNPs, implying that Torsin may be required for the scission step of the nuclear membrane (Jokhi et al., 2013). Therefore, we speculatively hypothesize that like Torsin, Msp1 participates in the budding of vesicles from mitochondria. Immuno-electron microscopy will be required to show the suborganellar localization of Msp1, including in mutants with these mitochondrial accumulations.

It is also a surprising and intriguing observation that the mitochondrial fusion protein, Fzo1, is required for Msp1 localization to peroxisomes. It is widely accepted that the same fission machinery is shared between mitochondria and peroxisomes in both yeast and mammals (Delille et al., 2009). The mitochondrial fusion machinery, however, has never been shown to play a role in any aspect of peroxisomal function. As Fzo1 mediates mitochondrial fusion by homo-oligomerization (Meeusen et al., 2004), we initially hypothesized that Fzo1 is present on both mitochondria and peroxisomes and that it mediates the fusion of the mitochondrial-derived Msp1-vesicles with peroxisomes. However, we have only been able to visualize the yeast Fzo1 protein localizing to mitochondria using the Fzo1 protein with different tags on either end (data not shown). Since the tagged proteins were not fully functional, these results were difficult to interpret and we cannot exclude the possibility that a small subset of Fzo1 localizes to peroxisomes. Nevertheless, given that a previous study showed that none of the fusion

proteins (MFN1, MFN2 and UGO1) localize to peroxisomes in mammalian cells (Bonekamp et al., 2012), it seems unlikely that the mitochondrial fusion machinery mediates fusion of the Msp1-decorated vesicles with perixosmes. An alternative possibility is that fusion of mitochondria might sequester proteins or lipids that are required for Msp1-decorated vesicle formation. Future studies will be required to uncover the role of the mitochondrial fusion proteins in this process.

Finally, we speculate that Msp1 could play a role in the *de novo* biogenesis of peroxisomes from mitochondria. Peroxisomes are currently believed to form either by self-dividing or by *de novo* synthesis from the ER subdomain (Smith and Aitchison, 2013). It is still debatable which of these mechanisms prevails under normal conditions. Both pathways have been verified in yeast, but fission is mostly likely the predominant mechanism of peroxisome proliferation under wild-type conditions (Motley and Hettema, 2007; Nagotu et al., 2008). It appears that cells only utilize *de novo* biogenesis under specific circumstances, because ER was found to be the receptive host for a subset of peroxins in peroxisome-deficient mutants. As we observed that some peroxins also localize to mitochondria in peroxisome-deficient mutants, we should consider the possibility that mitochondria also contribute to the biogenesis of peroxisomes. Another line of evidence supporting the possibility that mitochondria contribute to peroxisomal biogenesis is that artificially targeting Pex3 to mitochondria in the *pex3*Δ mutant fully regenerates peroxisomes (Rucktaschel et al., 2010). In our case, we have show that deletion of *MSP1* and *PEX19* leads to peroxin localization to mitochondria in yeast (Figure 4-6A). More importantly, we showed that in mammalian cells, overexpression of *ATAD1* is capable of removing peroxins from mitochondria in Zellweger syndrome

patient cells, and induces accumulation of the protein in vesicle-like cytoplasmic structures (Figure 4-6C). It is possible that under some conditions, a subset of peroxins may first target mitochondria and then be sorted into Msp1-decorated vesicles. These "pre-peroxisome" vesicles could then fuse with other pre-peroxisome vesicles, thereby delivering different peroxins to form mature peroxisomes. One potential experiment that would directly tackles this hypothesis would be to perform cell fusion assays. We plan to fuse the ATAD1-overexpressing ZS patient cells harboring GFP-tagged peroxins and wild-type cells and test if GFP-tagged peroxins will end up localized to peroxisomes. On the other hand, we also do not have enough evidence to completely exclude the possibility that the peroxin-containing vesicles are destined for degradation. Theses vesicles, instead of fusing with other pre-peroxisomal vesicles for peroxisomes biogenesis, might engage with lysosomes for protein turnover. Certainly, more work is needed to rigorously test these hypotheses.

In conclusion, we suggest that in addition to the role in protein quality control that we described previously, Msp1/ATAD1 performs a second role in mitochondria to peroxisome trafficking, which might directly impact peroxisome biogenesis. Give the importance of Msp1/ATAD1 in both mitochondria and peroxisomal functions, and the extent to which the integrity of both of these organelles directly impacts human health, we eagerly await a deeper understanding of the molecular mechanisms underlying the roles of the Msp1/ATAD1 protein family.

Materials and methods

Yeast strains and growth conditions

Saccharomyces cerevisiae W303-1a (*MATa, his3 leu2 met15 trp1 ura3*) was used in this study. The standard PCR-based homologous recombination method was used to generate all mutant strains. Briefly, drug selection cassette (KanMX4 or hphMX4) flanked with 45-bp fragments upstream and downstream of the gene of interest was PCR amplified and transformed into the wild-type diploid (Goldstein and McCusker, 1999) (Wach et al., 1994). The haploid strain was generated by sporulation and tetrad analysis. The genotype of the strain was verified by standard genotyping PCR. The genotypes of all yeast strains used in this study are listed in Table 4-1.

For yeast transformation, the standard lithium acetate procedure was used (Gietz et al., 1992). Transformed yeast cells were grown in synthetic complete dextrose (SD) medium lacking the appropriate amino acid(s) for auxotrophic selection purposes at 30°C. Media used in this study includes standard YP and synthetic minimal medium supplemented with 2% glucose or 3% glycerol. Oleate medium is composed of 0.67% yeast nitogen base without amino acid, 0.1% yeast extract, 0.1% oleate and 0.25% tween-40 and filter sterilized Solid plates contain 2.2% (w/v) agar.

Plasmid construction

The plasmids expressing nontagged, C-terminal HA or GFP-tagged Msp1 and Msp1^{E193Q} were reported previously (Chen et al., 2014). Msp1^{K139A}-GFP, Msp1^{R248E}-GFP and Msp1$^{W166G/Y167D}$-GFP were generated by site-directed mutagenesis. Tom70^{TMD}-

Table 4-1. Yeast strains used in this study

Number	Strains	Genotype	Source
JRY245	WT (W303)	*MAT**a** his3 leu2 lys2 met15 trp1 ura3*	David Stillman
JRY1816	*msp1*Δ	*MAT**a** his3 leu2 lys2 met15 trp1 ura3 msp1::kanMX4*	Chen et al., 2014
JRY1814	*get3*Δ *msp1*Δ	*MAT**a** his3 leu2 lys2 met15 trp1 ura3 get3::hphMX4 msp1::kanMX4*	Chen et al., 2014
JRY490	*rho*^{0}	*MAT**a** his3 leu2 lys2 met15 trp1 ura3* ρ^{0}	Jared Rutter
JRY2724	*pex19*Δ	*MAT**α** his3 leu2 lys2 met15 trp1 ura3 pex19::natMX*	This study
JRY2726	*msp1*Δ *pex19*Δ	*MAT**a** his3 leu2 lys2 met15 trp1 ura3 pex19::natMX msp1::kanMX4*	This study
JRY2618	*fis1*Δ	*MAT**a** ade2 his3 leu2 trp1 ura3 can1 fis1::His3MX*	Janet Shaw
JRY2617	*mdv1*Δ	*MAT**a** ade2 his3 leu2 trp1 ura3 can1 mdv1::His3MX*	Janet Shaw
JRY2616	*dmn1*Δ	*MAT**a** ade2 his3 leu2 trp1 ura3 can1 dmn1::His3MX*	Janet Shaw
JRY252	*fzo1*Δ	*MAT**a** ade2 his3 leu2 trp1 ura3 can1 fzo1::TRP1*	Janet Shaw
JRY1040	*mdm30*Δ	*MAT**a** his3 leu2 lys2 met15 trp1 ura3 mdm30::kanMX*	Janet Shaw
JRY2620	WT	*MAT**a** his3 leu2 LYS2 met15 trp1 ura3*	Janet Shaw
JRY2619	*fzo1-1*	*MAT**a** ade2 his3 leu2 trp1 ura3 fzo1-1*	Janet Shaw

Msp1-GFP was generated by fusing *MSP1* promoter (509 bp upstream of *MSP1* ORF), 1-30 amino acid of Tom70 and 31-364 amino acid of Msp1 by sawing PCR and ligating into a pRS416-based vector with a c-terminal GFP. Om45^{TMD}-Msp1-GFP was made similarly except that 1-26 amino acid of Om45 was fused with Msp1. *GAL1* promoter driven Msp1-GFP constructs were generated by ligating Msp1-GFP into pRS414-GAL1 vector (Mumberg et al., 1995). E193Q mutation was introduced by site-directed mutagenesis. RFP-tagged peroxin constructs were created by amplifying the ORF of each peroxin with about 500 bp upstream of the starting codon and ligated into a pRS414-based vector containing a c-terminal RFP tag. GFP-tagged PEX10 and PEX13 was generated by amplifying PEX10 and PEX13 ORF from human cDNA and ligated into a pLenti-CMV-GFP-Puro vector (Campeau et al., 2009). Peroxisomal fluorescent marker construct was made by fusing RFP protein with the peroxisomal targeting sequence (SKL) at the C-terminus.

Isolation of yeast mitochondria

Yeast cells were harvested at midlog phase (OD600=2-3) in 2% synthetic reffinose medium. Preparation of crude and purified mitochondria was as described previously (Boldogh and Pon, 2007). Yeast pellet was washed once with ddH2O, resuspended and incubated in TD buffer (100 mM Tris-SO4, pH 9.4 and 100 mM DTT) for 15 min at 30°C. Spheroplasts were obtained by incubating cells in SP buffer (1.2 M sorbitol and 20 mM potassium phosphate, pH 7.4) supplemented with lyticase (2 mg/g of cell pellet) (Sigma-Aldrich) for 1 hr at 30°C to digest the cell wall. Spheroplasts were gently washed once in ice-cold SHE buffer (1.2 M sorbitol, 20 mM HEPES-KOH, pH 7.4, 2 mM MgCl2, 1 mM EGTA, and 1 mM PMSF) and homogenized in ice-cold SHE buffer

that contains 0.6 M sorbitol and a Dounce homogenizer was applied with 10-20 strokes. The crude mitochondrial fraction was obtained by differential centrifugation. Protein concentration was determined using Bradford protein assay.

Fluorescence microscopy

Yeast samples were prepared by growing yeast cells to early-log phase (OD_{600}= 0.8-1) in synthetic dropout medium with appropriate carbon sources at 30°C or otherwise indicated. To prepare mammalian cell samples, we cultured cells on Poly-L-Lysine-coated Lab-Tek® II chamber slides for a day to allow them to fully attach. They were stained with 25 nM Mitotracker® Red CMXRos (Life Technologies) in FBS-free medium for 5 min at 37°C before being imaged. To examine morphological changes of peroxisomes on ATAD1-/- MEFs, cells were grown on coverslips, washed with PBS and fixed with 4% PFA in PBS for 20 min at room temperature. Cells were then blocked in 10% normal goat serum and 5% ultrapure BSA for 1 hr, stained with anti-PMP70 antibody (1/500, Abcam) and Alexa flour® 546 secondary antibody (Life Technologies). Cells were washed three times with PBS buffer and stained with DAPI. Cells were imaged on the Axio Observer.Z1 imaging system (Carl Zeiss) equipped with 40X and 100X objectives (oil-immersion). Digital fluorescence and differential interference contrast (DIC) images were acquired using a monochrome digital camera (AxioCam MRm, Carl Zeiss). The final images were adjusted and assembled using Adobe Photoshop CS5.1. Brightness and contrast were adjusted only using linear operation on the entire image.

Co-immunoprecipitation

One mg of crude mitochondria extracted from each strain was solubilized in 0.5% digitonin for 1 hr at 4°C. Cleared mitochondria lysates were mixed with anti-HA antibody conjugated agarose for 1 hr at 4°C. Agarose was washed two times with buffer containing 250 mM NaCl and 0.05% digitonin, and three times with buffer containing 600 mM NaCl and 0.05% digitonin. Laemmli buffer without β-ME was added to the agarose to elute proteins. Final eluate and 4-5% of the mitochondria lysate were resolved by 12% SDS-PAGE followed by immunoblot.

Mammalian cell culture

MEFs and HEK293T were maintained in DMEM with 10% FBS. Human fibroblasts were maintained in DMEM with 20% FBS. Cells were cultured at 37°C with 5% CO2. To establish stable cell lines, lentivirus was produced in HEK293T cells that were co-transfected with the vector containing the gene of interest, MDLg/pRRE, pRSV-Rev and pMD2.G. Retrovirus was produced in HEK293T cells that were co-transfected with the vector containing the gene of interest, Gag-pol and VSVG (amount ratio is 3:2:1). Transfection was performed using Lipofactamine 2000 according to the manufacturer's instructions. Lentivirus was harvested from the medium at 48 hr posttransfection and applied to the target cells. After 24 hr postinfection, target cells were selected in 4 μg/mL puromycin and/or 150 μg/mL zeocin for 5-7 days. Stable cell lines were maintained in the appropriate medium with 0.5 μg/mL puromycin and/or 20 μg/mL zeocin. MEFs were prepared from embryonic day 13 mouse pups as described previously (Chen et al., 2014).

References

Babst, M. (2005). A protein's final ESCRT. Traffic (Copenhagen, Denmark) *6*, 2-9.

Boldogh, I.R., and Pon, L.A. (2007). Purification and subfractionation of mitochondria from the yeast Saccharomyces cerevisiae. Methods Cell Biol *80*, 45-64.

Bonekamp, N.A., Sampaio, P., de Abreu, F.V., Luers, G.H., and Schrader, M. (2012). Transient complex interactions of mammalian peroxisomes without exchange of matrix or membrane marker proteins. Traffic (Copenhagen, Denmark) *13*, 960-978.

Braschi, E., Goyon, V., Zunino, R., Mohanty, A., Xu, L., and McBride, H.M. (2010). Vps35 mediates vesicle transport between the mitochondria and peroxisomes. Current Biology: CB *20*, 1310-1315.

Campeau, E., Ruhl, V.E., Rodier, F., Smith, C.L., Rahmberg, B.L., Fuss, J.O., Campisi, J., Yaswen, P., Cooper, P.K., and Kaufman, P.D. (2009). A versatile viral system for expression and depletion of proteins in mammalian cells. PLoS One *4*, e6529.

Chen, Y.C., Umanah, G.K., Dephoure, N., Andrabi, S.A., Gygi, S.P., Dawson, T.M., Dawson, V.L., and Rutter, J. (2014). Msp1/ATAD1 maintains mitochondrial function by facilitating the degradation of mislocalized tail-anchored proteins. Embo J *33*, 1548-1564.

Cohen, Y., Klug, Y.A., Dimitrov, L., Erez, Z., Chuartzman, S.G., Elinger, D., Yofe, I., Soliman, K., Gartner, J., Thoms, S.*, et al.* (2014). Peroxisomes are juxtaposed to strategic sites on mitochondria. Molecular bioSystems. *10*:1742-1748

Crane, D.I. (2014). Revisiting the neuropathogenesis of Zellweger syndrome. Neurochemistry International *69*, 1-8.

Delille, H.K., Alves, R., and Schrader, M. (2009). Biogenesis of peroxisomes and mitochondria: linked by division. Histochem Cell Biol *131*, 441-446.

Delille, H.K., Bonekamp, N.A., and Schrader, M. (2006). Peroxisomes and disease - an overview. International Journal of Biomedical Science : IJBS *2*, 308-314.

Dixit, E., Boulant, S., Zhang, Y., Lee, A.S., Odendall, C., Shum, B., Hacohen, N., Chen, Z.J., Whelan, S.P., Fransen, M.*, et al.* (2010). Peroxisomes are signaling platforms for antiviral innate immunity. Cell *141*, 668-681.

Gietz, D., St Jean, A., Woods, R.A., and Schiestl, R.H. (1992). Improved method for high efficiency transformation of intact yeast cells. Nucleic Acids Research *20*, 1425.

Goldstein, A.L., and McCusker, J.H. (1999). Three new dominant drug resistance cassettes for gene disruption in Saccharomyces cerevisiae. Yeast *15*, 1541-1553.

Hanson, P.I., and Whiteheart, S.W. (2005). AAA+ proteins: have engine, will work. Nat Rev Mol Cell Biol *6*, 519-529.

Heiland, I., and Erdmann, R. (2005). Biogenesis of peroxisomes. Topogenesis of the peroxisomal membrane and matrix proteins. The FEBS Journal *272*, 2362-2372.

Hermann, G.J., Thatcher, J.W., Mills, J.P., Hales, K.G., Fuller, M.T., Nunnari, J., and Shaw, J.M. (1998). Mitochondrial fusion in yeast requires the transmembrane GTPase Fzo1p. The Journal of Cell Biology *143*, 359-373.

Hettema, E.H., Girzalsky, W., van Den Berg, M., Erdmann, R., and Distel, B. (2000). Saccharomyces cerevisiae pex3p and pex19p are required for proper localization and stability of peroxisomal membrane proteins. Embo J *19*, 223-233.

Hoepfner, D., Schildknegt, D., Braakman, I., Philippsen, P., and Tabak, H.F. (2005). Contribution of the endoplasmic reticulum to peroxisome formation. Cell *122*, 85-95.

Hu, J., Baker, A., Bartel, B., Linka, N., Mullen, R.T., Reumann, S., and Zolman, B.K. (2012). Plant peroxisomes: biogenesis and function. The Plant Cell *24*, 2279-2303.

Jokhi, V., Ashley, J., Nunnari, J., Noma, A., Ito, N., Wakabayashi-Ito, N., Moore, M.J., and Budnik, V. (2013). Torsin mediates primary envelopment of large ribonucleoprotein granules at the nuclear envelope. Cell Reports *3*, 988-995.

Lazarow, P.B., and Fujiki, Y. (1985). Biogenesis of peroxisomes. Annual Review of Cell Biology *1*, 489-530.

Littleton, J.T., Barnard, R.J., Titus, S.A., Slind, J., Chapman, E.R., and Ganetzky, B. (2001). SNARE-complex disassembly by NSF follows synaptic-vesicle fusion. Proc Natl Acad Sci USA *98*, 12233-12238.

Lodhi, I.J., and Semenkovich, C.F. (2014). Peroxisomes: a nexus for lipid metabolism and cellular signaling. Cell Metab *19*, 380-392.

Meeusen, S., McCaffery, J.M., and Nunnari, J. (2004). Mitochondrial fusion intermediates revealed in vitro. Science *305*, 1747-1752.

Mohanty, A., and McBride, H.M. (2013). Emerging roles of mitochondria in the evolution, biogenesis, and function of peroxisomes. Frontiers in Physiology *4*, 268.

Motley, A.M., and Hettema, E.H. (2007). Yeast peroxisomes multiply by growth and division. The Journal of Cell Biology *178*, 399-410.

Mumberg, D., Muller, R., and Funk, M. (1995). Yeast vectors for the controlled expression of heterologous proteins in different genetic backgrounds. Gene *156*, 119-122.

Nagotu, S., Saraya, R., Otzen, M., Veenhuis, M., and van der Klei, I.J. (2008). Peroxisome proliferation in Hansenula polymorpha requires Dnm1p which mediates fission but not de novo formation. Biochim Biophys Acta *1783*, 760-769.

Nagotu, S., Veenhuis, M., and van der Klei, I.J. (2010). Divide et impera: the dictum of peroxisomes. Traffic (Copenhagen, Denmark) *11*, 175-184.

Neuspiel, M., Schauss, A.C., Braschi, E., Zunino, R., Rippstein, P., Rachubinski, R.A., Andrade-Navarro, M.A., and McBride, H.M. (2008). Cargo-selected transport from the mitochondria to peroxisomes is mediated by vesicular carriers. Current Biology: CB *18*, 102-108.

Opalinski, L., Kiel, J.A., Williams, C., Veenhuis, M., and van der Klei, I.J. (2011). Membrane curvature during peroxisome fission requires Pex11. Embo J *30*, 5-16.

Poirier, Y., Antonenkov, V.D., Glumoff, T., and Hiltunen, J.K. (2006). Peroxisomal beta-oxidation--a metabolic pathway with multiple functions. Biochim Biophys Acta *1763*, 1413-1426.

Rabouille, C., Levine, T.P., Peters, J.M., and Warren, G. (1995). An NSF-like ATPase, p97, and NSF mediate cisternal regrowth from mitotic Golgi fragments. Cell *82*, 905-914.

Rapaport, D., Brunner, M., Neupert, W., and Westermann, B. (1998). Fzo1p is a mitochondrial outer membrane protein essential for the biogenesis of functional mitochondria in Saccharomyces cerevisiae. J Biol Chem *273*, 20150-20155.

Rucktaschel, R., Halbach, A., Girzalsky, W., Rottensteiner, H., and Erdmann, R. (2010). De novo synthesis of peroxisomes upon mitochondrial targeting of Pex3p. European Journal of Cell Biology *89*, 947-954.

Sacksteder, K.A., Jones, J.M., South, S.T., Li, X., Liu, Y., and Gould, S.J. (2000). PEX19 binds multiple peroxisomal membrane proteins, is predominantly cytoplasmic, and is required for peroxisome membrane synthesis. The Journal of Cell Biology *148*, 931-944.

Schrader, M., Bonekamp, N.A., and Islinger, M. (2012). Fission and proliferation of peroxisomes. Biochim Biophys Acta *1822*, 1343-1357.

Schrader, M., and Yoon, Y. (2007). Mitochondria and peroxisomes: are the 'big brother' and the 'little sister' closer than assumed? BioEssays: News and Reviews in Molecular, Cellular and Developmental Biology *29*, 1105-1114.

Smith, J.J., and Aitchison, J.D. (2013). Peroxisomes take shape. Nat Rev Mol Cell Biol *14*, 803-817.

Soubannier, V., McLelland, G.L., Zunino, R., Braschi, E., Rippstein, P., Fon, E.A., and McBride, H.M. (2012). A vesicular transport pathway shuttles cargo from mitochondria to lysosomes. Current Biology : CB *22*, 135-141.

South, S.T., and Gould, S.J. (1999). Peroxisome synthesis in the absence of preexisting peroxisomes. The Journal of Cell Biology *144*, 255-266.

South, S.T., Sacksteder, K.A., Li, X., Liu, Y., and Gould, S.J. (2000). Inhibitors of COPI and COPII do not block PEX3-mediated peroxisome synthesis. The Journal of Cell Biology *149*, 1345-1360.

Sugiura, A., McLelland, G.L., Fon, E.A., and McBride, H.M. (2014). A new pathway for mitochondrial quality control: mitochondrial-derived vesicles. Embo J *33*, 2142-2156.

Theodoulou, F.L., Bernhardt, K., Linka, N., and Baker, A. (2013). Peroxisome membrane proteins: multiple trafficking routes and multiple functions? Biochem J *451*, 345-352.

Toro, A.A., Araya, C.A., Cordova, G.J., Arredondo, C.A., Cardenas, H.G., Moreno, R.E., Venegas, A., Koenig, C.S., Cancino, J., Gonzalez, A.*, et al.* (2009). Pex3p-dependent peroxisomal biogenesis initiates in the endoplasmic reticulum of human fibroblasts. Journal of Cellular Biochemistry *107*, 1083-1096.

van der Klei, I.J., and Veenhuis, M. (2013). The versatility of peroxisome function in filamentous fungi. Sub-cellular Biochemistry *69*, 135-152.

van der Zand, A., Gent, J., Braakman, I., and Tabak, H.F. (2012). Biochemically distinct vesicles from the endoplasmic reticulum fuse to form peroxisomes. Cell *149*, 397-409.

Wach, A., Brachat, A., Pohlmann, R., and Philippsen, P. (1994). New heterologous modules for classical or PCR-based gene disruptions in Saccharomyces cerevisiae. Yeast *10*, 1793-1808.

Woodman, P.G. (2003). p97, a protein coping with multiple identities. J Cell Sci *116*, 4283-4290.

Zhang, J., Wang, Y., Chi, Z., Keuss, M.J., Pai, Y.M., Kang, H.C., Shin, J.H., Bugayenko, A., Wang, H., Xiong, Y.*, et al.* (2011). The AAA+ ATPase Thorase regulates AMPA receptor-dependent synaptic plasticity and behavior. Cell *145*, 284-299.

CHAPTER 5

CONCLUDING REMARKS

Mitochondria play a critical role in many aspects of cell biology. Thus, dysfunction of this organelle is associated with many pathological conditions. To understand the etiology of these human diseases, we set out to characterize the molecular function of evolutionarily conserved mitochondrial proteins with unknown function in both yeast and mammalian cells. In this dissertation, the functions of two highly conserved mitochondrial proteins have been described. The first protein is a respiratory superocomplex stability factor, Rcf1, which is crucial for maintaining optimal efficiency of mitochondrial respiration and ATP production. The second protein, Msp1, is an AAA+ ATPase that possesses multiple functions including mitochondrial protein quality control and mitochondria-to-peroxisome communication. Both proteins act in important aspects of mitochondrial biology and are potentially related to human health.

Rcf1 is an evolutionarily conserved protein that is required for the normal assembly of respiratory supercomplexes. We demonstrate that Rcf1 acts like glue to stabilize the association of Complex III and Complex IV of the electron transport chain. In yeast, we demonstrate that deletion of the *RCF1* gene caused impaired respiration, possibly as a result of destabilization of respiratory supercomplexes. Consistent with the hypothetical function of these respiratory assemblies, loss of *RCF1* also caused elevated mitochondrial oxidative stress and damage. More importantly, we show that knockdown of *HIG2A*, a mammalian homolog of *RCF1*, causes impaired supercomplex formation in mammalian cells. In conclusion, we hypothesize that Rcf1/HIG2A is a member of an evolutionarily conserved protein family that acts to promote respiratory supercomplex assembly and activity. We propose that mutations on this protein family cause major impacts on human health as the integrity of the electron transport chain directly influences energy

homeostasis as well as ROS production.

Msp1 is an AAA+ ATPase that we have found to participate in two distinct functions. The first one is mitochondrial protein quality control in patrolling mitochondria for mislocalized TA proteins. ER-targeted TA proteins are inserted by the GET system and it has been shown that loss of GET system activity causes protein mislocalization to the mitochondria. In yeast, we show that deletion of *MSP1* causes two TA proteins, Pex15 and Gos1, to accumulate on mitochondria when the GET system is impaired. Likely as a result of failing to extract mislocalized TA proteins, yeast with combined mutation of the *MSP1* gene and the GET system exhibit strong synergistic growth defects and severe mitochondrial damage. In mammalian cells, the human homologue of Msp1, ATAD1 limits the mitochondrial mislocalization of PEX26 and GOS28, orthologs of Pex15 and Gos1, respectively. GOS28 protein level is also increased in multiple *ATAD1*$^{-/-}$ mouse tissues. In conclusion, we propose that yeast Msp1 and mammalian ATAD1 are conserved members of the mitochondrial protein quality control system that promote the extraction and degradation of mislocalized TA proteins to maintain mitochondrial integrity.

The additional and unexpected function of Msp1 that we identified is in mitochondria-to-peroxisome trafficking and perhaps peroxisome biogenesis. In yeast, Msp1 first localizes to mitochondria and from there, it traffics to peroxisomes in an ATPase activity-dependent manner. Probably due to failure of trafficking to peroxisomes, Msp1 localizes to vesicle-like puncta in the *pex19*Δ mutant that does not contain peroxisomes. Importantly, depletion of yeast *MSP1* and human *ATAD1* leads to fragmentation of peroxisome, suggesting that they posses an evolutionarily conserved

peroxisomal function. We also show that Msp1/ATAD1 might play a role in sorting peroxisome biogenesis factors (or peroxins) from mitochondria into vesicles. Therefore, we conclude that Msp1/ATAD1 might participate in sorting peroxins from mitochondria to peroxisomes *via* a vesicle trafficking pathway.

Our findings regarding both Rcf1 and Msp1 directly impact our understanding of mitochondrial diseases. First, mitochondrial ROS has been long known as an important contributor to organismal aging. As Rcf1-mediated stabilization of the respiratory supercomplex is crucial to limit mitochondrial oxidative stress, we believe that the function of Rcf1 might be related to the aging process. Therefore, the discovery of the function of the Rcf1/HIG2A protein family provides a perfect opportunity for the scientific community to explore the connection between respiratory supercomplexes and human health. Next, both impaired mitochondria and peroxisomes have major impact on brain function. We know that *ATAD1*$^{-/-}$ mice exhibit severe neurological defects and die at an early postnatal stage. According to the functional characteristics of the Msp1/ATAD1 protein family, members of this protein family play an important role not only in mitochondria but also peroxisomes. An interesting question that awaits to be answered is to what degree the two distinct functions of Msp1/ATAD1 contributes to the pathological phenotype of the *ATAD1*$^{-/-}$ mice. In conclusion, we are hoping that the findings regarding both of these two protein families will provide more insight into mitochondrial disease biology and even have clinical implications.